INVESTIGATING THE RELATIONSHIP BETWEEN ATMOSPHERIC MOISTURE TRANSPORT AND PRECIPITATION IN THE EASTERN UNITED STATES

By

NATALIE TEALE

A dissertation submitted to the

School of Graduate Studies

Rutgers, The State University of New Jersey

In partial fulfillment of the requirements

For the degree of

Doctor of Philosophy

Graduate Program in Geography

Written under the direction of

David A. Robinson

And approved by

_____

_____

_____

_____

New Brunswick, New Jersey

October, 2020

ABSTRACT OF THE DISSERTATION

Investigating the relationship between atmospheric moisture transport and precipitation in the eastern United States

By NATALIE TEALE

Dissertation Director:
Dr. David A. Robinson

This dissertation develops a climatology of water vapor fluxes for the eastern United States and investigates its relationship with precipitation. This approach enriches the current literature, which relates changes in precipitation in the eastern US to weather patterns but largely overlooks the role of moisture supply. Because atmospheric water vapor content is sensitive to temperature, this dissertation contributes new knowledge on how large-scale climate variability impacts regional precipitation. This knowledge is foundational for interpreting past, present, and projected changes in precipitation and understanding its impacts in regional climatology and water resources applications.

Major patterns of water vapor transport in the eastern US are identified using a self-organizing map methodology ingesting daily moisture fluxes from the European Centre for Medium-Range Weather Forecasts (ECMWF) ERA-Interim reanalysis from 1979–2017 for 30°–50°N × 60°–90°W. This procedure produces sixteen patterns of integrated water vapor transport (IVT) that encompass the variety of moisture transport through the region. Spatial and temporal characteristics of these patterns, including

moisture distribution across the domain, qualities of atmospheric rivers, frequency, seasonality, and persistence of the patterns are examined. This resulting climatology presents a precise and comprehensive framework for relating atmospheric moisture supply to precipitation.

This climatology is related to precipitation from 1981–2017 using PRISM daily precipitation data and is extended to 1900–2010 using empirical precipitation data and ECMWF ERA-20C IVT reanalysis. These relationships reveal that the semi-frequent patterns defined by moderate moisture transport are important contributors to annual precipitation, and that the majority of moisture transport patterns are associated with increasing amounts of heavy precipitation. Additionally, increases in the frequency and intensity of strong, meridional moisture transport patterns result in changes in the moisture patterns most often associated with heavy precipitation in the eastern US. These results demonstrate the sensitivity of the eastern US precipitation regime to variability in moisture transport, indicating a need for future studies of regional precipitation to include this information. Overall, this study of kinematic moisture transport provides a new framework for better understanding precipitation variability.

ACKNOWLEDGEMENTS

I would first like to express my deep gratitude to my advisor, Dr. David A. Robinson, for his insight and guidance on this research and in my professional development. His enthusiasm for this project is greatly appreciated, as is his role in creating opportunities for me to explore my interests and grow in the academic setting.

I offer my sincere thanks to the members of my committee, Dr. Åsa Rennermalm, Dr. Anthony Broccoli, and Dr. Thomas Mote, for their insight, expertise, and encouragement at various stages of this project. Their willingness to serve on the committee and provide feedback is much appreciated.

I would like to express my deep appreciation for the Department of Geography for its support throughout these years. I am especially grateful for multiple years of funding and the support to attend conferences and expand my knowledge. I also thank the Rutgers Climate Institute for their conference travel support to enrich my education, as well as the Rutgers Institute of Earth, Ocean, and Atmospheric Sciences for their funding and conference support. I am also greatly appreciative of the Presidential Fellowship and travel support from the School of Graduate Studies.

I thank my classmates and peers at Rutgers University for their support and friendship, especially my past and present officemates and the attendees of the Quantitative Geography lunches. Dr. Alexandra Ramos deserves special thanks for her companionship and encouragement from across the river. I am also profoundly thankful for my peers and friends in Geography outside Rutgers: in addition to their continuous

support, I am grateful to Mr. Manuel Hernandez, Mr. Daniel Vecellio, Ms. Victoria Ford, and Dr. Ryan Dicce for their helpful discussions about climatology, programming, statistics, and scholarship.

Finally, I am indebted to my family for their encouragement and understanding. I am eternally grateful to my husband, Matthew Samollow, for his unwavering support. He has made countless sacrifices to support my aspirations only to receive an unending and often unsolicited education in climatology and physical geography in return. I especially thank my sister, Dr. Stephanie Green, who has always been my biggest cheerleader. Finally, I thank my parents. I am grateful to my father for showing me a path in research, and my mother for her support of me following that path. In recognition of her “pearls of wisdom” and her exemplification of grace under pressure, I would like to dedicate this dissertation to my mother.

TABLE OF CONTENTS

LIST OF TABLES

LIST OF FIGURES

1. INTRODUCTION

1.1. Hydroclimatology and climate change

Hydroclimatology is the "study of cyclical, multidirectional interactions between the climate system and the hydrologic cycle on a variety of spatial and temporal scales" (Teale 2020). Because the hydrologic cycle is inextricably connected to the climate system through an array of intrinsic relationships, variability in the climate system is impressed upon hydrologic system. One such relationship, among many, includes how moisture is transported from global to local scales and the resulting precipitation patterns.

The effect of global temperatures on atmospheric moisture can be described through the Clausius-Clapeyron relationship, in which atmospheric moisture content theoretically increases approximately 7% per degree Celsius of warming assuming constant relative humidity (Trenberth 2011; Held and Soden 2006; Boer 1993). The increase in global-mean precipitation is less than the Clausius-Clapeyron relation, being shown as a 3–4% increase per degree Celsius in climate models (Allen and Ingram 2002, Skliris et al. 2016), though this rate has been closer to the relation in other datasets (Wentz et al. 2007). Heavy precipitation has been shown to be more sensitive to global temperature increases than global-mean precipitation, resulting in an increased frequency and intensity of heavy and extreme precipitation events (Trenberth 1999; Allen and Ingram 2002; Pall et al. 2007; Donat et al. 2016). This shift in precipitation characteristics has impacts throughout water resources, flooding hazards, and other hydroclimatic applications.

Increases in the water vapor holding capacity of the atmosphere and in precipitation are not spatially uniform. Instead, the hydroclimatic response to climate change is often discussed as an intensification of the water cycle, with increases in evaporation and precipitation resulting in wet areas becoming wetter and dry areas becoming drier (Huntington 2006; Byrne and O'Gorman 2015; Wentz et al. 2007). While convenient to visualize for general purposes, this phrasing overlooks factors that drive regional responses to climate change. Bryne and O'Gorman (2015), for example, show that accounting for latitude and horizontal temperature gradients in this scaling yields moisture budgets that better agree with model projections than the simple "wet-get-wetter" scaling alone. Bordi et al. (2015) also show considerable regional variability in atmospheric moisture, demonstrating that in South America, the influence of both regional vegetation greening as well as intensification of monsoon activity result in spatially uneven total column water vapor. Beyond monsoons, the influence of atmospheric circulation in arranging heterogeneous water vapor magnitudes is a topic of interest in hydroclimatology not just for its impact on the water vapor feedback (Held and Soden 2000) or meridional moisture and energy transport (Knippertz and Wernli 2010), but also for its role in precipitation. Trenberth et al. (2003) show that precipitation is fueled by water vapor transported from ranges several times the size of a storm itself. This mechanism enables precipitation totals to be considerably higher than mean global total column water vapor depths and extremely spatially variable, and also creates major conduits of water vapor transport that comprise the majority of global moisture transport (Zhu and Newell 1998).

This process of moisture advection resulting in localized areas of high water vapor content has been given extensive attention in the past several years through the study of atmospheric rivers. Atmospheric rivers refer to narrow corridors of strong, horizontal water vapor transport responsible for much of the horizontal moisture transport in the midlatitudes (American Meteorological Society 2020). These features are frequently linked with heavy precipitation when the enhanced moisture transport filament is forced to rise. Because of the varied impacts of this precipitation, many studies have turned to assessing water vapor transport to better understand regional precipitation. Such efforts to characterize moisture transport to better understand precipitation and other hydrologic processes have been undertaken for western North America (Ralph et al. 2006; Payne and Magnusdottir 2014; Rutz et al. 2015; Warner et al. 2015; Radić et al. 2015; Guan et al. 2016; Hu et al. 2017; and others), the intermountain West (Swales et al. 2016), the central United States (Moore et al. 2011; Lavers and Villarini 2013), the southeastern United States (Mahoney et al. 2016, Debbage et al. 2017), Greenland (Mattingly et al. 2016), coastal Europe and the United Kingdom (Lavers and Villarini 2015; Ramos et al. 2015; Brands et al. 2017), and even Antarctica (Gorodetskaya et al. 2014; Wille et al. 2019). However, the climatology of water vapor transport, much less the role of moisture transport in precipitation, has not been studied sufficiently for the northeastern US or the eastern US as a whole.

1.2. Precipitation variability of the Eastern United States

Moderate annual precipitation and a seasonal temperature cycle define the hydroclimatology of the eastern US. Like much of the midlatitudes, the eastern US experiences a strong seasonal amplitude in temperature, controlled largely by latitude and

elevation (Figure 1.1). Precipitation within the eastern US demonstrates less of a seasonal cycle, though totals are generally more spatially homogeneous in the summer months than the winter (Figure 1.1). In general, the eastern US receives higher precipitation in the summer and winter than elsewhere in the United States, with few exceptions (Figure 1.1). Prominent hydroclimatic events since the early twentieth century include the drought of the 1960s (Namias 1966) and the following shift to wetter conditions (Seager et al. 2012; Kelly-Voicu and Frei 2019), and the onset of enhanced precipitation in the 1990s (Huang et al. 2017; Kelly-Voicu and Frei 2020).

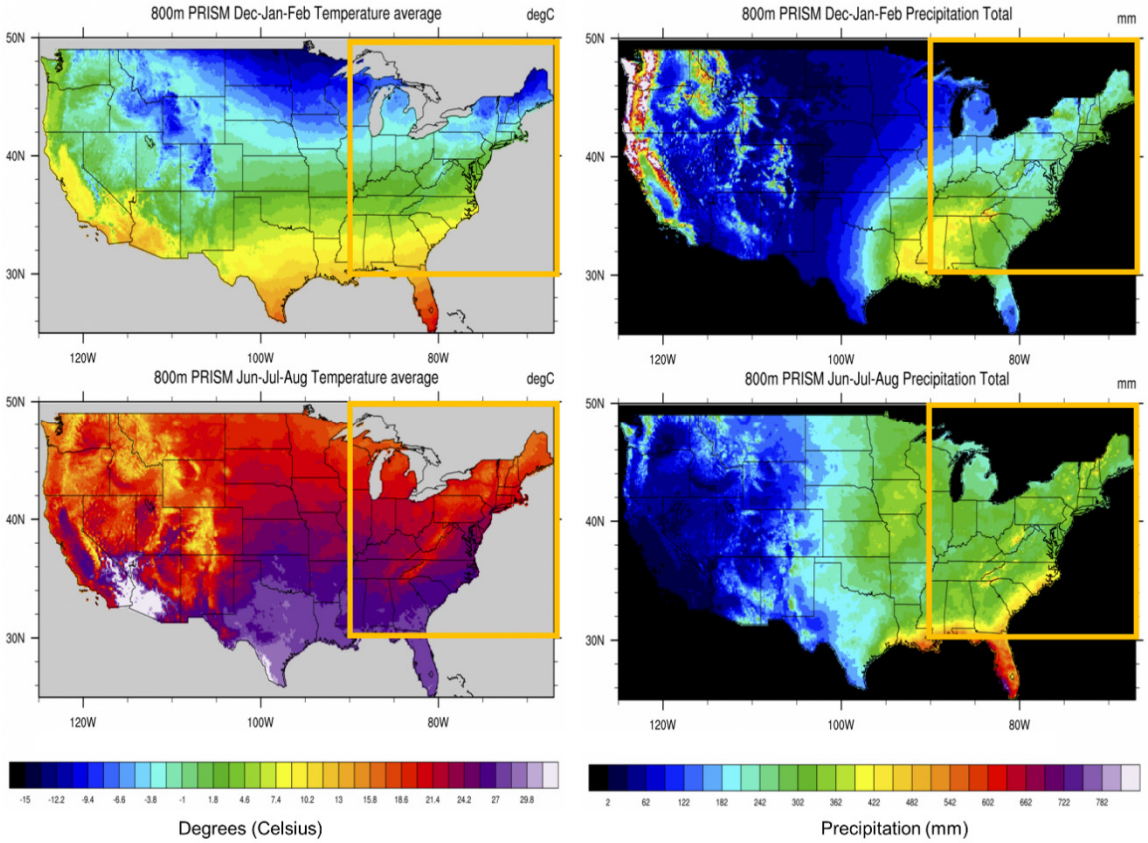

Figure 1.1. Winter (top) and summer (bottom) temperature and precipitation for the contiguous United States from 1981–2010, modified from National Center for Atmospheric Research, climatedataguide.ucar.edu (D. Schneider). The eastern US as defined in this study is approximated by the box.

Increases in annual precipitation have been observed for much of the eastern US since 1900 (Figure 1.2). These changes are variable throughout the eastern US (Figure 1.3). While the Midwest, Northeast, and Southeast—all included within the eastern US domain of this study—each show increases in annual precipitation after the 1970s, the percent change is considerably lower in the Southeast than the other eastern regions. Furthermore, while the Midwest and Northeast each show increasing annual precipitation totals throughout the region, areas of decreasing annual precipitation emerge in the Southeast, particularly in the piedmont region of the Carolinas.

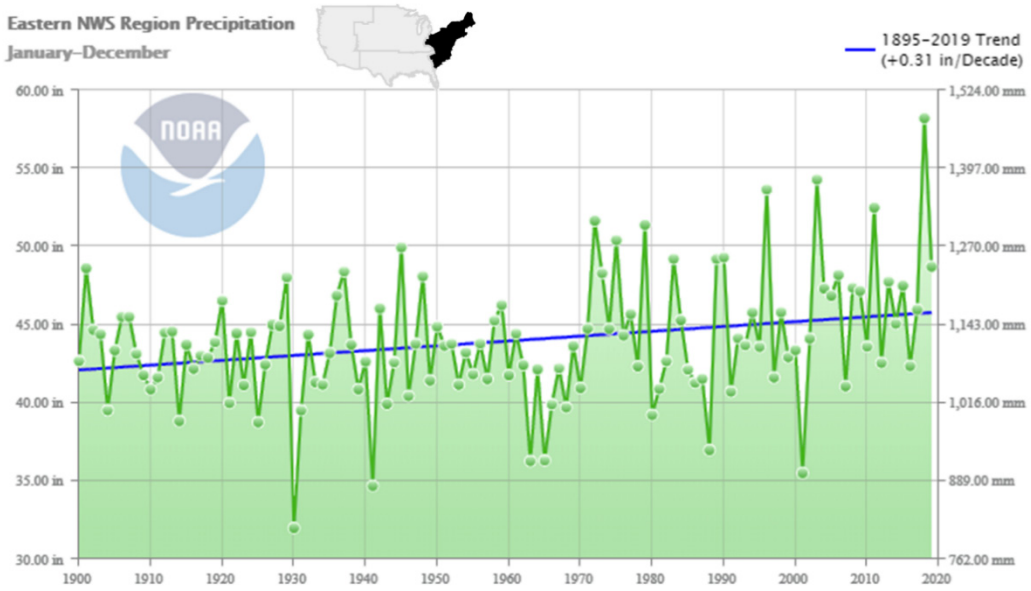

Figure 1.2. Annual precipitation for the eastern US. Figure from NOAA Climate at a Glance (https://www.ncdc.noaa.gov/cag).

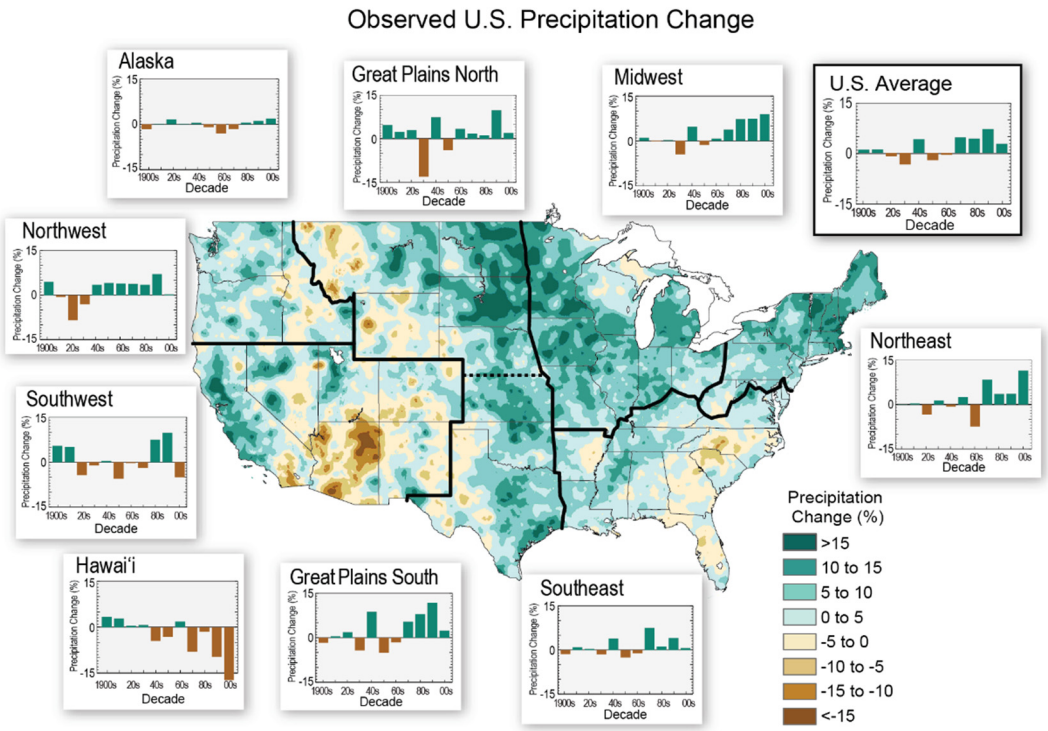

Figure 1.3. Change in annual precipitation for each decade relative to 1901–1960 average. Adapted from Peterson et al. (2013).

The eastern US has experienced strong increases in heavy precipitation (Figure 1.4) Some of the greatest changes in heavy precipitation have been observed in the Northeast, including a 71% increase in the amount of precipitation falling in the heaviest 1% of precipitation events (Walsh et al. 2014). Many studies have shown increases in heavy precipitation in the eastern US. Positive trends in frequency of moderate and extreme precipitation events in the eastern and northeastern US are shown in Degaetano (2009). Douglas and Fairbank (2011) show increases in the frequency of heavy precipitation events in New England since the 1950s as well as in the magnitude of annual precipitation since the 1970s. A similar increase in more frequent precipitation extremes since the 1950s is also shown in Thibeault and Seth (2014). Huang et al. (2017) show

significant increases in both annual precipitation and extreme precipitation, and that these rates of increase intensify after the late 1990s and early 2000s. In the southeastern US, trends are less consistent. For instance, dry spells have become shorter since the 1950s in the southern US (Trepanier et al. 2015), though trends in precipitation frequency vary spatially and temporally throughout the Southeast since the 1960s (Bartels et al. 2020). Similar to the Northeast, increases in the intensity of heavy precipitation have been observed in the Southeast. In particular, increases in the 90th percentile of hourly precipitation events increased since the 1960s (Brown et al. 2020).

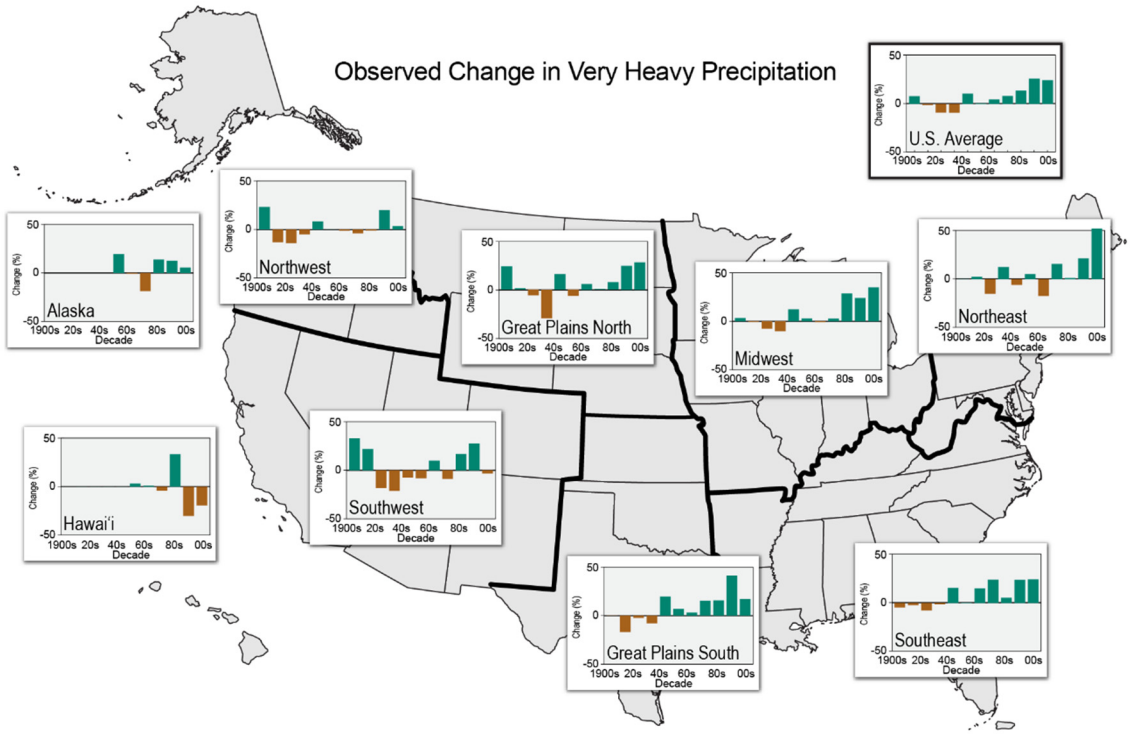

Figure 1.4. Percent changes in the amount of precipitation falling in heaviest 1% of events annually, relative to the 1901–1960 average. Figure adapted from NOAA NCDC / CICS-NC, as in Walsh et al. (2014).

Efforts have been undertaken to determine the mechanisms or storm types related to eastern US precipitation events, if not the trends associated with them. For instance, Kunkel et al. (2013) analyze trends in extreme precipitation through their associations with various meteorological causes, such as extratropical cyclones, fronts, and mesoscale convective systems. Other studies employ a typing approach that identifies major atmospheric features and patterns associated with heavy precipitation. For instance, Konrad (1997) employs a synoptic typing methodology to identify atmospheric features associated with heavy precipitation in the southeastern US. A typing methodology based on principle component analysis is employed to identify synoptic-scale pressure patterns associated with heavy precipitation in New York in Teale et al. (2017). Agel et al. (2018) apply k-means clustering to the dynamic tropopause pressure field to identify major patterns associated with extreme precipitation in the Northeast. Other studies relating extreme precipitation events to large-scale meteorological patterns are reviewed in Barlow et al. (2019).

These classification and synoptic typing studies describe the conditions surrounding many precipitation events in the eastern US. This approach reduces the dimensionality of the climate system to reveal a small number of patterns frequently associated with heavy precipitation, enabling analysis of the frequencies of these weather patterns. These studies provide a great deal of information regarding the hydroclimatology of the eastern US. However, this body of literature surrounding regional precipitation currently possesses two major knowledge gaps that will be addressed by this dissertation.

The first knowledge gap is that the majority of the literature does not account for variability in the water vapor providing moisture for precipitation. As previously discussed, increases in water vapor have been observed and projected globally, with corresponding increases in precipitation. While most of the studies assessing precipitation in the eastern US discuss the frequency of the precipitation-generating weather patterns, the picture is not complete without an understanding of water vapor transport, as variability in water vapor supply would fundamentally affect the precipitation produced by any weather pattern. Water vapor transport, a variable commonly used in the aforementioned atmospheric rivers literature, is a useful variable for precipitation applications because it combines columnar water vapor content with horizontal velocity. These components together capture the magnitude of total water vapor flux as well as the moisture trajectory, both of which can be important in determining the characteristics of any associated precipitation.

The second knowledge gap is that most of the studies relating precipitation to weather patterns focus on precipitation of a certain magnitude, often heavy precipitation and extreme precipitation. This problem is complicated by the wide range of thresholds and methods used to determine what constitutes heavy or extreme precipitation currently in use in the literature. While heavy precipitation is of great importance to the regional hydroclimatology due to its potential for life-threatening flooding and its intensification over the past century, it is only a small part of the precipitation regime in the eastern US. Water resources, agriculture, and other applications are also sensitive to variability in moderate precipitation events. An analysis of a precipitation regimes as a whole would provide a comprehensive insight into the variability of precipitation impacting the region.

This dissertation addresses these knowledge gaps by developing a climatology of water vapor transport and relating this climatology to precipitation in the eastern US. This novel characterization of present and historical moisture transport provides important background information for interpreting historical datasets as well as climate model projections of water vapor and precipitation. Furthermore, the structure of this dissertation enables the study of not just heavy precipitation, but of the precipitation regime as a whole. In this way, this dissertation offers a comprehensive description of atmospheric moisture and associated precipitation in the eastern US.

1.3. Dissertation organization

To achieve the goal of developing a climatology of water vapor transport in the eastern US and relating it to the precipitation regime, this research is structured in three studies focused on developing the water vapor transport climatology, relating the major patterns to regional precipitation, and extending the climatology back through the twentieth century.

The first study, Chapter 2, identifies the major patterns of moisture transport impacting the eastern US. This procedure is undertaken using reanalysis data from 1979–2017. Several analyses are implemented to characterize these patterns, describing the frequency, persistence, and seasonality of the moisture transport patterns as well as the confinement of moisture within the patterns. These patterns and the produced understanding of the multifaceted water vapor transport through the eastern US provide the primary dataset used in the subsequent studies.

In Chapter 3 the patterns of water vapor transport are related to eastern US precipitation. Gridded, high-resolution precipitation data from 1981–2017 are employed to determine the magnitude of precipitation associated with each pattern throughout the eastern US as well as how often precipitation occurs with each moisture transport pattern. These analyses are undertaken seasonally to better understand the impact of different moisture fluxes throughout the year. This study also demonstrates the contribution of each pattern to the annual precipitation totals of the study domain. Overall, the findings from this research describe the relationship between each of the moisture patterns and precipitation within the eastern US.

Chapter 4 extends the water vapor transport patterns back through the twentieth century. This extension is executed by classifying a historical reanalysis water vapor transport product into the patterns identified in the first study. The long-term variability of these patterns is compared with variability in heavy precipitation in the region, as shown through empirical precipitation data from 1900–2010 from several stations throughout the study domain. This final study provides a long-term perspective on the variability of moisture transport, precipitation extremes, and their relationship throughout the eastern US.

1.4. References

Agel, L., M. Barlow, S. B. Feldstein, and W. J. Gutowski, 2018: Identification of large-scale meteorological patterns associated with extreme precipitation in the US northeast. *Clim. Dyn.*, **50**, 1819–1839, https://doi.org/10.1007/s00382-017-3724-8.

Allen, M. R., and W. J. Ingram, 2002: Constraints on future changes in climate and the hydrologic cycle. *Nature*, **419**, 224–232, https://doi.org/10.1038/nature01092.

American Meteorological Society, 2020: Atmospheric river. http://glossary.ametsoc.org/wiki/Atmospheric_river.

Barlow, M., and Coauthors, 2019: North American extreme precipitation events and related large-scale meteorological patterns: a review of statistical methods, dynamics, modeling, and trends. *Clim. Dyn*., **53**, 6835–6875 pp., https://doi.org/10.1007/s00382-019-04958-z.

Bartels, R. J., A. W. Black, and B. D. Keim, 2020: Trends in precipitation days in the United States. *Int. J. Climatol.*, **40**, 1038–1048, https://doi.org/10.1002/joc.6254.

Brands, S., J. M. Gutiérrez, and D. San-Martín, 2017: Twentieth-century atmospheric river activity along the west coasts of Europe and North America: algorithm formulation, reanalysis uncertainty and links to atmospheric circulation patterns. *Clim. Dyn.*, **48**, 2771–2795, https://doi.org/10.1007/s00382-016-3095-6.

Boer, G. J., 1993: Climate change and the regulation of the surface moisture and energy budgets. *Clim. Dyn.*, https://doi.org/10.1007/BF00198617.

Bordi, I., R. De Bonis, K. Fraedrich, and A. Sutera, 2015: Interannual variability patterns of the world's total column water content: Amazon River basin. *Theor. Appl. Climatol.*, **122**, 441–455, https://doi.org/10.1007/s00704-014-1304-y.

Brown, V. M., B. D. Keim, and A. W. Black, 2020: Trend Analysis of Multiple Extreme Hourly Precipitation Time Series in the Southeastern United States. *J. Appl. Meteorol. Climatol.*, **59**, 427–442, https://doi.org/10.1175/jamc-d-19-0119.1.

Byrne, M. P., and P. A. O'Gorman, 2015: The response of precipitation minus evapotranspiration to climate warming: Why the "Wet-get-wetter, dry-get-drier" scaling does not hold over land. *J. Clim.*, **28**, 8078–8092, https://doi.org/10.1175/JCLI-D-15-0369.1.

Daly, Christopher & National Center for Atmospheric Research Staff (Eds). Last modified 12 Dec 2019. "The Climate Data Guide: PRISM High-Resolution Spatial Climate Data for the United States: Max/min temp, dewpoint, precipitation." Retrieved from https://climatedataguide.ucar.edu/climate-data/prism-high-resolution-spatial-climate-data-united-states-maxmin-temp-dewpoint.

Debbage, N., P. Miller, S. Poore, K. Morano, T. Mote, and J. Marshall Shepherd, 2017: A climatology of atmospheric river interactions with the southeastern United States coastline. *Int. J. Climatol.*, **37**, 4077–4091, https://doi.org/10.1002/joc.5000.

Degaetano, A. T., 2009: Time-dependent changes in extreme-precipitation return-period amounts in the continental United States. *J. Appl. Meteorol. Climatol.*, **48**, 2086-2099. https://doi.org/10.1175/2009JAMC2179.1.

Donat, M. G., A. L. Lowry, L. V. Alexander, P. A. O'Gorman, and N. Maher, 2016: More extreme precipitation in the world's dry and wet regions. *Nat. Clim. Chang.*, **6**, 508-513. https://doi.org/10.1038/nclimate2941.

Douglas, E. M., and C. A. Fairbank, 2011: Is Precipitation in Northern New England Becoming More Extreme? Statistical Analysis of Extreme Rainfall in Massachusetts, New Hampshire, and Maine and Updated Estimates of the 100-Year Storm. *J. Hydrol. Eng.*, **16**, 203–217, https://doi.org/10.1061/(ASCE)HE.1943-5584.0000303.

Gorodetskaya, I. V., M. Tsukernik, K. Claes, M. F. Ralph, W. D. Neff, and N. P. M. Van Lipzig, 2014: The role of atmospheric rivers in anomalous snow accumulation in East Antarctica. *Geophys. Res. Lett.*, **41**, https://doi.org/10.1002/2014GL060881.

Guan, B., D. E. Waliser, F. M. Ralph, E. J. Fetzer, and P. J. Neiman, 2016: Hydrometeorological characteristics of rain-on-snow events associated with atmospheric rivers. 2964–2974, https://doi.org/10.1002/2016GL067978.

Held, I. M., and B. J. Soden, 2000: Water Vapor Feedback and Global Warming. *Annu. Rev. Energy Environ.*, **25**, 441–475.

Held, I. M., and B. J. Soden, 2006: Robust Responses of the Hydrological Cycle to Global Warming. *J. Clim.*, **19**, 5686–5699.

Hu, H., F. Dominguez, Z. Wang, D. A. Lavers, G. Zhang, and F. M. Ralph, 2017: Linking Atmospheric River Hydrological Impacts on the U.S. West Coast to Rossby Wave Breaking. *J. Clim.*, JCLI-D-16-0386.1, https://doi.org/10.1175/JCLI-D-16-0386.1.

Huang, H., J. M. Winter, E. C. Osterberg, R. M. Horton, and B. Beckage, 2017: Total and extreme precipitation changes over the Northeastern United States. *J. Hydrometeorol.*, **18**, 1783–1798, https://doi.org/10.1175/JHM-D-16-0195.1.

Huntington, T. G., 2006: Evidence for intensification of the global water cycle: Review and synthesis. *J. Hydrol.*, **319**, 83–95, https://doi.org/10.1016/j.jhydrol.2005.07.003.

Kelly-Voicu, P., and A. Frei, 2019: Hydrological and temperature variations between 1900 and 2016 in the Catskill Mountains, New York, USA. *Int. J. Climatol.*, 1–21, https://doi.org/10.1002/joc.6289.

——, and ——, 2020: Hydrological and temperature variations between 1900 and 2016 in the Catskill Mountains, New York, USA. *Int. J. Climatol.*, **40**, 1586–1606, https://doi.org/10.1002/joc.6289.

Knippertz, P., and H. Wernli, 2010: A lagrangian climatology of tropical moisture exports to the northern hemispheric extratropics. *J. Clim.*, **23**, 987–1003, https://doi.org/10.1175/2009JCLI3333.1.

Konrad, C. E., 1997: Synoptic-scale features associated with warm season heavy rainfall over the interior southeastern United States. *Weather Forecast.*, **12**, 557–571, https://doi.org/10.1175/1520-0434(1997)012<0557:SSFAWW>2.0.CO;2.

Kunkel, K. E., and Coauthors, 2013: Monitoring and understanding trends in extreme storms: State of knowledge. *Bull. Am. Meteorol. Soc.*, **94**, 499–514, https://doi.org/10.1175/BAMS-D-11-00262.1.

Lavers, D. A., and G. Villarini, 2013: Atmospheric Rivers and Flooding over the Central United States. *J. Clim.*, **26**, 7829–7836, https://doi.org/10.1175/JCLI-D-13-00212.1.

——, and ——, 2015: The contribution of atmospheric rivers to precipitation in Europe and the United States. *J. Hydrol.*, **522**, 382–390, https://doi.org/10.1016/j.jhydrol.2014.12.010.

Mahoney, K., and Coauthors, 2016: Understanding the Role of Atmospheric Rivers in Heavy Precipitation in the Southeast United States. *Mon. Weather Rev.*, **144**, 1617–1632, https://doi.org/10.1175/MWR-D-15-0279.1.

Mattingly, K. S., C. A. Ramseyer, J. J. Rosen, T. L. Mote, and R. Muthyala, 2016: Increasing water vapor transport to the Greenland Ice Sheet revealed using self-organizing maps. *Geophys. Res. Lett.*, 9250–9258, https://doi.org/10.1002/2016GL070424.Received.

Moore, B. J., P. J. Neiman, F. M. Ralph, and F. E. Barthold, 2011: Physical Processes Associated with Heavy Flooding Rainfall in Nashville , Tennessee , and Vicinity during 1 – 2 May 2010 : The Role of an Atmospheric River and Mesoscale Convective Systems *. 358–378, https://doi.org/10.1175/MWR-D-11-00126.1.

Namias, J., 1966: Nature and Possible causes of the Northeastern United States Drought During 1962- 1965. *Mon. Weather Rev.*, **94**, 543–557.

NOAA National Centers for Environmental information, Climate at a Glance: Global Mapping, published April 2020, retrieved on April 26, 2020 from https://www.ncdc.noaa.gov/cag/

Pall, P., M. R. Allen, and D. A. Stone, 2007: Testing the Clausius-Clapeyron constraint on changes in extreme precipitation under CO2 warming. *Clim. Dyn.*, **28**, 351–363, https://doi.org/10.1007/s00382-006-0180-2.

Payne, A. E., and G. Magnusdottir, 2014: Dynamics of Landfalling Atmospheric Rivers over the North Pacific in 30 Years of MERRA Reanalysis. *J. Clim.*, **27**, 7133–7150, https://doi.org/10.1175/JCLI-D-14-00034.1.

Peterson, T. C., and Coauthors, 2013: Monitoring and understanding changes in heat waves, cold waves, floods, and droughts in the United States: State of knowledge. *Bull. Am. Meteorol. Soc.*, **94**, 821–834, https://doi.org/10.1175/BAMS-D-12-00066.1.

Radić, V., A. Cannon, B. Menounos, and N. Gi, 2015: Future changes in autumn atmospheric river events in British Columbia, Canada, as projected by CMIP5 global climate models. *J. Geophys. Res. Atmos.*, **120**, 1300–1321, https://doi.org/10.1002/2014JD021963.Received.

Ralph, F. M., P. J. Neiman, G. a. Wick, S. I. Gutman, M. D. Dettinger, D. R. Cayan, and A. B. White, 2006: Flooding on California's Russian River: Role of atmospheric rivers. *Geophys. Res. Lett.*, **33**, 3–7, https://doi.org/10.1029/2006GL026689.

Ramos, A. M., R. M. Trigo, M. L. R. Liberato, and R. Tomé, 2015: Daily precipitation

extreme events in the Iberian Peninsula and its association with atmospheric rivers. *J. Hydrometeorol.*, **16**, 579–597, https://doi.org/10.1175/JHM-D-14-0103.1.

Rutz, J. J., W. J. Steenburgh, and F. M. Ralph, 2015: The Inland Penetration of Atmospheric Rivers over Western North America: A Lagrangian Analysis. *Mon. Weather Rev.*, **143**, 1924–1944, https://doi.org/10.1175/MWR-D-14-00288.1.

Seager, R., N. Pederson, Y. Kushnir, J. Nakamura, and S. Jurburg, 2012: The 1960s drought and the subsequent shift to a wetter climate in the Catskill Mountains region of the New York City watershed. *J. Clim.*, **25**, 6721–6742, https://doi.org/10.1175/JCLI-D-11-00518.1.

Skliris, N., J. D. Zika, G. Nurser, S. A. Josey, and R. Marsh, 2016: Global water cycle amplifying at less than the Clausius-Clapeyron rate. *Sci. Rep.*, **6**, 1–9, https://doi.org/10.1038/srep38752.

Swales, D., M. Alexander, and M. Hughes, 2016: Examining moisture pathways and extreme precipitation in the U.S. Intermountain West using self-organizing maps. 1727–1735, https://doi.org/10.1002/2015GL067478.Received.

Teale, N., 2020: Hydroclimatology and Climate Variability. *Oxford Bibliogr. Geogr.*, 1–16, https://doi.org/10.1093/obo/9780199874002-0216.

——, S. M. Quiring, and T. W. Ford, 2017: Association of synoptic-scale atmospheric patterns with flash flooding in watersheds of the New York City water supply system. *Int. J. Climatol.*, **37**, 358–370, https://doi.org/10.1002/joc.4709.

Thibeault, J. M., and A. Seth, 2014: Changing climate extremes in the Northeast United States: observations and projections from CMIP5. *Clim. Change*, **127**, 273–287, https://doi.org/10.1007/s10584-014-1257-2.

Trenberth, K. E., 1999: Conceptual framework for changes of extremes of the hydrological cycles with climate change. *Clim. Change*, https://doi.org/10.1023/A:1005488920935.

Trenberth, K. E., A. Dai, R. M. Rasmussen, and D. B. Parsons, 2003: The changing character of precipitation. *Bull. Am. Meteorol. Soc.*, **84**, 1205-1217+1161, https://doi.org/10.1175/BAMS-84-9-1205.

Trenberth, K. E., 2011: Changes in precipitation with climate change. *Clim. Res.*, **47**, 123–138, https://doi.org/10.3354/cr00953.

Trepanier, J. C., M. J. Roberts, and B. D. Keim, 2015: Trends and spatial variability in dry spells across the south-central United States. *J. Appl. Meteorol. Climatol.*, **54**, 2261–2272, https://doi.org/10.1175/JAMC-D-14-0319.1.

Walsh, J., D. Wuebbles, K. Hayhoe, J. Kossin, K. Kunkel, G. Stephens, P. Thorne, R. Vose, M. Wehner, J. Willis, D. Anderson, S. Doney, R. Feely, P. Hennon, V. Kharin, T. Knutson, F. Landerer, T. Lenton, J. Kennedy, and R. Somerville, 2014: *Ch. 2: Our Changing Climate. Climate Change Impacts in the United States: The*

Third National Climate Assessment, J. M. Melillo, Terese (T.C.) Richmond, and G. W. Yohe, Eds., U.S. Global Change Research Program, 19-67. doi:10.7930/J0KW5CXT.

Warner, M. D., C. F. Mass, and E. P. Salathé, 2015: Changes in Winter Atmospheric Rivers along the North American West Coast in CMIP5 Climate Models. *J. Hydrometeorol.*, **16**, 118–128, https://doi.org/10.1175/JHM-D-14-0080.1.

Wentz, F. J., L. Ricciardulli, K. Hilburn, and C. Mears, 2007: How much more rain will global warming bring? *Science (80-.).*, **317**, 233–235, https://doi.org/10.1126/science.1140746.

Wille, J. D., V. Favier, A. Dufour, I. V. Gorodetskaya, J. Turner, C. Agosta, and F. Codron, 2019: West Antarctic surface melt triggered by atmospheric rivers. *Nat. Geosci.*, **12**, 911–916, https://doi.org/10.1038/s41561-019-0460-1.

Zhu, Y., and R. E. Newell, 1998: A Proposed Algorithm for Moisture Fluxes from Atmospheric Rivers. *Mon. Weather Rev.*, **126**, 725–735, https://doi.org/10.1175/1520-0493(1998)126<0725:APAFMF>2.0.CO;2.

2. PATTERNS OF WATER VAPOR TRANSPORT IN THE EASTERN UNITED STATES

Abstract

This study presents a climatology of water vapor fluxes for the eastern US and adjacent Atlantic with particular focus on the Northeast. Pathways of moisture transport comprising this climatology were discerned using a self-organizing map methodology ingesting daily integrated vapor transport data from ECMWF ERA-Interim Reanalysis from 1979–2017 at a 2.5°× 2.5° spatial resolution. Sixteen spatially distinct moisture transport patterns capture the variety of water vapor transport in the region. The climatology of water vapor transport is precisely and comprehensively defined via synthesis of spatial and temporal characteristics of the fluxes. Each flux has a distinct seasonality and frequency. The fluxes containing the highest amounts of moisture transport occur less frequently than those with less moisture transport. Because the patterns showing less moisture transport are prevalent, they are major contributors to the manner in which water vapor is moved through the eastern US. The spatial confinement of fluxes is inversely related to persistence, with strong, narrow bands of enhanced moisture transport most often moving through the region on daily timescales. Many moisture fluxes meet a threshold-based definition of atmospheric rivers, with the diversity in trajectories and moisture sources indicating that a variety of mechanisms develop these enhanced moisture transport conditions. Temporal variability in the monthly frequencies of several of the fluxes in this study aligns with changes in the

regional precipitation regime, demonstrating that this water vapor flux climatology provides a precise moisture-delivery framework from which changes in precipitation can be investigated.

2.1. Introduction

Substantial changes in the precipitation regime, particularly in heavy precipitation, have been observed in the northeastern United States (e.g., Groisman et al. 2005, 2004; Karl et al. 2009; Walsh et al. 2014; Douglas and Fairbank 2011; Matonse and Frei 2013; Frei et al. 2015). So too have particularly large increases in the magnitude of extreme precipitation events been observed (e.g., Groisman et al. 2005, 2004; Karl et al. 2009). The National Climate Assessment shows a 71% increase in the amount of precipitation falling in the top 1% of precipitation events (Walsh et al. 2014). This assessment also shows that the amount of precipitation falling in the heaviest precipitation events has increased disproportionately in the northeastern US compared to other regions. These findings corroborate a suite of literature reporting changes in heavy precipitation in the Northeast. For example, Douglas and Fairbank (2011) show that heavy precipitation has become more frequent in New England since the 1950s, and the magnitude of the annual maximum precipitation has increased since the 1970s. Additionally, Matonse and Frei (2013) report an increased frequency of extreme events in southern New York since 1985, mostly in the warm season. They also find the rate of increase of frequency of extreme events accelerated in the 1990s to unprecedented reported levels (Matonse and Frei 2013). Kunkel et al. (2013) find statistically significant

increases in total fall precipitation and total annual precipitation since 1970, though they report no significant change in winter or summer precipitation. They also report an increase in the amount of precipitation variability over the past 80 years (Kunkel et al. 2013). Groisman et al. (2005) show that the number of days receiving precipitation increased for the first several decades of 20th century in the northeastern and midwestern US; however, the frequency of precipitation days decreased alongside an increase in very heavy precipitation over the past 30 years. These results indicate that the precipitation regime of the region is changing.

One potential explanation for the changing Northeast precipitation regime is a change in the magnitude of water vapor delivered to the region. Precipitation is dependent on an atmospheric moisture source to condense and precipitate. Higher temperatures, such as those observed and projected in models of anthropogenic global warming, are projected to alter precipitation regimes through an intensification of the water cycle (Huntington 2006). The Clausius-Clapeyron equation shows that for every 1°C of warming, the saturation vapor pressure of the atmosphere increases 7% (Trenberth 2011). This means that while air may reach saturation less frequently in warmer climates, resulting in less frequent precipitation, due to the higher air temperatures there may be more moisture to precipitate out once saturation is met (Trenberth et al. 2003).

Changes in regional precipitation may also be associated with changes in the trajectory of water vapor fluxes. Trenberth et al. (2003) demonstrate that transport of water vapor from a distance is required to achieve even moderate precipitation events, and that precipitation can be sourced from water vapor transported from a distance of 3-5 times the radius of the precipitation event. With small storms this source area may be

fairly small, on the order of kilometers, but with large extratropical cyclones the source region may be thousands of kilometers away, and water vapor may be transported for days before being precipitated (Trenberth et al. 2003). Changes in synoptic scale circulation associated with natural variability and anthropogenically induced climate change may also alter the patterns of precipitation by changing relationships and transport distances between moisture source and deposition (Trenberth et al. 2003). These changes may also affect the direction from which the moisture is arriving, which can change the precipitation mechanism (such as orographic lifting) or the moisture content (such as lake-effect moisture). These changes in transport distance and direction are important because they may also lead to shifts in timing and direction of moisture delivery. Changes in the delivery of moisture may affect flooding through the delivery of precipitation that exceeds saturation (e.g., Villarini et al. 2014; Douglas and Fairbank 2011; Mallakpour and Villarini 2015) or by triggering rain-on-snow events in winter months (Guan et al. 2016, Ye et al. 2008). This is important for water resources. For example, precipitation delivered as rain instead of snow in winter months may cause seasonal snowmelt to occur earlier and therefore reduce water availability in summer months (Barnett and Adam 2005; Trenberth et al. 2003; Matonse and Frei 2013). Because regional hydroclimatic regimes are intrinsically tied to life and infrastructure as well as to hazards such as floods, understanding the potential changes in these patterns is important for protecting life and property. While multiple studies examine the role of large-scale meteorological patterns in precipitation in the northeastern US (e.g., Agel et al. 2015, Roller et al. 2016, Teale et al. 2017, Agel et al. 2018, Barlow et al. 2019), none consider moisture transport in the pattern identification or classification procedure.

An additional topic in the study of atmospheric water vapor is that of atmospheric rivers (ARs). ARs are filamentary structures of enhanced water vapor that are considered to account for 90% of meridional moisture transport while covering only 10% of the globe at a given time (Zhu and Newell 1998). ARs have been studied at length along the US west coast and in the Pacific Basin, and increasingly in western Europe and the southeastern US (e.g., Dettinger et al. 2011, Lavers et al. 2015, Mahoney et al 2016, Debbage et al. 2017). Because ARs are responsible for a large magnitude of moisture transport and precipitation, changes in ARs that impact the northeastern US may greatly influence the regional precipitation regime in the presence of precipitation-generating mechanisms. However, at this time there has been no study of ARs on the US east coast at large, or in the northeastern US, so it is not known if ARs influence the regional climatology or if changes in ARs are associated with the observed changes in precipitation. This gap cannot be addressed without first understanding the nature of the water vapor fluxes influencing the region.

At present, a precise characterization of the primary patterns of water vapor transport does not exist for the region. Here we generate a comprehensive climatology of moisture transport for the Northeast, the eastern US, and adjacent Atlantic at large. This kinematics of water vapor transport will provide the atmospheric foundation for understanding the causes behind observed and projected changes in precipitation in the Northeast. This is the first paper in a series of three characterizing the relationship between moisture transport patterns and precipitation in the eastern US. This first paper develops the moisture transport climatology; the second paper explores the relationship and variability therein between these moisture transport patterns and precipitation; the

third investigates long-term variability of the moisture transport climatology and its relationship with heavy precipitation.

The comprehensive climatology of water vapor transport discerned in this study is comprised of both spatial and temporal descriptions of each of the moisture transport pathways for the eastern US and adjacent Atlantic Ocean. By integrating assessments of the magnitude of moisture transport throughout the study region with the shape (i.e., location, width, and direction) of the moisture transport patterns, a general overview of each is provided. The fluxes are further characterized by assessing the temporal aspects of the patterns, as understood through their individual frequency, persistence, and seasonality. Interpretations of each component of these spatial and temporal descriptions alone or in tandem with another component provide unique insight into the characterization of the moisture fluxes; all together, these components form the climatology of moisture transport. A conceptual framework of how each of these transport patterns can be interpreted in isolation and in pairs before being synthesized to understand the comprehensive climatology is illustrated in Figure 2.1.

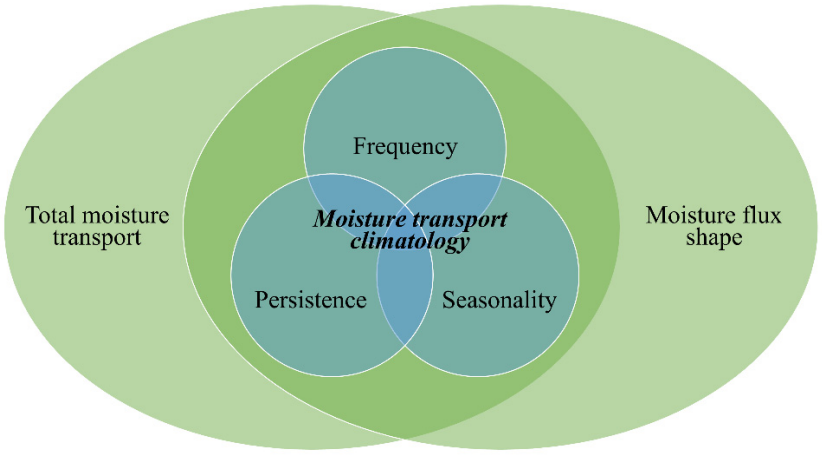

Figure 2.1. Conceptual framework demonstrating the interrelationships between variables comprising the water vapor flux climatology. Outer circles (green) represent spatial descriptions; inner circles (blue) represent temporal characteristics.

2.2. Data & Methods

2.2.1. Water vapor transport patterns

Water vapor transport patterns are discerned using daily integrated water vapor transport (IVT). IVT is a useful variable in identifying and characterizing horizontal water vapor fluxes, as it accounts for both the moisture content as well as the horizontal velocity and direction of the movement. Derived from column-integrated water vapor and zonal and meridional wind and calculated in units of kg m^{-1} s^{-1}, IVT has been used to characterize features of water vapor transport in many regions (Gimeno et al. 2014). In this study, daily IVT is calculated:

$$\text{IVT}=\sqrt{(IVT_v)^2+(IVT_u)^2}$$

Here, IVT_v and IVT_u are daily vertical integrals of northward and eastward water vapor fluxes, respectively, each obtained from the ERA-Interim dataset from the European Centre for Medium-Range Weather Forecasts (ECMWF) data portal (Dee et al. 2011). IVT_v and IVT_u are defined in the ECMWF ERA-Interim documentation (Berrisford et al. 2011) as:

$$IVT_v = \frac{1}{g}\int_0^1 vq\frac{\partial p}{\partial \eta}\partial\eta$$

And,

$$IVT_u = \frac{1}{g}\int_0^1 uq\frac{\partial p}{\partial \eta}\partial\eta$$

In which vq is northward water vapor flux and uq is eastward water vapor flux.

Daily IVT is calculated from 1979–2017, inclusively, at 2.5°× 2.5° horizontal spatial resolution (Dee et al. 2011). This spatial resolution is optimal for this study as the major synoptic-scale flux features are identifiable without the addition of noise from minor or mesoscale variations in the fluxes. The study area is bounded by 30°—50°N and 60°—90°W. This domain approximates other studies investigating large-scale atmospheric patterns related to the hydroclimatology of the eastern and northeastern US, including Agel et al. (2015), Roller et al. (2016), and Agel et al (2018). This time period is selected to make use of the entirety of the ERA-Interim reanalysis dataset, which begins in 1979.

The ERA-Interim dataset from the European Centre for Medium-Range Weather Forecasts (ECMWF; Dee et al. 2011) is widely used for calculating IVT (e.g., Guan and

Waliser 2015; Knippertz and Wernli 2010, Lavers and Villarini 2013; Rutz et al. 2015), and is the optimal choice for hydroclimatological analyses due to its improved representation of moisture and precipitation compared to earlier reanalyses (Lynch et al. 2016).

2.2.2. Self-organizing maps

Classification (or "typing") of climate data is essential to reduce prohibitive dimensionality and complexity in large datasets. Similarly, classification of climate data also facilitates assessment of the variability of distinct events or patterns. In this study, a self-organizing map (SOM) methodology is employed to differentiate the patterns of water vapor transport through the study region. SOMs have become increasingly popular in climate research (e.g., Hewitson and Crane 2002; Crane and Hewitson 2003; Sheridan and Lee 2011; Ford et al. 2014, Cassano et al. 2015), including studies of precipitation and moisture fluxes (e.g., Mattingly et al. 2016; Swales et al. 2016; Cassano et al. 2007). SOMs use an unsupervised, self-learning, neural network procedure to form a matrix of classes where each class is more related to the classes around it than classes at a distance. The SOM classification begins with randomly placed clusters which evolve and shift with the addition of more data, as samples are sorted into the nearest cluster by Euclidean distance (Sheridan and Lee 2011). This learning in the SOM process results in more clusters being located over the densest part of the data cloud and does not force outliers to be assigned to ill-fitting clusters; instead, it is inclusive of transitional phases (Sheridan and Lee 2011). Furthermore, the locations of the resulting patterns are meaningful: as patterns gradually transition across the SOM layout, patterns that are in close proximity share more resemblance than patterns on opposite sides of the SOM. This process is

repeated until no clusters are modified by additional iterations. Therefore, SOMs create a two-dimensional spectrum of patterns that captures both major and transitional conditions. Other automated classification methodologies, including principal component analysis (PCA) and empirical orthogonal function (EOF) analysis, are restricted by their requirements of orthogonal relationships between classes (Yarnal 1993). While these linear methods can draw out major modes of variation efficiently, they can be a limiting factor for geoscientific data that often contain intermediate and transitional modes. Given the complex geography of the Northeast with its numerous internal and external influences (e.g., topography, land-ocean interactions, etc.) as well as the ephemeral nature of IVT, intermediate patterns must be included in the analysis, making the SOM methodology a suitable approach for the classification of regional moisture fluxes.

The number of nodes produced within the SOM is defined by the user, based on the purpose of the classification and the utility of the patterns identified. We tested all combinations of nodes from 2 × 2 to 6 × 6, finding that several of the nodes did not add meaningful information when the SOM size was at the upper limits of the range. Conversely, we found that employing too few nodes did not capture the variability of the atmospheric hydroclimatology of the study region. The most usable number of SOM nodes in this study ultimately was decided based on a subjective assessment of how well the SOM nodes captured the spatial variability of IVT while minimizing the number of nodes that do not contribute useful information. In this way, the SOM nodes represent the full range of major water vapor transport patterns in the region without essentially "overfitting" the climatology.

The SOM was run over daily IVT for all days over the entirety of the study period (14,245 days) and was adjusted over 10,000 iterations. The study area used for the SOM classification was the same as the ERA-Interim reanalysis-derived IVT (30°—50°N and 60°—90°W boundary, 2.5°× 2.5° spatial resolution). A pilot study indicated that a smaller area focused directly over the Northeast did not sufficiently capture the character of the moisture fluxes influencing the area. Mid-level atmospheric pressure composites of 500 mb geopotential height from ECMWF ERA-Interim reanalysis for the same spatial resolution, not included in the SOM development, were plotted over the IVT patterns to indicate steering mechanisms for the moisture fluxes.

2.2.3. Climatology development

The IVT patterns identified in the SOM are analyzed in a variety of ways. These analyses describe the spatial patterns as well as the temporal characteristics of each water vapor transport pattern. These analyses in concert define the regional climatology of moisture transport, as shown in Figure 2.1.

2.2.3.1. Spatial description of water vapor transport patterns

First, the "domain-total" IVT is calculated to compare the magnitude of moisture transport by each pattern by summing the IVT value for all the individual grid cells in each of the sixteen nodes. This process then allows each node to be ranked by the amount of water vapor transported over the entire study region, enabling comparisons of the magnitude of moisture transport by each pattern. This process is useful, as moderate water vapor transport patterns can appear unimportant next to extreme patterns but in fact may transport considerable moisture over a broad area.

To quantify the concentration of water vapor transport of each node, the Gini coefficient is next determined for each node. The Gini coefficient, also known as the index of dissimilarity, represents how evenly a variable is distributed across an area or population. This metric has been used in climate literature, such as examining the distribution of climate change impacts (Tol et al. 2004) and assessing the distribution of monsoonal precipitation (Bombardi et al. 2020). The Gini coefficient is commonly used in economic geography to represent the spatial distribution of wealth across an area (Barber 1988). We employ the Gini coefficient here to represent the degree to which the water vapor is either concentrated or evenly distributed over the study area (i.e., transport through a narrow pathway or in a broad swath), providing an index for the moisture plume width. One a scale of 0–1, high Gini coefficients indicate a high degree of inequality (i.e., high moisture transport confined to a narrow pathway) while low Gini coefficients indicate more homogenous distribution of moisture transport across the study area. This multi-step calculation is carried out using the Lengwiler (2020) MATLAB function.

Most of the definitions of ARs used in practice account for enhanced water vapor content coupled with a transport component, frequently employing IVT to detect ARs. Following with atmospheric rivers literature closest to this study region, the 85th percentile of IVT is calculated for the study region as the threshold above which moisture transport is considered an AR (Mahoney et al. 2016). The 85th percentile of IVT was calculated from daily IVT values for the entirety of the study area. Due to the high background water vapor content of the region, the 95th percentile of IVT is also calculated. Locations within the transport patterns where these thresholds are exceeded

are displayed to determine if and where each of the SOM-determined water vapor transport patterns fit this commonly used definition of an AR.

2.2.3.2. Water vapor content

Because IVT combines water vapor content with velocity, it is possible that combinations of slow-moving yet water vapor-rich patterns and fast-moving yet relatively dry patterns produce the same IVT value despite substantial mechanical differences.

Water vapor content for each of the patterns is analyzed using the vertically integrated water vapor from ERA-Interim at 2.5×2.5° resolution for the same study area. Vertically integrated water vapor content for the study area is aggregated for each instance of each water vapor pattern. Hartigan's dip test, also known as the Dip Test of Unimodality (Hartigan and Hartigan 1985) is used to determine if multiple discernable wet and dry sub-patterns of water vapor are included in each SOM-identified IVT node. This nonparametric statistical test requires no prior knowledge of the distribution and has been used to detect multimodality distributions of water vapor in the climate literature (e.g., Louf et al. 2015; Zhang et al. 2003). When used in conjunction with histograms, we find that this test is useful in characterizing the bimodality of distribution in water vapor distributions. Mean sea level pressure from ERA-Interim at 0.75×0.75° resolution for the study area is employed to further assess the potential for discernable sub-patterns of water vapor in the IVT nodes.

2.2.3.3.Temporal characteristics of water vapor transport patterns

The SOM node into which each daily IVT pattern is sorted is catalogued for temporal analyses. The number of days sorted into each SOM node is assessed to indicate

which patterns dominate the climatology, and which patterns are relatively rare. The temporal persistence of each node is also assessed to determine how many days the water vapor transport patterns potentially impact a region consecutively. The persistence of each node is particularly important in interpreting its impacts. In addition to overall frequency, the number of times each node occurred during each calendar month is tabulated over the study period. This enables investigation into the seasonality of each node.

To determine if months of unusually high or low numbers of each transport pattern occurred during the study period, monthly departures are assessed. For this analysis, overall mean node occurrence is calculated for each month and each node for the study period, 1979–2017. Then, departures are measured as a percent of normal on a monthly basis.

2.3. Results

2.3.1. Spatial descriptions of water vapor transport patterns

Water vapor transport patterns in the northeast US are best represented by sixteen nodes in a self-organizing map (Figure 2.2). This number allows variety among the patterns to be discerned without duplication. IVT values below 150 $kg^{-1}s^{-1}$ are omitted from Figure 2.2 for visual clarity, though these values were included in the development of the SOM nodes. 500 mb wind vector composites and 500 mb geopotential height contours (not ingested by the SOM procedure) indicate how the fluxes are steered as well as to provide climatological context for the flux patterns. Characteristics of the IVT features defining each node, such as axis, location, and intensity, transition gradually

across the 4 × 4 SOM layout. This indicates that both major and transitional moisture transport patterns are represented through this methodology.

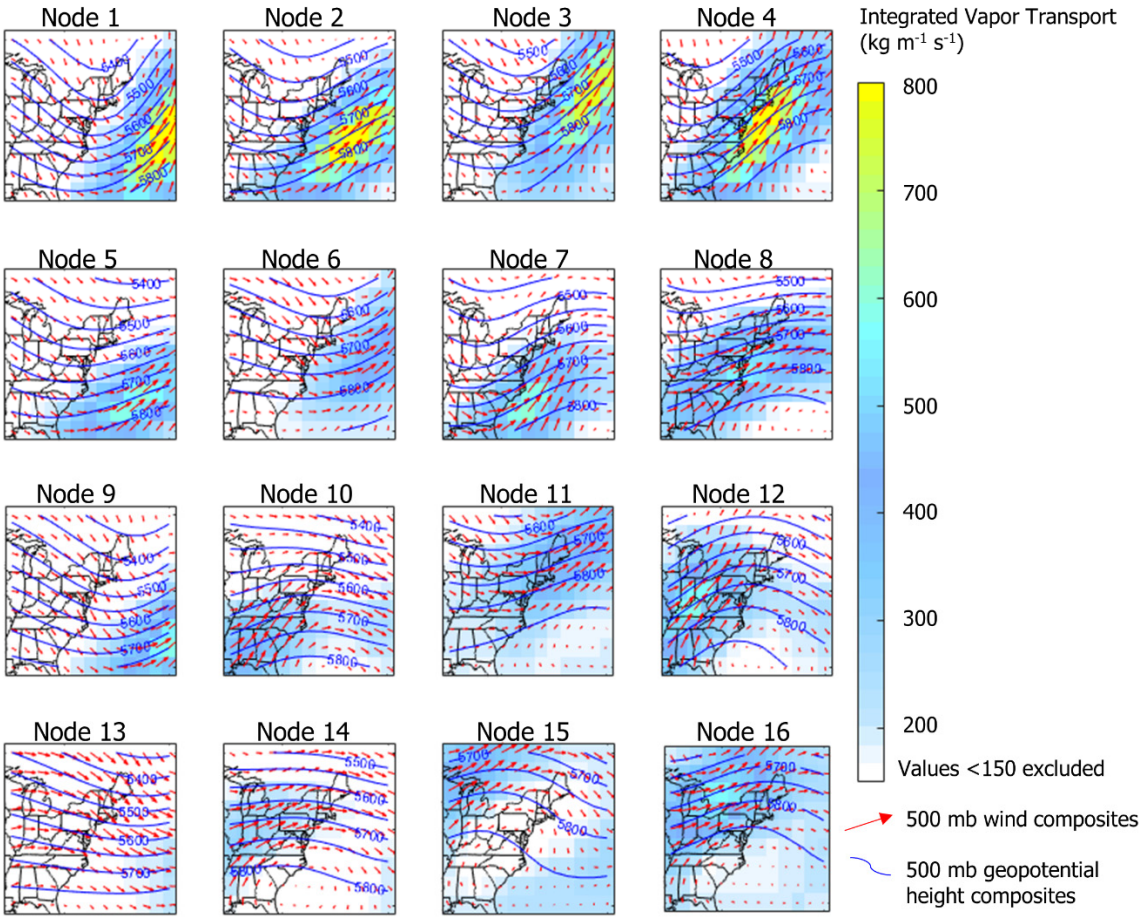

Figure 2.2. SOM-derived node central IVT patterns in kg m^{-1} s^{-1}. Composites of 500 mb wind vectors and 500 mb geopotential height isobars are plotted for context. IVT values below 150 kg m^{-1} s^{-1} are not shown.

Substantial variety in the magnitude and location of moisture fluxes exists in this classification, with the magnitude, direction, and placement of moisture fluxes unique to each pattern. Nodes 1-4 contain the highest maximum IVT values. However, the location of the IVT maxima is different in each of these nodes. Node 1 shows moisture transport offshore with very low moisture transport through the eastern US. The band of enhanced

moisture in this node shows a strong southwesterly component on the lee side of a trough over the East Coast. Node 2 shows a band of moisture transport maxima offshore as well but shows slightly increased transport in the Carolinas and southeastern US. The axis of moisture transport in Node 2 is more westerly than that of Node 1. The area of maximum IVT is positioned to the north in Node 3, with some increased IVT impacting Maine. However, as with Nodes 1 and 2, most of the enhanced moisture transport in Node 3 takes place offshore. Node 4 shows the highest IVT band impacting the US eastern coastline. The IVT maxima stretches along the coastline from North Carolina through Massachusetts, with high IVT surrounding the maximum channel. Nodes 1-4 each have relatively high Gini coefficients, between 0.33 and 0.42, indicating that the moisture transport is concentrated within narrow pathways in these patterns (Figure 2.3).

In contrast to the high moisture plumes in Nodes 1–4, other nodes show more homogenous and lower IVT values. For example, Node 13 contains very low IVT values for most of the study area (Figure 2.2). Nodes 12, 14 and 15 show IVT pathways along the Ohio River Valley and the Midwest. Node 12 shows strong moisture transport through the Ohio River Valley west of the Appalachian Mountains, with the greatest IVT over Kentucky, Indiana, and Ohio, and strong winds continuing northward through southern Canada where they diverge. While representing relatively low magnitudes of IVT, Node 14 shows strong southwesterly flow in the Midwest as part of strong anticyclonic circulation centered off the coast of Georgia, as suggested in the 500 mb wind vectors. Node 10 also shows anticyclonic circulation off the coast of Georgia but with enhanced southwesterly moisture transport throughout the southeastern states. Node 8 shows moderate IVT values through much of the eastern US, but the moisture transport

is not as strongly confined to a narrow pathway as is seen in other nodes. Instead, Node 8 shows a broad, southwesterly flow of moisture transport from the Gulf of Mexico area turning offshore in the Mid-Atlantic. The relatively low Gini coefficients of these nodes (Nodes 8, 10, 12–15) indicate that the moisture present in these patterns is somewhat equally distributed across the study region or in a broad swath as opposed to being confined in a narrow plume (Figure 2.3).

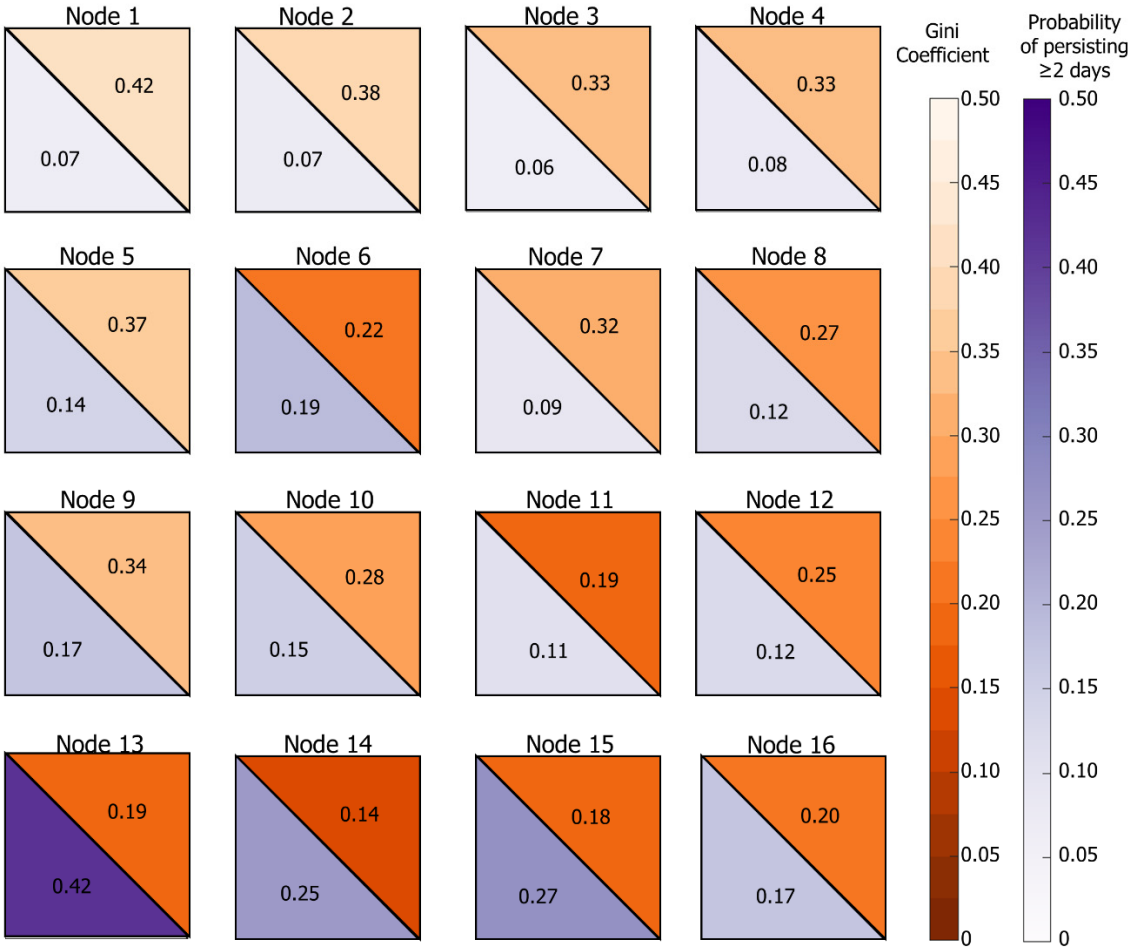

Figure 2.3. The Gini Coefficient of Dissimilarity for each node (upper right triangle; orange) shown alongside the probability of each node persisting for two or more days (lower left triangle; purple).

Summing the IVT values across each node pattern or calculating the domain-total IVT for each node (Figure 2.4) reveals that Node 4 contains the highest overall IVT. Nodes 2 and 16 represent patterns with the second and third highest amounts of water vapor transport overall, though in starkly different ways: Node 2 shows confined transport of water vapor, with very high IVT magnitudes extending over a narrow band (Gini coefficient = 0.38, Figure 2.3) offshore, while Node 16 shows widespread water vapor transport throughout the study area (Gini coefficient = 0.20, Figure 2.3) with the exception of a dry center of anticyclonic motion centered over North Carolina (Figure 2.2). Generally, the nodes depicting the greatest overall IVT patterns are distributed along the top and right edges of the SOM. Four of the nodes with the greatest overall IVT are located along the right column of the SOM, with Nodes 4, 8, 12, and 16 among the six nodes with greatest overall IVT (Figure 2.4) but having decreasing confinement of moisture transport (i.e., decreasing Gini coefficient) downward from the top right corner of the SOM (Figure 2.3). The other two nodes with relatively greatest overall IVT are Nodes 2 and 3, both of which show a confined pathway of southwesterly water vapor transport

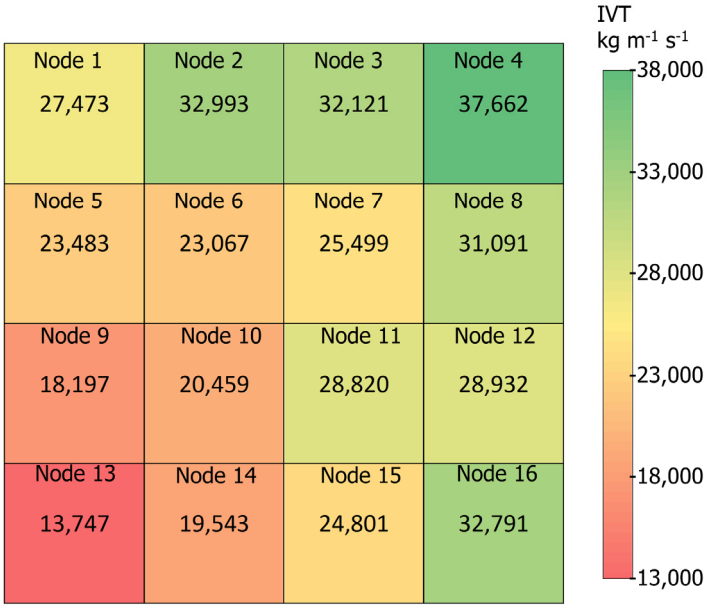

Figure 2.4. Domain-total IVT of each SOM node pattern, in kg m^{-1} s^{-1}.

offshore and relatively high Gini coefficients. Node 1 shows a similarly well-structured pathway of water vapor transport with the highest Gini coefficient of all the nodes (Gini coefficient = 0.42), but the far southeast position of the IVT maxima band and very low IVT values outside of that pathway cause that node to be ranked 8 of 16 in terms of total IVT in the study region. The four nodes comprising the bottom-left of the SOM (Nodes 13, 9, 14, and 10) contain the patterns with the least overall moisture flow, in the order listed. In general, the bottom left diagonal of the SOM layout contains patterns with less overall IVT, while the top right diagonal houses patterns with greater IVT. This distribution suggests that the SOM was successful in adjusting the node patterns to best capture the range in water vapor fluxes of the study area in a two-dimensional spectrum of patterns.

The AR threshold, or 85th percentile of IVT calculated from daily data 1979–2017 for the study region, is 354.2 kg m^{-1} s^{-1}. This threshold was exceeded in 14 of the 16 SOM-derived water vapor transport patterns (Figure 2.5). Several of these potential AR bands exist over the Atlantic Ocean and have little bearing on the land mass of the study region, such as Nodes 1–3, 5, 6, and 9. However, Nodes 4, 7, 8, 10–12, 15 and 16 contain AR patterns directly impacting the continent. The trajectories of the Node 4 and Node 7 pathways of enhanced moisture transport parallel to the Atlantic Coast suggest that the Atlantic Ocean may be a primary source of moisture for these water vapor fluxes. In contrast, the Node 16 band of enhanced moisture transport is proximal and downwind of the Great Lakes. The southwesterly flow of the moisture pathways in Nodes 8 and 10, indicate that these bands of enhanced moisture transport originate in the Gulf of Mexico and southeastern US. Node 12 shows a pathway of enhanced moisture transport through

the Ohio River Valley with an orientation comparable to the Great Plains low-level jet. This variety in origin, potential moisture source, and directionality of these bands of enhanced moisture transport indicate that AR conditions in the eastern US may be a function of a multitude of climatological factors.

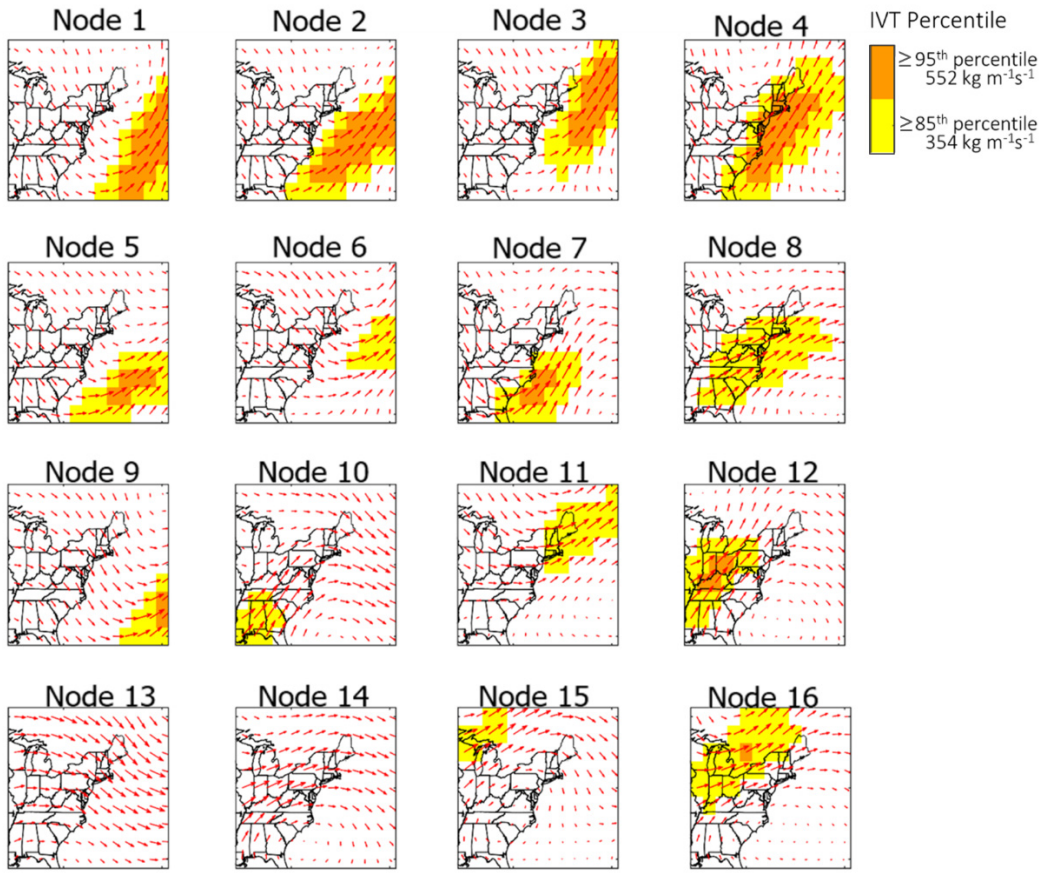

Figure 2.5. The 85th percentile of overall IVT (yellow) and 95th percentile of overall IVT (orange) shown in the SOM nodes. Percentiles calculated using daily IVT data 1979–2017. Wind vectors at the 500 mb level are plotted for reference.

2.3.2. Temporal characterization of moisture transport patterns

The number of days assigned to each node are shown in Figure 2.6. The variability in node frequency is distributed throughout the SOM node layout, with the most frequent nodes generally in the bottom left corner of the SOM node layout and the least frequent nodes extending along the top and right edges of the node layout. The smooth transitions between adjacent node frequencies suggests that each node pattern is adjusted successfully during the SOM development to smoothly incorporate all of the daily fluxes impacting the region. The most common water vapor transport pattern is that of Node 13, occurring 2467 times from 1979–2017, an equivalent of more than 6.5 years. This pattern contains the lowest overall IVT values (Figure 2.4); however, because of its high frequency, this pattern overall accounts for the most water vapor transport through the region over the 39-year study period. Wind vectors at the 500 mb level indicate westerly to northwesterly atmospheric flow over much of the study area, suggesting low moisture content. The least frequent water vapor transport pattern is Node 4, occurring only 317 times in the 39-year study period.

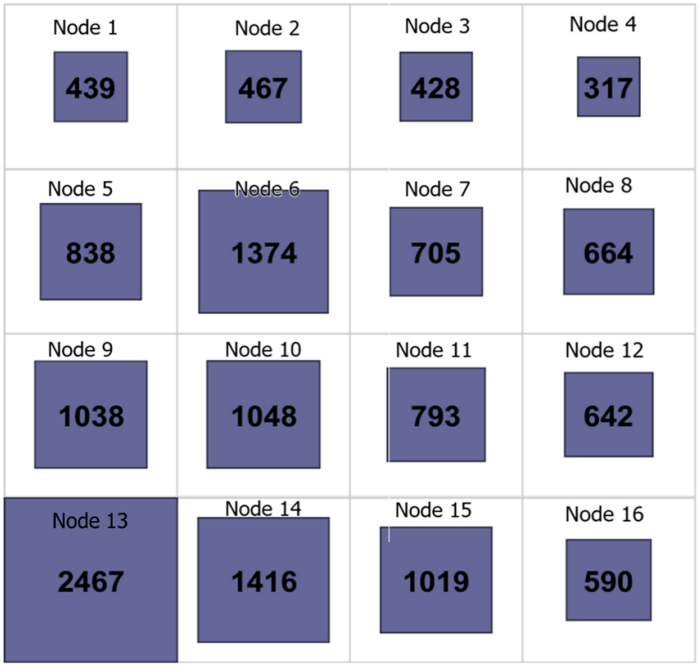

Figure 2.6. Node counts showing the number of days each occurred during the 1979–2017 study period.

Node 4 shows strong moisture transport directly over the US East Coast, therefore suggesting the greatest potential for extreme precipitation. Because of its high moisture transport, this pattern is likely disproportionately impactful in the regional hydroclimatology and meridional moisture transport relative to its frequency.

A seasonal climatology of the water vapor transport patterns for the eastern US is discerned in Figure 2.7. The seasonality of these nodes illustrates the seasonal and intraseasonal procession of water vapor fluxes over the eastern US, including seasonally shifting magnitudes, sources, and trajectories. Winter months are dominated by the Node 13 water vapor transport pattern, with Node 13 being the most frequently occurring pattern from October through April. This is unsurprising, given that Node 13 is by far the most frequently occurring pattern, and most days with little moisture transport to classify

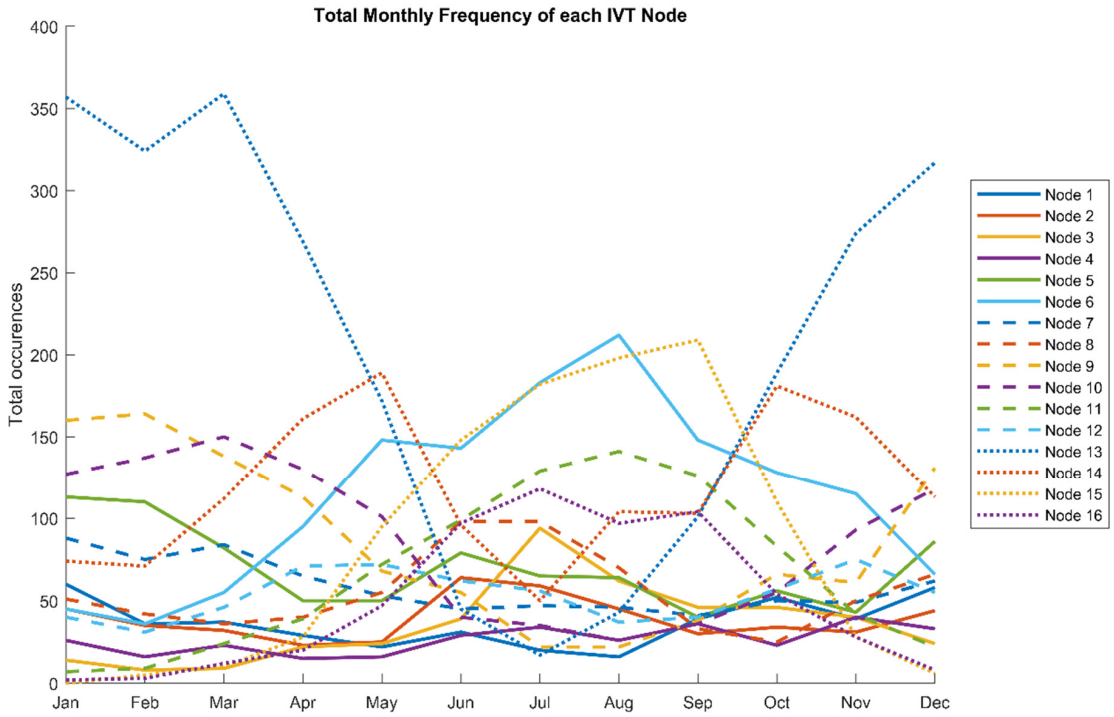

Figure 2.7. Node seasonality as shown through monthly frequencies, 1979–2017.

are sorted into this node. The absence of strong water vapor fluxes in the winter months, resulting in the prevalence of the low-IVT pattern of Node 13 during those months, reflects the relatively dry atmosphere in the cool seasons in the eastern US compared to the warm seasons. The appearance of marked atmospheric moisture transport in the warmer atmosphere of the warm seasons results in a decreased frequency of low-IVT patterns, such as Node 13, in the summer months. Other than Node 13, Node 9 is the most common water vapor transport pattern for December through February, with northwesterly flow over much of the study area and minor water vapor transport over the Atlantic Ocean far from the coastline. The third most frequent winter pattern is Node 10, with strong water vapor transport in the southeastern US and strong 500 mb winds extending through the study region parallel to the coastline and IVT curling offshore near the Carolinas. Patterns showing strong advection of moisture in the Northeast are relatively infrequent in the winter months. At this scale, local-scale systems such as atmospheric moisture conditions for lake-effect snow are not visible. Summer months of June through September are dominated by Nodes 6 and 15 moisture transport patterns. These nodes are starkly different from each other, with Node 6 showing a trough centered over northeast New England and enhanced moisture transport off the East Coast, and Node 15 showing anticyclonic motion over Appalachia blocking moisture transport over much of the Eastern Seaboard (Figure 2.2).

Other patterns peak in frequency in the transitional seasons. Node 14, showing strong moisture transport along the Ohio River Valley as part of an anticyclonic circulation centered off the Georgia coast, is the most frequent transport pattern in May (Figure 2.7). While the Node 13 pattern (i.e., pattern with very little advection of

moisture) is the most frequent pattern occurring in October, Node 14 is also very common in October. This suggests that that Node 14, with a band of moisture transport through the central US, is a dominant pattern in transitional seasons and is demonstrative of moisture variability from changing synoptic pressure systems.

The monthly departures from the average frequency for each moisture transport pattern for the 1979–2017 study period are shown in Figure 2.8. This figure shows that there are months of higher-than-usual and lower-than-usual frequencies of each node pattern. This figure shows increasing frequencies of the Node 4 pattern—enhanced moisture transport confined in an atmospheric channel over the East Coast—beginning

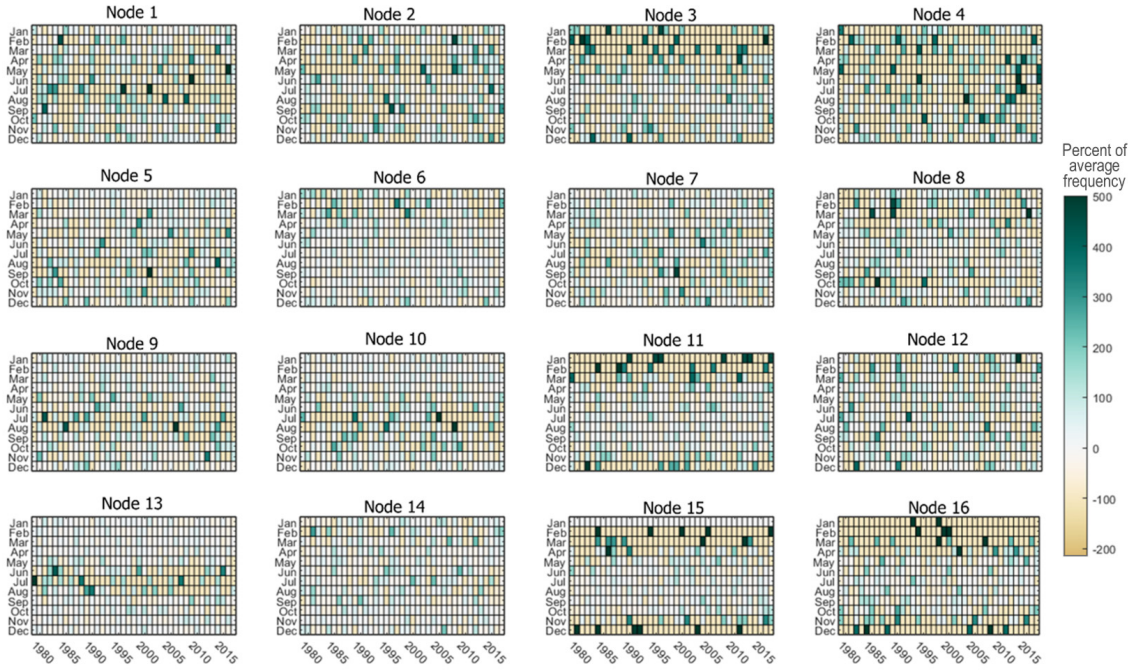

Figure 2.8. Percent of average monthly frequency for each month, 1979–2017. Average node frequency was calculated for each month in the 39-year study period. Departure from the monthly average is indicated by color in each grid cell. For each month, brown colors indicate fewer node occurrences than average; teal colors show more node occurrences than average. For each subfigure, each of the 39 years of the study are shown along the horizontal axis; months of the year are shown along the vertical axis.

around 2010, particularly in the warm season. Months of anomalously high frequencies of the zonal and dry Node 13 decrease in the last 25 years of the time period, particularly in the summer months (Figure 2.8). This shift reflects the increasing frequency of moisture-rich water vapor fluxes in the warm season at the expense of low-IVT pattern days. Additionally, occurrences of Node 16 shifted from early winter (October–December) to late winter (January–March) in the 1990s and early 2000s. Because the Node 16 pattern is distinguished by moisture transport over the Great Lakes, this seasonal shift may be related to variability in the freezing date of the Great Lakes as a moisture source. This variability in the number of Node 16 days in the winter months is likely driven by a small number of days relative to its annual frequency, as this pattern is considerably more common in summer months.

The probability of each node persisting for two or more days is inversely related to the Gini coefficient (Figure 2.3). In other words, the more confined the moisture transport is in a pattern, the less likely it is that the pattern will persist over the region for multiple days. The probability of Node 13, the driest and least-confined moisture pattern, persisting in the study region for two or more days is 42%, making this the longest-persisting pattern. This low-IVT zonal to northwesterly flow pattern persisted up to seven days during the study period. In contrast, the patterns with some of the most confined moisture pathways and therefore highest Gini coefficients, Nodes 1–4, each occurred more than 92% of the time in isolation. While a variety of weather patterns with similar low-IVT characteristics are likely represented in the less-defined nodes, the inverse relationship between moisture confinement and persistence demonstrates how the well-

structured moisture patterns evolve quickly from one to another as the plume migrates over the region.

2.3.3. Water Vapor Content

Hartigan's dip test is employed to determine if the IVT patterns included multiple distinguishable patterns of water vapor content. Five of the sixteen nodes (Nodes 2–4, 6, and 8) are found to reject the null hypothesis of a unimodal distribution of water vapor (Figure 2.9). Histograms of spatially summed water vapor content reveal that these IVT patterns each contain two distinct distributions of water vapor content: a "wet" version and a "dry" version (Figure 2.9). Composites of the vertically integrated water vapor content for each of these wet and dry sub-patterns show that while there is a marked difference in the total amount of water vapor present, the location and directionality of the water vapor distribution is the same (not shown).

The seasonality of each of these wet and dry bimodal sub-patterns shows the wet pattern prevailing in summer months and the dry pattern being more frequent in the winter months (not shown). An assessment of mean sea level pressure indicates different strengths of the same pressure patterns involved in the wet and dry sub-patterns; namely, strong pressure gradients existing during the dry sub-patterns, and weaker pressure gradients present during the wet sub-patterns. A timeseries of the annual frequencies of the wet and dry sub-patterns does not indicate any temporal trends in the sub-patterns at the annual scale for the 39 years of this study.

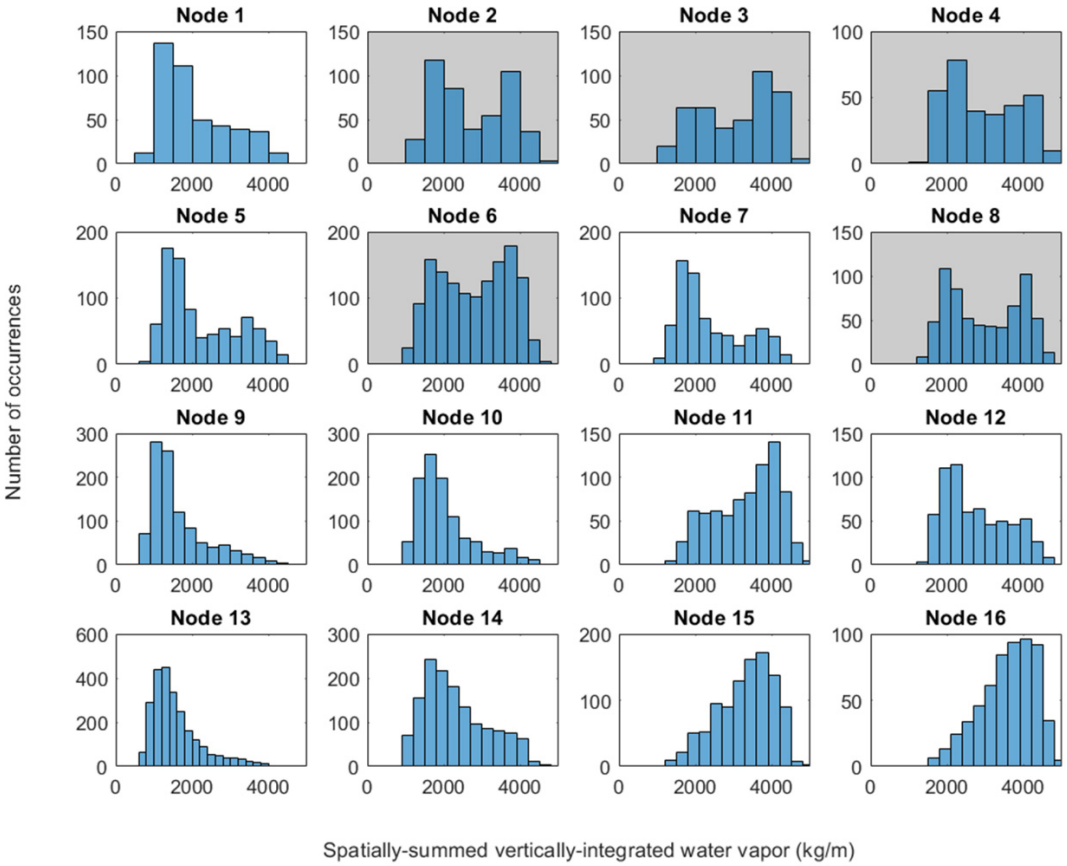

Figure 2.9. Histograms of vertically integrated water vapor content for each of the moisture fluxes. Nodes which reject the null hypothesis of unimodality of the Hartigan's dip test are shown with darkened backgrounds.

2.4. Discussion & Conclusion

The climatology of moisture transport discerned in this study show that water vapor moves through the eastern US via distinct pathways or patterns, each with a specific spatial distribution and directionality of moisture transport. Each of these patterns comprising the climatology has its own seasonality, frequency, and persistence probability. These spatial and temporal characteristics together define a water vapor transport climatology for the eastern US, as shown in Figure 2.1. While almost all IVT

patterns show a strong southwesterly flow in the eastern US, variations in the axis, magnitude, confinement, and location of the maxima are noted among the sixteen water vapor transport patterns identified by the SOM (Figure 2.2). The spatial characteristics of these moisture transport patterns with their unique behaviors define the climatology of water vapor transport through the eastern and northeastern US.

The differences in node frequency (Figure 2.6) allow each moisture transport pattern to be contextualized within the broader regional hydroclimatology. Specifically, this approach allows less-frequent but high-magnitude water vapor transport patterns to be identified and related to potential impacts on the regional hydroclimatology. The isolation of these influential water vapor transport patterns has applications in extreme precipitation studies. In particular, Node 4 shows extremely high IVT across the study region, particularly along the coastline and over the continent. This moisture transport pattern is likely linked to extreme precipitation in the Northeast in the presence of triggering mechanisms and therefore may have a disproportionate impact on the regional hydroclimatology relative to its frequency. The extent to which this flux, as well as the other fluxes, contributes to the precipitation regime of the region is explored in Chapter 3. This approach will reveal if the observed changes in precipitation outlined in previous studies are related to changes in moisture flux behavior. Similarly, because of the large magnitude of IVT in the narrow pathway of the Node 4 moisture pattern, changes in frequency of this pattern likely have disproportionate effects on meridional moisture transport. The frequency of these fluxes is currently being examined on longer timescales in an extension of this research.

The water vapor transport patterns Nodes 1–4 each are responsible for the least amount of water vapor transport overall through the study region from 1979–2017 despite their high values of IVT, due to their limited frequency. Node 13, despite exhibiting low IVT, is responsible for the most transport of water vapor through the study region due to its high frequency. Nodes 6 and 14 represent, respectively, the second and third most water vapor transport through the study region. This estimation of domain-total IVT multiplied by frequency should only be considered in a general sense, as it assumes that all days of a node pattern have IVT patterns that are identical to that node pattern. In reality, while the SOM sorts the daily IVT patterns into the most-similar node, the daily IVT patterns in each node will have some variation in magnitude and location. However, this assessment demonstrates the dual importance of infrequent yet extreme water vapor fluxes alongside common yet moderate water vapor fluxes in the regional water vapor transport climatology.

The persistence of each moisture transport pattern, or the probability of the pattern existing for consecutive days, is unique for each node (Figure 2.3). The persistence of each node has important implications for impacts, particularly if a mechanism triggering precipitation is present. The confined, moisture-rich transport patterns may have considerable hydroclimatological impacts as extreme single-day precipitation events. They may produce severe local and regional impacts such as flooding before the atmospheric moisture source progresses into a different node pattern. Similarly, multi-day precipitation events may trigger widespread impacts, as flooding may occur if soils exceed saturation over multiple days with consistent moderate precipitation. This consideration is particularly demonstrable when recognizing that the

IVT variable contains both moisture and horizontal transport components, so relatively low IVT values may indicate a moist weather system moving slowly or stalled across the region. Therefore, the moisture fluxes with lower, more widespread values of IVT with higher probability of persisting over a region for multiple days may also be of concern for flood impacts. Further analysis discerning the precipitation impacts produced by each of these water vapor fluxes is being undertaken as a next step of this Northeast research endeavor.

The increase in the occurrences of the Node 4 water vapor transport pattern in the last decade of the study likely has bearing on the increases in extreme precipitation observed in the study region (Walsh et al. 2014). The advection of an intense water vapor plume along the East Coast is likely associated with precipitation in the area if a precipitation-generating mechanism is present. The seasonal timing of the increasing frequency of this pattern in summer months may be compounded by warm-season meteorological systems not visible in the scale of this study, including convective systems which may provide the vertical lifting required to produce extreme precipitation. The combination of positive and negative anomalies of monthly moisture flux pattern frequency found in this study is generally in line with Kunkel et al. (2013), who reported overall increasing trends in precipitation since 1970 but no statistically significant trends in spring, summer, or winter seasons. Similarly, the positive monthly frequency anomalies of high-IVT Node 4 in the summer months with the negative monthly frequency anomalies of low-IVT Node 13 in summer months in the later part of the timeseries aligns with the temporal changes in precipitation patterns observed by Ahn and Steinschneider (2019). The observed variability in pattern frequency over this 39-year

study period warrants investigation of these fluxes over the past century to determine if these changes are related to hydroclimatic variability on sub-decadal or multi-decadal timescales. The current study utilizes the entirety of the ERA-Interim record to develop this baseline moisture transport climatology; work on the extended timescale of these moisture fluxes is undertaken in the next phase of this research through the incorporation of reanalyses with longer records.

Strong IVT or AR patterns occur regularly throughout the year. With 14 of the 16 moisture transport patterns meeting the IVT threshold of ARs, the identification of ARs by this method suggests that AR activity may have existed in the study region on nearly 73% of days from 1979–2017. Even while considering only the AR-magnitude IVT patterns impacting widespread land areas (Nodes 4, 8, 12, and 16), the number of times these patterns occur amounts to nearly 6 years of AR activity in the study region. The frequency of moisture transport patterns exceeding the AR-threshold in the southeastern US generally follows the seasonality of ARs outlined in Mahoney et al. (2016), with reduced frequency in AR patterns in summer months coupled with relatively frequent occurrences in the cool and shoulder seasons. The strong IVT patterns showing the longest trajectories of enhanced moisture transport, Nodes 1–4, show little seasonality, other than a slight preference for Node 3 to occur in the summer months. This warm season tendency for Node 3 is likely related to the need for a warm, moist atmosphere for this farthest-poleward moisture flux to develop fully. The other water vapor transport pattern comparably poleward as Node 3 is Node 16; however, Node 16 forms in the lee of a trough over the Great Lakes. This directionality signals the potential importance of the Great Lakes as atmospheric moisture sources, especially as this moisture transport

pathways occurs relatively frequently in the warm months and rarely in the winter months when evaporation is inhibited by cold temperatures and ice cover. Several other water vapor patterns exceeding the AR-threshold indicate trajectories similar to the Great Plains low level jet, with high pressure located on the eastern side of the study region steering enhanced moisture transport poleward from the Gulf of Mexico through the Ohio River Valley. The wide variety in mechanisms and pressure patterns associated with the multiple different transport patterns meeting the AR definition in the eastern US demonstrates the limitations of a threshold-based AR definition in a region where the hydroclimatology comprised of a myriad of atmospheric conditions, especially when considering the full annual climatology as a whole.

The wet and dry sub-patterns in Nodes 2, 3, 4, 6, and 8 reflect the general atmospheric moisture content in the presence of the pressure patterns steering the moisture transport. The wet sub-patterns dominate during the summer months when the atmospheric moisture content is generally greater. The dry sub-patterns dominate during the winter months when the cooler atmosphere does not contain as much water vapor. Nayak and Villarini (2016) report that similar flux patterns could be produced by different mechanisms; they demonstrate that the Great Plains low-level jet and extratropical cyclones produce the same moisture flux signature in the central US, despite differing mechanisms. An assessment of the mean sea level pressure patterns associated with the wet and dry sub-patterns reveal that the same pressure patterns appear in both the wet and dry sub-pattern days, but with varying strength. The sea level pressure composites for the dry sub-patterns all show stronger and more pronounced pressure gradients than the sea level pressure composites for the wet sub-patterns. The stronger

pressure gradients suggest that transport velocity is greater during the dry sub-pattern days and is reduced during the wet sub-pattern days. This demonstrates how fast-moving but dry moisture fluxes and slow-moving but moisture-rich fluxes produce the same IVT signature. The next phase of this project, relating these moisture fluxes to precipitation, will reveal if or how these sub-patterns impact the precipitation regime differently.

This research develops a climatology of water vapor fluxes which did not previously exist for the eastern US. By examining the IVT variable in multiple ways, we are able to identify the major water vapor fluxes influencing the region and outline the spatial and temporal characteristics of each, as framed in Figure 2.1. In doing so, we have shown:

- A self-organizing map methodology performed with IVT discerns regional moisture fluxes with sufficient detail to capture transition patterns and seasonal changes.
- The summer and shoulder months show a diversity of pathways in which water vapor is transported through the eastern US. The winter months are dominated by a moisture flux pattern with very little moisture transport in the eastern US (Node 13), though multiple other pathways are still shown to transport water vapor during the cold season.
- The moisture patterns containing the highest amounts of moisture transport occur less frequently than the patterns with less moisture transport. Because the patterns showing less moisture transport are most prevalent, they are major contributors to the manner in which water vapor is moved through the eastern US. In Chapter 3, the contribution of each of these fluxes to annual precipitation is investigated.

- Moisture flux confinement is generally inversely related to persistence, suggesting that strong, narrow bands of enhanced moisture transport move through the region on daily timescales and generally do not stall over a narrow region for multiple days. Subsequent chapters reveal the hydrological contributions of strong but ephemeral patterns compared to mild to moderate but persistent patterns.
- There is temporal variability in the monthly frequencies of several of the fluxes in the 39-year study period. Future work will apply longer timescales of daily IVT to these moisture flux patterns to investigate if the variability indicated by these monthly anomalies is related to large-scale climate modes on the sub-decadal to multidecadal time periods.
- Several of the nodes are dually comprised of slow-moving but moisture-rich sub-patterns and fast-moving but dry patterns. While the mechanisms for these sub-patterns appear to be the same, future work will reveal if these sub-patterns contribute to the regional precipitation regime differently.
- Many moisture transport pathways meet the threshold-based definition of ARs, despite the diversity in trajectories, locations, associated moisture sources suggesting a variety of mechanisms developing the AR conditions. The high frequency with which the threshold-based definition of ARs is met in this study region indicates that this definition needs improvement for regions with a myriad of climate controls, such as that of the Northeast.

Overall, this study of water vapor fluxes influencing the northeastern US sets the stage for an investigation of how changing water vapor fluxes may relate to changes in the regional precipitation regime. This includes an in-depth analysis relating these water

vapor patterns to precipitation to quantify the contribution of each to the annual regional precipitation. Additionally, time series analyses of these fluxes are being conducted to determine if and, if so, how these transport patterns have changed over the past century. Future work should examine possible changes in the seasonality and phase of precipitation produced by each of the pattern, as well as relationships between the North Atlantic Oscillation, the Pacific North American pattern, and other large-scale climate modes and the water vapor transport climatology of the northeastern US. Future work should also further investigate how seasonal or long-term variability in the velocity and moisture content separately affect moisture transport in this and other midlatitude domains. We recommend that this be explored in both reanalysis products as well as climate model projections.

2.5. References

Agel, L., M. Barlow, J. H. Qian, F. Colby, E. Douglas, and T. Eichler, 2015: Climatology of daily precipitation and extreme precipitation events in the Northeast United States. *J. Hydrometeorol.*, **16**, 2537–2557, https://doi.org/10.1175/JHM-D-14-0147.1.

——, ——, S. B. Feldstein, and W. J. Gutowski, 2018: Identification of large-scale meteorological patterns associated with extreme precipitation in the US northeast. *Clim. Dyn.*, **50**, 1819–1839, https://doi.org/10.1007/s00382-017-3724-8.

Ahn, K., and S. Steinschneider, 2019: Seasonal Predictability and Change of Large-Scale Summer Precipitation Patterns over the Northeast United States. *J. Hydrometeor*, **20**, 1275–92, https://doi.org/10.1175/jhm-d-18-0252.1.

Barber, G.M., 1988. Elementary Statistics for Geographers. The Guilford Press, New York.

Barlow, M., and Coauthors, 2019: North American extreme precipitation events and related large-scale meteorological patterns: a review of statistical methods, dynamics, modeling, and trends. *Clim. Dyn.*, **53**, 6835–6875 pp., https://doi.org/10.1007/s00382-019-04958-z.

Berrisford, P., D. Dee, P. Poli, R. Brugge, K. Fielding, M. Fuentes, P. Kallberg, S. Kobayashi, S., Uppala, and A. Simmons, 2011: *The ERA-Interim archive, version 2.0.* ERA report series. 1. Technical Report. ECMWF pp23.

Barnett, T. P., and J. C. Adam, 2005: Potential impacts of a warming climate on water availability in snow-dominated regions. *Nature*, **438**, 303–309, http://dx.doi.org/10.1038/nature04141.

Bombardi, R. J., V. Moron, and J. S. Goodnight, 2020: Detection, variability, and predictability of monsoon onset and withdrawal dates: A review. *Int. J. Climatol*., **40**, 641–667, https://doi.org/10.1002/joc.6264.

Cassano, J. J., P. Uotila, A. H. Lynch, and E. N. Cassano, 2007: Predicted changes in synoptic forcing of net precipitation in large Arctic river basins during the 21st century. *J. Geophys. Res. Biogeosciences*, **112**, https://doi.org/10.1029/2006JG000332.

Cassano, E. N., J. M. Glisan, J.J. Cassano, W. J. Gutowski Jr., M.W. Seefeldt, 2015: Self-organizing map analysis of widespread temperature extremes in Alaska and Canada. *Clim. Res.,* **62**,199-218, https://doi.org/10.3354/cr01274.

Crane, R. G., and B. C. Hewitson, 2003: Clustering and upscaling of station precipitation records to regional patterns using self-organizing maps (SOMs). *Clim. Res.*, **25**, 95–107, https://doi.org/10.3354/cr025095.

Debbage, N., P. Miller, S. Poore, K. Morano, T. Mote, and J. Marshall Shepherd, 2017: A climatology of atmospheric river interactions with the southeastern United States coastline. *Int. J. Climatol.*, **37**, 4077–4091, https://doi.org/10.1002/joc.5000.

Dee, D., and Coauthors, 2011: The ERA - Interim reanalysis: Configuration and performance of the data assimilation system. *Quaterly J. R. Meteorol. Soc.*, **137**, 553–597, https://doi.org/10.1002/qj.828.

Dettinger, M. D., F. M. Ralph, T. Das, P. J. Neiman, and D. R. Cayan, 2011: Atmospheric Rivers, Floods and the Water Resources of California. *Water*, **3**, 445–478, https://doi.org/10.3390/w3020445.

Douglas, E. M., and C. A. Fairbank, 2011: Is Precipitation in Northern New England Becoming More Extreme? Statistical Analysis of Extreme Rainfall in Massachusetts, New Hampshire, and Maine and Updated Estimates of the 100-Year Storm. *J. Hydrol. Eng.*, **16**, 203–217, https://doi.org/10.1061/(ASCE)HE.1943-5584.0000303.

Frei, A., Kunkel Kenneth E., Matonse Adao, 2015, The Seasonal Nature of Extreme Hydrological Events in the Northeastern United States, *J. Hydrometeorol*, **16**, No. 5, p. 2065-2085, doi:10.1175/JHM-D-14-0237.1

Ford, T. W., S. M. Quiring, O. W. Frauenfeld, and A. D. Rapp, 2014: Synoptic conditions related to soil moisture-atmosphere interactions and unorganized convection in

Oklahoma. *J. Geophys. Res. Atmos.*, **11**, 519–535, https://doi.org/10.1002/2015JD023975.

Gimeno, L., R. Nieto, M. Vázquez, and D. A. Lavers, 2014: Atmospheric rivers: a mini-review. *Front. Earth Sci.*, **2**, 1–6, https://doi.org/10.3389/feart.2014.00002.

Groisman, P. Y., and Coauthors, 2004: Contemporary Changes of the Hydrological Cycle over the Contiguous United States: Trends Derived from In Situ Observations. *J. Hydrometeorol.*, **5**, 64–85, https://doi.org/10.1175/1525-7541\.

——, R. W. Knight, D. R. Easterling, T. R. Karl, G. C. Hegerl, and V. N. Razuvaev, 2005: Trends in intense precipitation in the climate record. *J. Clim.*, **18**, 1326–1350, https://doi,org/10.1175/JCLI3339.1.

Guan, B., and D. E. Waliser, 2015: Detection of atmospheric rivers: Evaluation and application of an algorithm for global studies. *J. Geophys. Res. Atmos.*, 1–19, https://doi.org/10.1002/2015JD024257.

——, ——, F. M. Ralph, E. J. Fetzer, and P. J. Neiman, 2016: Hydrometeorological characteristics of rain-on-snow events associated with atmospheric rivers. *Geophys. Res. Lett.*, https://doi.org/10.1002/2016GL067978.

Hartigan, J. A. and P. M. Hartigan, 1985: The Dip Test of Unimodality. *Ann. Statist.,* **13**,1, 70-84, https://doi.org/10.1214/aos/1176346577.

Hewitson, B. C., and R. G. Crane, 2002: Self-organizing maps: Applications to synoptic climatology. *Clim. Res.*, **22**, 13–26, https://doi.org/10.3354/cr022013.

Huntington, T. G. (2006). Evidence for intensification of the global water cycle: Review and synthesis. *J. Hydrol.*, **319**,1–4, 83–95. https://doi.org/10.1016/j.jhydrol.2005.07.003.

Karl, T. R., J. M. Melillo, and T. C. Peterson, 2009: *Global Climate Change Impacts in the United States*. Cambridge University Press, 196 pp. www.globalchange.gov/usimpacts.

Knippertz, P., and H. Wernli, 2010: A lagrangian climatology of tropical moisture exports to the northern hemispheric extratropics. *J. Clim.*, **23**, 987–1003, https://doi.org/10.1175/2009JCLI3333.1.

Kunkel, K. E., and Coauthors, 2013: Regional climate trends and scenarios for the US national climate assessment. Part 1. Climate of the northeast US. 1–87.

Lavers, D. A., and G. Villarini, 2013: Atmospheric Rivers and Flooding over the Central United States. *J. Clim.*, **26**, 7829–7836, https://doi.org/10.1175/JCLI-D-13-00212.1.

——, and ——: The contribution of atmospheric rivers to precipitation in Europe and the United States. *J. Hydrol.*, **522**, 382–390, https.//doi.org/10.1016/j.jhydrol.2014.12.010.

Lengwiler, Y., (2020). Gini coefficient and the Lorentz curve (https://www.mathworks.com/matlabcentral/fileexchange/28080-gini-

coefficient-and-the-lorentz-curve), MATLAB Central File Exchange. Retrieved May 7, 2020.

Louf, V., O. Pujol, H. Sauvageot, and J. Riédi, 2015: Seasonal and diurnal water vapour distribution in the Sahelian area from microwave radiometric profiling observations. *Q. J. R. Meteorol. Soc*., **141**, 2643–2653, https://doi.org/10.1002/qj.2550.

Lynch, C., A. Seth, and J. Thibeault, 2016: Recent and projected annual cycles of temperature and precipitation in the Northeast United States from CMIP5. *J. Clim.*, **29**, 347–365, https://doi.org/10.1175/JCLI-D-14-00781.1.

Mahoney, K., and Coauthors, 2016: Understanding the Role of Atmospheric Rivers in Heavy Precipitation in the Southeast United States. *Mon. Weather Rev.*, **144**, 1617–1632, http://journals.ametsoc.org/doi/10.1175/MWR-D-15-0279.1.

Mallakpour, I., and G. Villarini, 2015: The changing nature of flooding across the central United States. *Nat. Clim. Chang.*, **5**, 250–254, https://doi.org/10.1038/nclimate2516.

Matonse, A. H., and A. Frei, 2013: A seasonal shift in the frequency of extreme hydrological events in Southern New York State. *J. Clim.*, **26**, 9577–9593, https://doi.org/10.1175/JCLI-D-12-00810.1.

Mattingly, K. S., C. A. Ramseyer, J. J. Rosen, T. L. Mote, and R. Muthyala, 2016: Increasing water vapor transport to the Greenland Ice Sheet revealed using self-organizing maps. *Geophys. Res. Lett.*, **43**, 9250–9258, https://doi.org/10.1002/2016GL070424.

Nayak, M. A., and G. Villarini, 2016: A long-term perspective of the hydroclimatological impacts of atmospheric rivers over the central United States. *Water Resour. Res.*, **52**, 1–20, https://doi.org/10.1002/2014WR015716.

Roller, C. D., J. H. Qian, L. Agel, M. Barlow, and V. Moron, 2016: Winter weather regimes in the northeast United States. *J. Clim.*, **29**, 2963–2980, https://doi.org/10.1175/JCLI-D-15-0274.1.

Rutz, J.J., W.J. Steenburgh, and F.M. Ralph, 2015: The Inland Penetration of Atmospheric Rivers over Western North America: A Lagrangian Analysis. *Mon. Weather Rev.*, **143**, 1924–1944, https://doi.org/10.1175/MWR-D-14-00288.1

Sheridan, S. C., and C. C. Lee, 2011: The self-organizing map in synoptic climatological research. *Prog. Phys. Geogr.*, **35**, 109–119, https://doi.org/10.1177/0309133310397582.

Swales, D., M. Alexander, and M. Hughes, 2016: Examining moisture pathways and extreme precipitation in the US Intermountain West using self-organizing maps. *Geophys. Res. Lett.*, 43, 1727– 1735, https://doi.org/10.1002/2015GL067478.

Teale, N. G., S. M. Quiring, and T. W. Ford, 2017: Association of synoptic-scale atmospheric patterns with flash flooding in watersheds of the New York City water supply system. *Int. J. Climatol.*, **37**, 358–370, https://doi.org/10.1002/joc.4709.

Tol, R. S. J., T. E. Downing, O. J. Kuik, and J. B. Smith, 2004: Distributional aspects of climate change impacts. *Glob. Environ. Chang.,* **14**, 259–272, https://doi.org/10.1016/j.gloenvcha.2004.04.007.

Trenberth, K. E., 2011: Changes in precipitation with climate change. *Clim. Res.*, **47**, 123–138, https://doi.org/10.3354/cr00953.

——, A. Dai, R. M. Rasmussen, and D. B. Parsons, 2003: The changing character of precipitation. *Bull. Am. Meteorol. Soc.*, **84**, 1205–1217+1161, https://doi.org/10.1175/BAMS-84-9-1205.

Villarini, G., R. Goska, J. A. Smith, and G. A. Vecchi, 2014: North atlantic tropical cyclones and US flooding. *Bull. Am. Meteorol. Soc.*, **95**, 1381–1388, https://doi.org/10.1175/BAMS-D-13-00060.1.

Walsh, J., D. Wuebbles, and K. Hayhoe, 2014: Chapter 2: our changing climate. *Clim. Chang. Impacts United States Third Natl. Clim. Assessment.*, 19–67, doi:10.7930/J0KW5CXT.

Yarnal, B., 1993: *Synoptic Climatology in Environmental Analysis*. Belhaven Press, London, 195 pp.

Ye, H., D. Yang, and D.A. Robinson, 2008: Winter Rain on Snow and Its Association with Air Temperature in Northern Eurasia. *Hydrol. Processes* 22: 2728–2736, https://doi.org/10.1002/hyp.7094.

Zhang, C., B. E. Mapes, and B. J. Soden, 2003: Bimodality in tropical water vapour. *Q. J. R. Meteorol. Soc.*, **129**, 2847–2866, https://doi.org/10.1256/qj.02.166.

Zhu, Y., and R.E. Newell, 1998: A Proposed Algorithm for Moisture Fluxes from Atmospheric Rivers. *Monthly Weather Review* **126**, 3, 725–35. https://doi.org/10.1175/1520-0493(1998)126<0725:APAFMF>2.0.CO;2.

3. EASTERN US PRECIPITATION INVESTIGATED THROUGH PATTERNS OF MOISTURE TRANSPORT

Abstract

This paper examines the precipitation associated with large-scale patterns of water vapor transport in the eastern United States. Here we define the eastern US study area as 30°–50°N × 60°–90°W. Daily PRISM 4 km gridded precipitation from 1981–2017 is sorted into subsets according to previously-defined patterns of daily water vapor transport supplying the moisture. These subsets are then subjected to a suite of analyses to characterize the precipitation associated with each water vapor transport pattern. The frequency of precipitation occurring with each pattern varies spatially throughout the eastern US. Each pattern is associated with at least occasional precipitation. Highest precipitation averages emanate from near-offshore and coastal transport patterns, though fluxes from the Gulf of Mexico are associated with the highest inland totals. The spatial distribution and the amount of precipitation occurring with each of the water vapor transport patterns varies seasonally. Each transport pattern has a spatially distinct contribution to annual and seasonal precipitation totals. The water vapor transport patterns of moderate intensity and moderate associated precipitation impart the greatest contribution to average annual precipitation. Each of the water vapor transport patterns is associated with some area of heavy ($x \geq 50$ mm), moderate ($25 \text{ mm} \leq x < 50$ mm), and light ($0 \text{ mm} < x < 25$ mm) precipitation. Most of the transport patterns (10 of 16) are associated with statistically significant increases in areas of heavy precipitation over the study period; some patterns are also associated with statistically significant increases in

areas of moderate and/or light precipitation. These increases include the coastal transport pattern associated with the most consistent heavy precipitation of all the moisture delivery patterns. By identifying which water vapor transport patterns are issuing larger areas of moderate and heavy precipitation, and by characterizing the precipitation totals and contribution associated with each pattern, this paper demonstrates the utility of examining precipitation variability through moisture transport.

3.1. Introduction

This study investigates and characterizes relationships between precipitation and water vapor transport patterns in the eastern United States. Such a study is beneficial to understanding the precipitation that falls out of the variety of storms and other precipitation-generation mechanisms that impact this region. This study characterizes relationships between all patterns of water vapor transport and regional precipitation rather than focusing on only enhanced moisture transport or extreme precipitation events. This holistic approach permits a thorough investigation of the trends, changes, and variability in the moisture and precipitation climatologies.

Changing precipitation regimes have been a central topic in climatological research in recent years. Increases in heavy precipitation have been observed for much of the United States, with the largest increases in both intensity and frequency of heavy precipitation events observed in the Northeast (Easterling et al. 2017). Griffiths and Bradley (2007) found trends toward wetter conditions in the Northeast from 1926–2000.

Douglas and Fairbank (2011) found significant rises in maximum precipitation as well as precipitation events exceeding 50 mm at stations in coastal New England from 1970–2008 and 1954–2005, respectively. Thibeault and Seth (2014) showed that the northeastern US experienced an increase in the frequency of precipitation extremes from 1980–2010. Changes in heavy precipitation such as these are of particular interest due to the potential for increased frequency of flood-related hazards. In the eastern US, for example, observations of flooding becoming more frequent over the past century are well documented (e.g., Kunkel et al. 2013, Peterson et al. 2013).

Efforts have been undertaken to identify the meteorological causes of individual extreme precipitation events. Using a manual classification procedure, Kunkel et al. (2012) showed that precipitation in the eastern United States is driven by a wide variety of meteorological systems. They identify extratropical cyclones, frontal systems, and tropical cyclones as being associated with significant increases in heavy precipitation in the eastern US. Because frequencies of extratropical cyclones and landfalling tropical cyclones have not increased (Colle et al. 2015; Kunkel et al. 2012; Karl et al. 2009), increases in heavy precipitation associated with these events must be driven by other changes in these systems.

Changes in a precipitation regime, particularly increases in heavy precipitation, are related to the intensification of the water cycle due to increasing global temperatures. This increase in atmospheric moisture content with warmer temperatures proportional to the Clausius-Clapeyron relationship is well known (Trenberth 1999; Held and Soden 2006; Huntington 2006; Pall et al. 2007; Trenberth et al. 2005; O'Gorman and Schneider 2009). For each degree Celsius of warming, the capacity of the atmosphere to retain

water vapor increases by 7% (Trenberth 2011). In addition, the rate of increases in heavy precipitation vary from the Clausius-Clapeyron rate, as precipitation-generating systems may consolidate and precipitate moisture from an area 3–5 times the radius of the storm (Trenberth et al. 2003). This finding highlights the spatial heterogeneity of moisture in the atmosphere and the importance of moisture transport and entrainment in precipitation events.

The impact of a more moisture-rich atmosphere has been observed in shifting moisture transport and storm tracks, particularly in the midlatitudes. These changes include increases in the horizontal transport of atmospheric moisture (Lavers et al. 2015). However, Lavers et al. (2015) note that variability in atmospheric moisture content does not directly impact precipitation; lifting mechanisms to force condensation and precipitation of the moisture are still necessary. Kunkel et al. (2013) also state that while thermodynamically driven changes in water vapor content may be partly responsible for shifts in precipitation amounts, the role of dynamical variability must still be considered.

There has been little study on the water vapor transport patterns across the eastern US and how they may relate to precipitation. This paper contributes to filling this gap as the second paper in a series of three investigating the role of water vapor transport in eastern US precipitation. In the first paper, Teale and Robinson (under review; hereafter referred to as T&R) develop a comprehensive climatology of water vapor transport patterns to account for all pathways of moisture through the eastern US. While this research identifies and describes the pathways of moisture transport through this region, it does not investigate the relationship between water vapor transport and precipitation. In this second paper, the primary patterns of moisture transport identified in T&R are

associated with precipitation to identify the impact of each unique water vapor transport pattern on the precipitation distribution of the eastern US. In the third part of the project, we assess the long-term behavior of these patterns and their relationships with precipitation over the twentieth century.

To achieve our goal of characterizing the precipitation associated with moisture transport patterns, the paper is structured as follows. In section 3.2, study data are presented along with methodologies utilized to calculate precipitation frequency, magnitudes, and contributions for each water vapor transport pattern. Study results presented in Section 3.3 include the relationship between vertical velocity and water vapor transport (3.3.1), the frequency of precipitation issued from each water vapor transport pattern (3.3.2), the characterization of annual and seasonal precipitation magnitudes associated with each water vapor transport pattern (3.3.3), the contribution to annual and seasonal precipitation associated with each pattern as well as the relationships between precipitation frequency, magnitude, and contribution (3.3.4), and the relationship between water vapor transport patterns and light, moderate, and heavy precipitation (3.3.5). A discussion and concluding remarks follow in Section 3.4.

3.2. Data & Methods

3.2.1. Water vapor transport patterns

Water vapor transport patterns employed in this study were previously identified and described in T&R. In T&R, a self-organizing map (SOM) methodology was employed. In general, SOMs utilize unsupervised machine learning to ingest data and form a user-specified number of groups to represent the major patterns within those data.

The output patterns are portrayed as nodes distributed within the dimensions of the self-organizing map. The SOM methodology in T&R ingested daily integrated vapor transport (IVT), calculated from European Centre for Medium-Range Weather Forecasts (ECMWF) ERA-Interim reanalysis products, from 1979–2017 at a 2.5°×2.5° spatial resolution for the eastern US (30°–50°N × 60°–90°W). This study domain, which is large enough to capture synoptic-scale systems, is comparable to that of Agel et al. (2018) in their analysis of large-scale meteorological systems related to extreme precipitation in the eastern US, as well as that of Roller et al. (2016) in their identification of winter weather regimes in the northeastern US. The SOM procedure produced sixteen nodes, or unique patterns, of moisture transport. These moisture transport patterns, also called water vapor transport patterns in this paper, are shown in the SOM in Figure 3.1. These node patterns are amalgams of the daily moisture fluxes comprising each group; that is, while these nodes depict the general pattern of moisture transport for each group, each daily pattern may vary slightly. The layout of the sixteen nodes produced by the SOM is not coincidental. Following the patterns in the daily data, nodes with similar characteristics are located closer together, and patterns with opposing features are located at maximum distance. This creates a gradient of features across the SOM.

Most of the moisture transport patterns identified in T&R demonstrate moderate to strong seasonal signals; few patterns show little to no seasonality. The frequency of each of the patterns range from common (more than 17% of days, 1979–2017) to rare (2% of days, 1979–2017). In general, the magnitudes of daily water vapor transport as well as moisture confinement are inversely associated with both pattern frequency and pattern longevity. Put differently, the most confined water vapor pathways are the least

frequent and the least persistent but contain the highest values of moisture transport. Thus, while rare, these events have a potential for high impact due to their high moisture content.

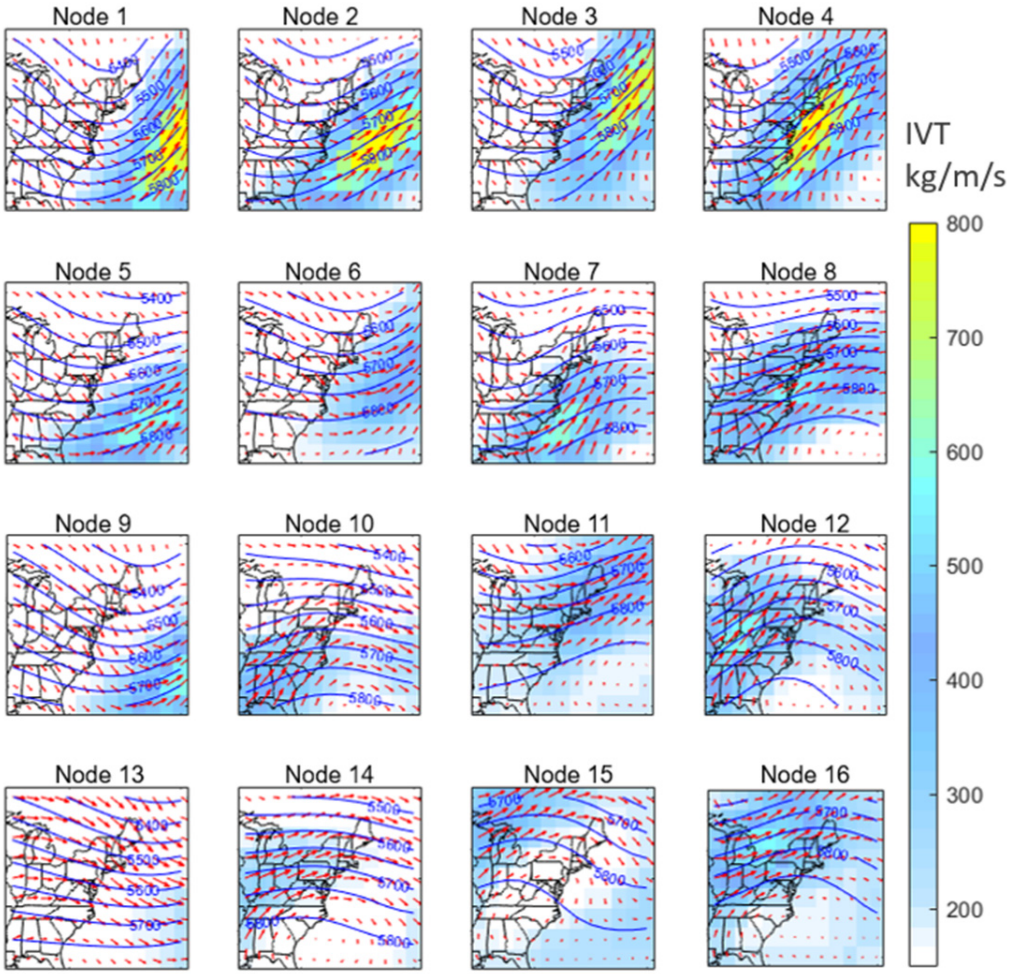

Figure 3.1. Water vapor fluxes identified by T&R. Integrated vapor transport (shading) is shown for the study area. 500 mb wind vectors (arrows) and 500 mb geopotential height (contours), not included in the SOM generation, are shown for reference.

Conversely, the water vapor pathways that are the least confined and move the least moisture tend to be most frequent and are more likely to persist for two or more days.

While common, they have relatively low impact on synoptic-scale moisture transport due to their low moisture content. This combination of rare-but-high-impact with common-but-low-impact events illustrates the complexity of the atmospheric moisture climatology of the eastern US, particularly the impact each of these patterns has on the regional precipitation regime.

The dates on which each moisture transport pattern occurred are established in T&R. Daily precipitation data corresponding with the dates of each moisture transport pattern are extracted and analyzed separately. This isolates the precipitation characteristics associated with each moisture transport pattern. The water vapor transport patterns are developed independently of other climatological variables, such as synoptic scale pressure patterns or mesoscale storm systems. This disentangles the role of variability in the moisture supply patterns from other variables that influence precipitation, such as frequencies of extratropical and tropical cyclones, cutoff lows, convergence, or other lifting mechanisms. The number of days assigned to each pattern, both annually and seasonally, are analyzed for trends using a nonparametric Mann-Kendall trend test to determine if significant changes ($p < 0.05$) in pattern frequency occurred from 1981–2017.

3.2.2. Vertical velocity

Vertical velocity is employed to relate integrated water vapor transport to precipitation. Daily vertical velocity is acquired from ECMWF ERA-Interim reanalysis from 1979–2017 at a 2.5°×2.5° spatial resolution, matching the domain and resolution of water vapor transport in T&R. Vertical velocities for the subset of days experiencing each

unique water vapor transport pattern from T&R are averaged to determine the average vertical velocity over the study area associated with each moisture transport pattern.

3.2.3. Precipitation data

Daily gridded precipitation data from 1981–2017 used in this study are generated by the Parameter-elevation Regression on Independent Slopes Model (PRISM) Climate Group at a 4 km grid resolution. PRISM ingests station data, digital elevation models, and other variables to estimate precipitation amounts between stations (Daly et al. 1992). This gridded precipitation dataset has advantages over station data because it provides equal data density over the study area for the entirety of the time period, thus limiting issues introduced by irregular station spacing and incomplete time records. PRISM's higher resolution is a key advantage over reanalysis precipitation. This gridded precipitation is acquired for land areas within the study region of T&R.

3.2.4. Precipitation frequencies

For each node, the percent of node days in which precipitation was recorded was tabulated for each grid cell. This is mapped to show the spatial distribution of precipitation occurrences associated with each node. These frequencies are calculated overall and annually from 1981 to 2017.

3.2.5. Precipitation averages

For each node, the average amount of precipitation produced by each water vapor transport pattern is calculated for each grid cell. This is done for each grid cell by averaging all non-zero precipitation received within that grid cell on node days. This procedure reveals the average precipitation distribution across the study area associated with each of the sixteen nodes.

This is repeated for spring (MAM), summer (JJA), fall (SON), and winter (DJF). Precipitation patterns at seasonal timescales reveal variability in the magnitude of precipitation associated with each pattern throughout the year. All averages in this study are calculated from 1981–2017: the entirety of the precipitation record for this dataset.

To assess the total precipitation produced by each water vapor transport pattern, a single-value metric is needed. A Riemann sum procedure is adapted for this purpose, as it is typically used to approximate an integral by summing the area of finite subintervals under a two-dimensional or three-dimensional curve (Hughes-Hallet et al. 2005). We adapt this procedure to sum the average precipitation received in the study area as suggested by Sigrist et al. (2012). This metric depicts the magnitude of precipitation over the study area more accurately for our purpose than a domain average or median value because it eliminates the need for prior knowledge of the distribution of the data values. Furthermore, the Riemann summation, as opposed to a domain-average, does not imply spatial cohesiveness of the precipitation values, which can be problematic due to the high spatial variability and discontinuity of precipitation in the eastern US as discussed in Agel et al. (2015). Riemann sums are calculated for each set of pattern days by summing the average on seasonal and annual timescales:

Riemann sum of average precipitation = Σ Average precipitation received in each grid cell

3.2.6. Precipitation contribution

We investigate the percent of overall precipitation that is associated with each water vapor transport pattern. To identify how much each pattern's associated

precipitation contributes to the regional precipitation regime, the precipitation contribution for each grid cell is calculated as:

$$\text{Precipitation contribution} = \frac{\text{Amount of precipitation produced by each transport pattern}}{\text{Total amount of precipitation}}$$

This calculation is performed on annual and seasonal timescales. A nonparametric Mann-Kendall trend test on the adapted Riemann sum is employed on both timescales to determine if significant changes in the precipitation contribution of each transport pattern occurred between 1981–2017.

3.2.7. Precipitation magnitudes

The extent to which each water vapor transport pattern is associated with daily heavy precipitation ($x \geq 50$ mm), moderate precipitation ($25 \text{ mm} \leq x < 50$ mm), and light precipitation ($0 \text{ mm} < x < 25$ mm) is investigated. For each day within each pattern subset, the number of grid cells receiving precipitation within each category is recorded. This number of grid cells is then averaged to represent precipitation on seasonal and yearly timescales for each moisture transport pattern. These average areas are converted to percent of the study area. For each pattern, Mann-Kendall trend tests determine if the seasonal and annual average areas receiving precipitation of each magnitude from each moisture transport pattern changed significantly between 1981–2017.

3.3. Results

3.3.1. Vertical velocity

Areas of greatest vertical lifting (Figure 3.2) align closely with areas of high moisture transport, frequently on the lee side of troughs as seen in Figure 3.1. The strongest lifting values are observed with the highest IVT values, as especially seen along the top row of the figure. The nodes in the bottom left corner of the self-organizing map have widespread neutral and positive values, indicating little uplift throughout the region, particularly in Node 13. Some of the patterns along the right side of the SOM, such as Node 16, are associated with uplift through much of the study area.

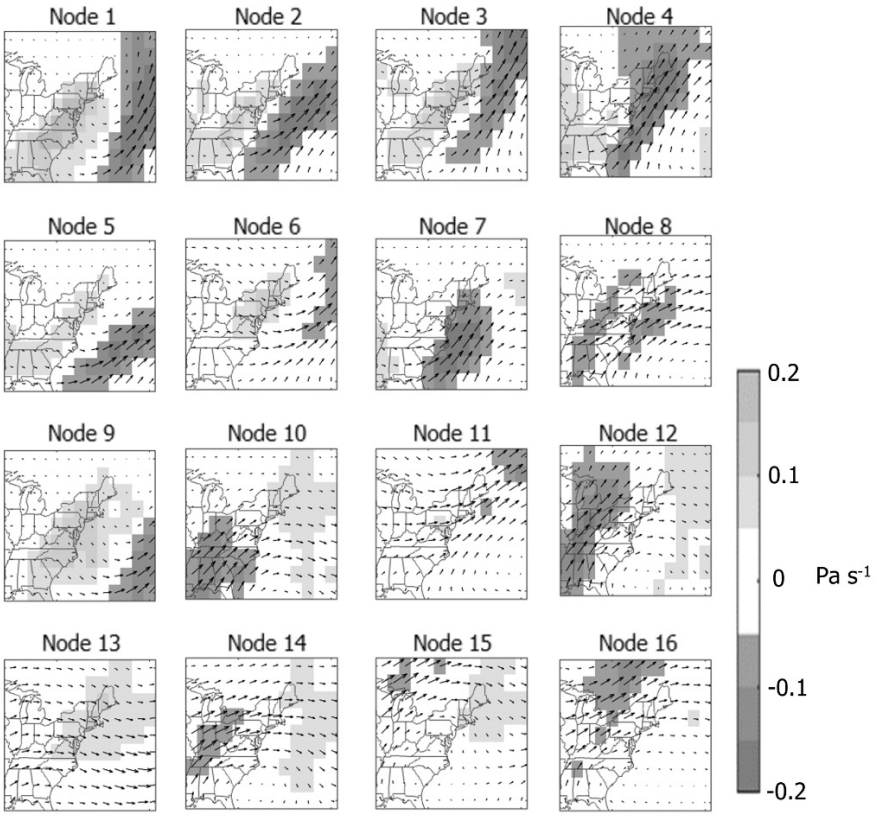

Figure 3.2. Vertical velocity composites for each of the water vapor fluxes in pascals per second. Positive values indicate atmospheric subsidence; negative values indicate lifting. Arrows indicate IVT; arrow length corresponds to IVT magnitude.

Seasonal vertical velocity composites for each water vapor transport pattern exhibit the same spatial patterns as the overall patterns shown in Figure 3.2. The only differences in seasonal compared to overall composites are in the intensity of the motion (figures not shown). Both ascending and descending vertical velocities are highest in winter and lowest in summer. Spring vertical velocities are higher than those of fall.

3.3.2. Precipitation frequencies

Each water vapor transport pattern is associated with at least occasional precipitation throughout the study period (Figure 3.3). The frequency with which precipitation occurs with each moisture transport pattern varies spatially within the study region. The water vapor patterns located throughout the top right corner of the SOM (i.e., the top right corners of Figure 3.1 and Figure 3.3) are associated with precipitation more frequently than the other patterns. The Node 4 pattern, characterized by strong moisture transport along the Atlantic coastline, consistently occurs concurrently with widespread precipitation over much of the eastern seaboard. This transport pattern is associated with precipitation in nearly 100% of the instances in which it occurs, particularly over the Appalachian Mountains and New England. Node 8 and Node 12 produce consistent precipitation in the Midwest. These precipitation patterns align with the vertical velocities observed with these moisture fluxes (Figure 3.2).

The water vapor transport patterns located along the left column and bottom of the SOM produce precipitation infrequently in much of the eastern US. Node 13, which is a common pattern with little moisture transport, is associated with infrequent precipitation for most of the study region. The most frequent precipitation with this low-IVT pattern occurs in northern New York and through northern New England, and the

high elevations of the Appalachians. The otherwise fragmented distribution of precipitation occurrences with this transport pattern, coupled with generally neutral vertical velocities (Figure 3.2), suggests that precipitation associated with this pattern is generated from mesoscale systems or other lifting mechanisms that are not resolved at the spatial or temporal resolution of vertical lifting in this study.

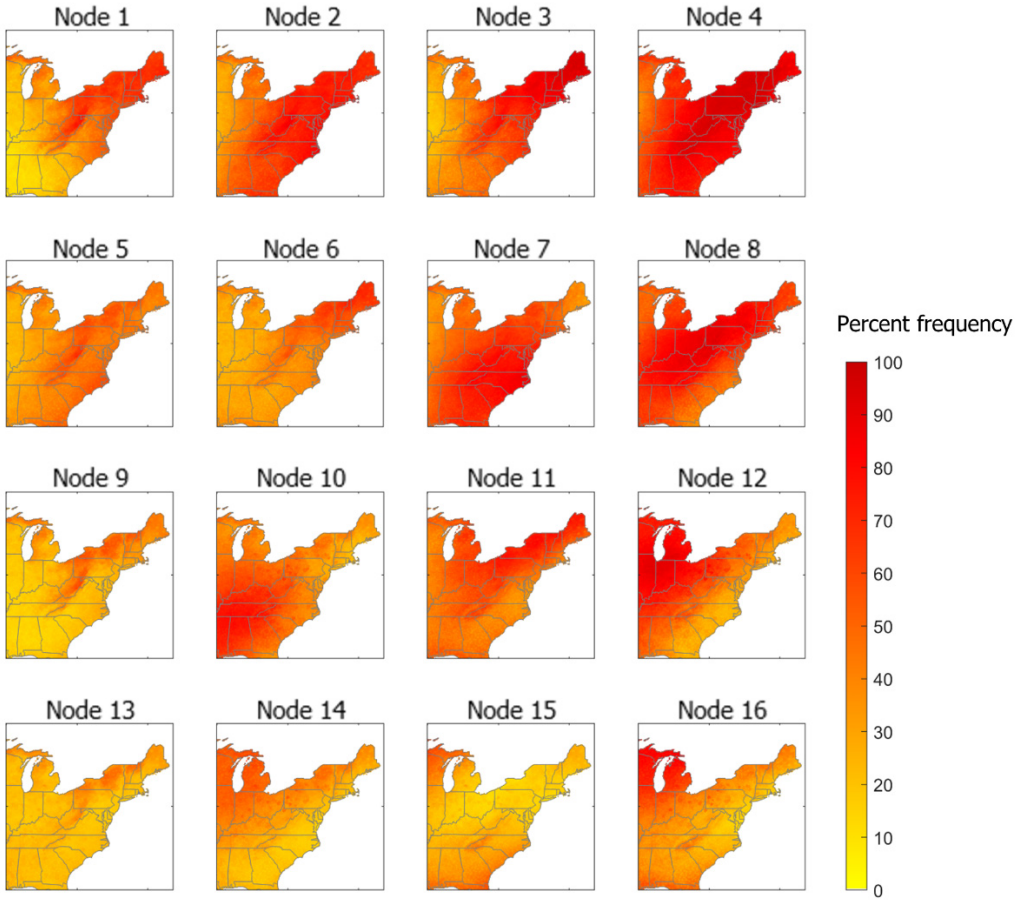

Figure 3.3. For each node, the frequency with which precipitation is observed, 1981–2017.

3.3.3. Precipitation averages

Daily precipitation totals associated with each moisture transport pattern varies throughout the study region. Areas of greatest average daily precipitation (Figure 3.4) align with areas of uplift shown in Figure 3.2. The greatest values are produced by the coastal Node 4 water vapor transport pattern, with daily precipitation nearing 25 mm on average at high elevations. Other patterns are regionally associated with high precipitation magnitudes. Offshore Node 3 patterns occur with the next highest precipitation values in the Northeast after the coastal Node 4 pattern. The southern states receive high precipitation from both Nodes 7 and 10; the coastal Node 7 pattern is associated with high precipitation along the Atlantic coastline, and the Node 10 pattern from the Gulf of Mexico delivers high precipitation inland. The Midwest receives high precipitation associated with the Node 12 pattern of moisture transport up the Ohio River Valley. The central part of the study region, including the Appalachians, receives high precipitation associated with the strong southwesterly moisture transport of the Node 8 pattern.

3.3.4. Precipitation totals: Seasonal timescales

3.3.4.1. Spring

Node 4, defined by strong moisture transport along the eastern seaboard, produces daily precipitation of 10 mm–20 mm on average in the spring months from 1979–2010 for much of the study region; the highest average precipitation of all the patterns (Figure 3.5A). The Atlantic southeast receives precipitation values exceeding 10 mm on average on Node 7 days, aligning with the enhanced water vapor flux along the southeastern coastline that characterizes this transport pattern. Similar magnitudes of precipitation are

observed through the Midwest on Node 12 days, matching the corresponding moisture flux extending from the Gulf Coast through the Great Lakes. The highest average spring precipitation values in the central portion of the study region, upwards of 15 mm, are associated with Node 8 water vapor transport patterns.

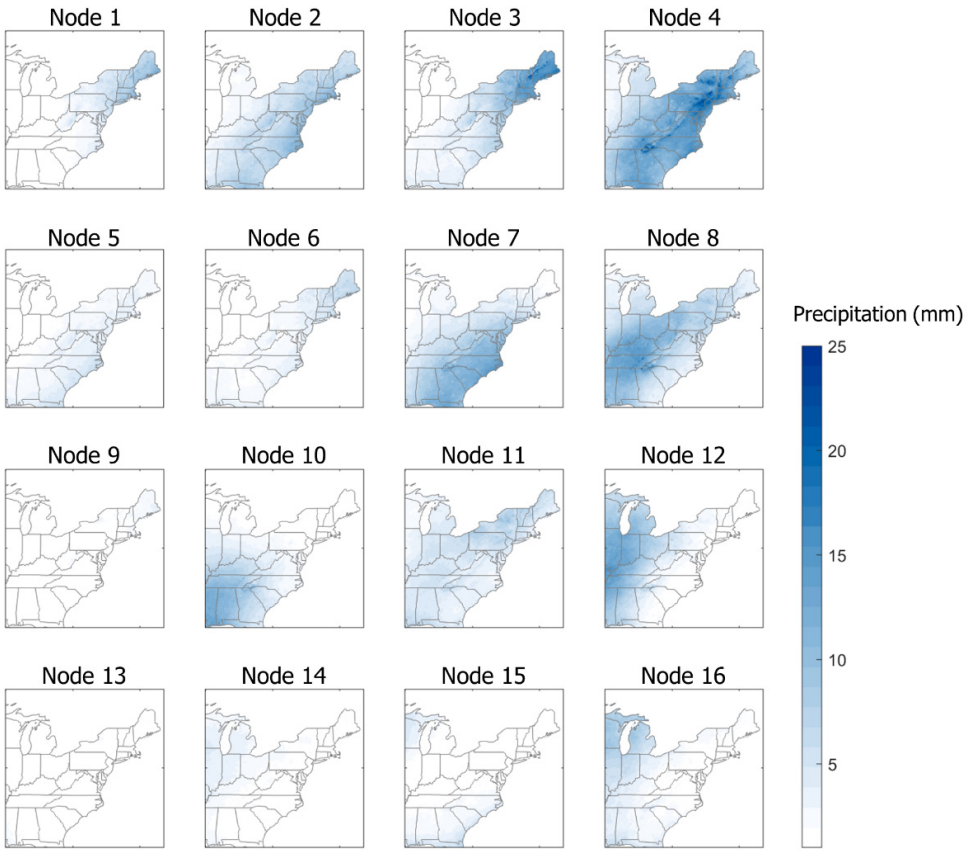

Figure 3.4. Average daily precipitation associated with each of the nodes, 1981–2017.

The offshore atmospheric moisture transport patterns depicted by Nodes 1, 5, and 9 produce low average precipitation in the spring months in the eastern US (Figure 3.5A). Similarly, the Node 15 and 16 patterns characterized by high moisture transport over the Midwest and Great Lakes are associated with very little spring precipitation.

3.3.4.2. Summer

The summer months bring light precipitation to the eastern US through more water vapor transport patterns than in the spring months (Figure 3.5B). Node 8 is associated with the most widespread precipitation, averaging more than 10 mm through the Ohio Valley, where the water vapor transport is also the strongest for this transport pattern. The Node 4 flux pattern along the Atlantic coastline issues upwards of 15 mm–20 mm of precipitation throughout much of the eastern US. On average, 10 mm–15 mm of precipitation from the Gulf of Mexico through western North Carolina in the summer months is associated with the southerly Gulf of Mexico fluxes depicted by Node 10.

Precipitation amounts in Maine occurring with the offshore moisture patterns Nodes 1 and 3 are higher than throughout the rest of the study area. This suggests that the summer hydroclimatology of Maine is distinct from that of the rest of the northeastern US due to its far northern and eastern location and apparent greater response to maritime influences.

Average precipitation within Node 7, 10, and 12 moisture transport patterns is lower in the summer months than in spring.

3.3.4.3. Fall

Fall brings higher average precipitation magnitudes than in summer (Figure 3.5C). Maximum values are observed with the coastal moisture transport patterns of Nodes 3 and 4. Daily magnitudes exceeding 20 mm in New England occur with the Node 3 coastal moisture transport pattern over Maine and offshore. The coastal Node 4 pattern is associated with precipitation upwards of 20 mm on average for much of the study area. Precipitation associated with this pattern is particularly high from the Outer Banks

through the Long Island Sound and at the high elevations paralleling the coast from North Carolina through Maine.

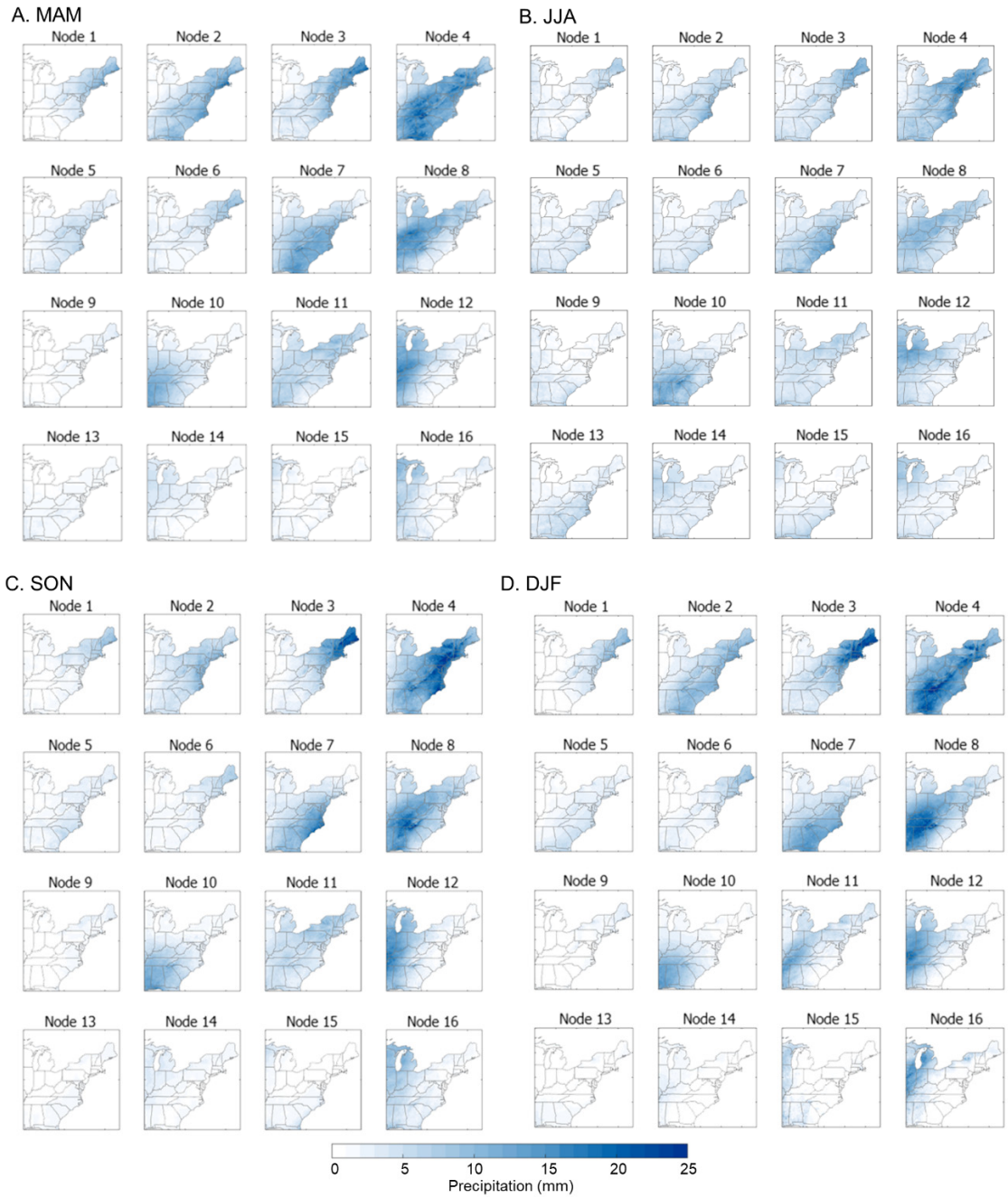

Figure 3.5. Precipitation composites as in Figure 3.4 for (A) MAM, (B) JJA, (C) SON, (D) DJF for each of the fluxes, 1981–2017.

The Node 12 pattern, characterized by strong moisture transport from the Gulf of Mexico through the Ohio River Valley and the Northeast, averages 10 mm–20 mm of precipitation through portions of western Tennessee and Kentucky and southern Illinois. This pulse of enhanced precipitation resembles that found in the spring (Figure 3.5A). Node 10, another flux originating from the Gulf of Mexico but extending over the Southeast, is associated with high fall precipitation relative to other moisture transport patterns, with an average of 10 mm–15 mm of precipitation occurring on days when this pattern of atmospheric transport is present.

3.3.4.4. Winter

The maximum precipitation values are more spatially confined and shifted slightly to the south in winter (Figure 3.5D) than in the fall. As with other seasons, the coastal Node 4 pattern is associated with the highest average precipitation magnitudes for much of the study area. The precipitation associated with other transport patterns is more regional than widespread. The highest average winter precipitation values in New England are associated with near-offshore fluxes, with upwards of 25 mm of precipitation associated with Node 3 days. The southwestern portion of the study region receives its highest average precipitation, exceeding 20 mm on Node 8 pattern days, with southwesterly moisture transport over much of the study area. The southern Atlantic region receives precipitation averaging over 15 mm in the winter months with the Node 7 patterns, reflecting the high moisture transport located offshore of the southeastern US that characterizes this pattern. The far southwestern portion of the study region, including Mississippi and Alabama, receives high precipitation magnitudes on Node 10 pattern

days. In many patterns, including the offshore moisture fluxes of Nodes 1, 3, 6, and 9, New England receives light precipitation, while the rest of the study region remains dry.

3.3.5. Precipitation contribution

Each water vapor transport pattern contributes precipitation to the regional precipitation regime differently (Figure 3.6). The largest contributions to annual precipitation by a single pattern—more than 20% of annual precipitation—appear in Mississippi and Alabama with Node 10 pattern days, and in the upper Midwest on Node 12 pattern days. The contribution from these respective water vapor moisture transport patterns is the result of high moisture transport and moderate frequency of these regional fluxes. The Northeast receives upwards of 40% of its precipitation with the offshore Node 3 and Node 6 patterns. The southern Atlantic region from Florida through Maryland receives more than 15%–20% of its average annual precipitation with the coastal fluxes of Node 7 offshore of the Carolinas.

The water vapor transport patterns represented on the left side of the SOM contribute very little to annual precipitation. Far-offshore fluxes Nodes 1 and 9 contribute the least overall to annual precipitation (Figure 3.6 & Supplemental Figure 3.1). The importance of moisture flux location is also apparent with the Node 3 pattern. These northeastern offshore moisture fluxes produce precipitation that accounts for 12-16% of the annual precipitation in northern New England and Maine but contributes little to no precipitation through the western portion of the study region.

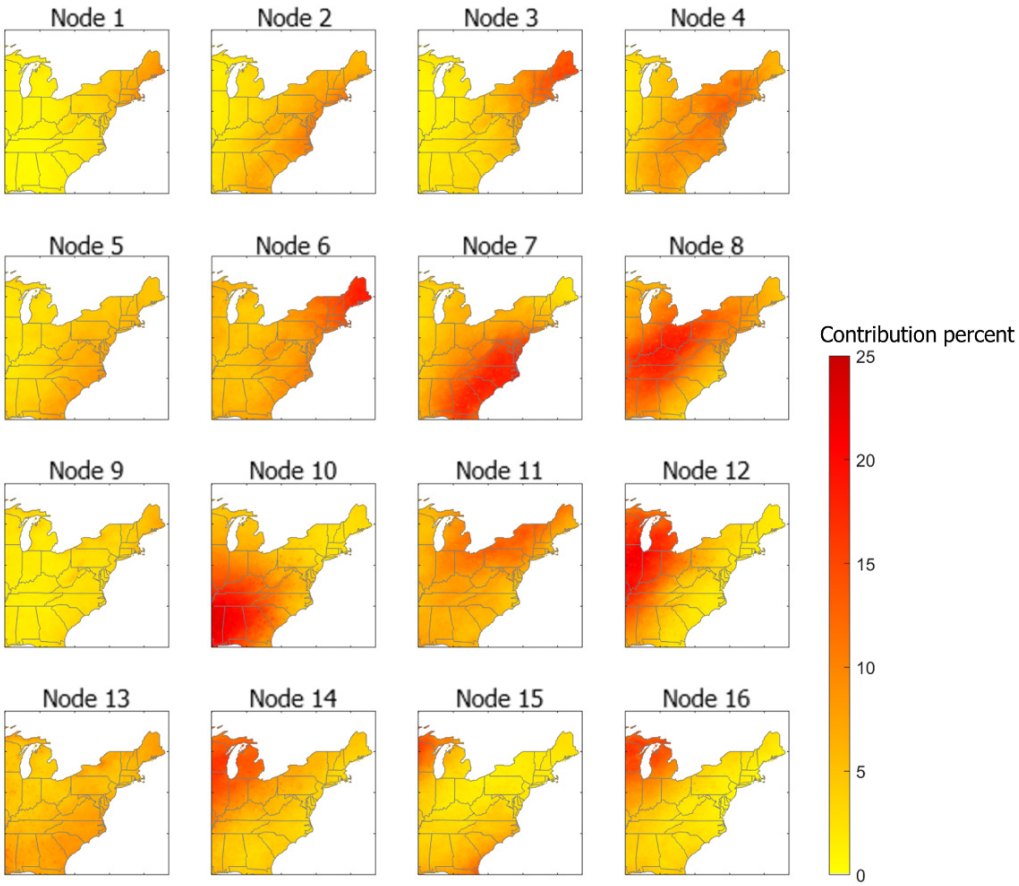

Figure 3.6. Average percentage of annual precipitation associated with each node, 1981–2017.

3.3.5.1. Precipitation contribution: Seasonal timescales

Spring. Nodes 7, 10, and 14 each contribute high percentages of total spring precipitation in select areas of the study region (Figure 3.7A). The southern Atlantic coastal region receives 25% of spring precipitation on average with the Node 7 pattern, characterized by strong moisture transport along the southeastern coastline peaking offshore of the Carolinas. Much of the study area west of the eastern seaboard receives up to 25% with the southwesterly Gulf of Mexico moisture associated with the Node 10 pattern. The high moisture transport centered over the Ohio River Valley and Great Lakes

region that defines Node 12 and 14 patterns is associated with approximately 30-45% in the upper Midwest.

While Node 13 is characterized by low moisture transport, this pattern stands out as having a moderate contribution to spring precipitation throughout the study area due to its high frequency (Figure 3.7A). The widespread moderate contribution associated with this water vapor transport pattern suggests that the mechanisms generating precipitation from this atmospheric moisture are spatially variable.

Node 6 transport patterns, distinguished by moisture transport offshore of New England, produce precipitation comprising 20% of spring precipitation for much of Maine (Figure 3.7A); the highest of the moisture transport patterns. A Mann-Kendall trend test on the Riemann's sum of contribution showed that the precipitation contribution by Node 6 significantly decreased from 1981–2017 (figure not shown; $p < 0.05$). Because the frequency of this pattern in spring did not change significantly during the study time period, this decreasing contribution suggests that changes in daily fluxes assigned to this pattern in the spring may be containing less moisture, are located further offshore, or encountering fewer lifting mechanisms in recent years than earlier in the study period.

Summer. Nodes 6, 8, and 11 emerge as notable contributors to summer precipitation (Figure 3.7B). These patterns (centered offshore New England, through the eastern US, and over New England, respectively) are associated with more than 10% of summer precipitation for most of the study region. Much of the precipitation in the upper Midwest occurs with the Ohio River Valley and Great Lakes fluxes of Nodes 12, 14, and

16. The offshore Node 3 pattern is associated with high precipitation contribution in the Northeast, while contributing very little precipitation elsewhere in the study region.

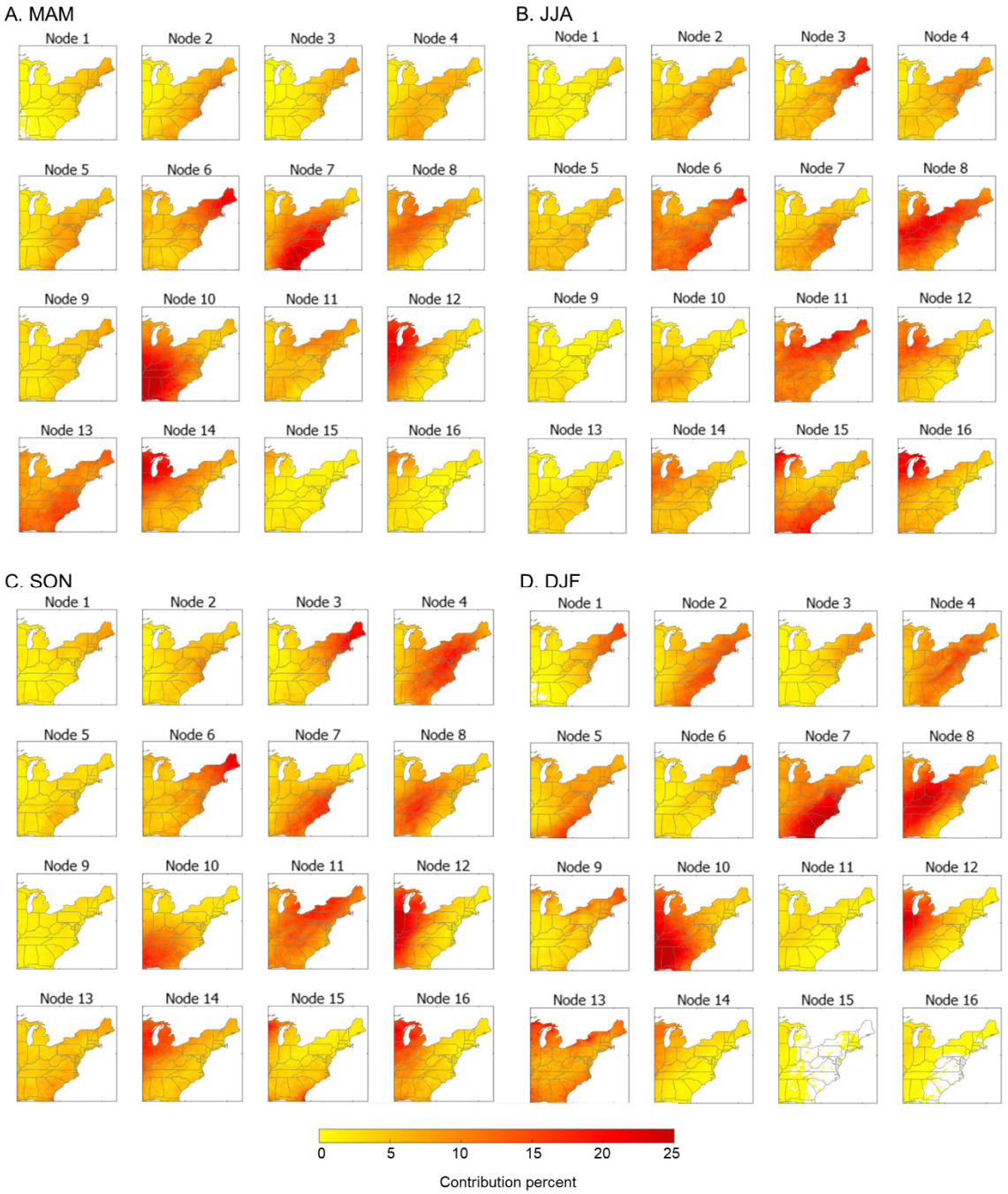

Figure 3.7. Average percent of (A) MAM, (B) JJA, (C) SON, (D) DJF precipitation produced by each node, 1981–2017.

A Mann Kendall trend test on yearly Riemann's sum of summer contribution showed that the yearly summer precipitation contribution of Nodes 1 and 13 significantly decreased ($p < 0.05$) from 1981–2017. Since there were no positive or negative trends in node frequency by season, the seasonal decreases in precipitation contribution must be associated with changes in precipitation production by the unique daily moisture fluxes. Because the contribution of precipitation produced by each pattern is relative to the precipitation produced by the other patterns, these decreases could also reflect subtle and insignificant increases in precipitation contribution from multiple other water vapor transport patterns throughout the 37 years of the study period.

Fall. Many water vapor transport patterns are associated with moderate contributions to fall precipitation (Figure 3.7C). Notably, precipitation associated with the Node 12 water vapor transport pattern alone contributes upwards of 25% of fall precipitation along the western portion of the study domain. New England receives approximately 40% with Nodes 3 and 6, which are the moisture patterns with the most northern water vapor fluxes (Figure 3.7C). This potentially reflects the impact of warm SSTs on precipitation in the region through this season relative to continental patterns. The upper Midwest receives similar contributions on Nodes 14 and 16 days alone. Much of the eastern seaboard receives 30%-40% of its fall precipitation with coastal Node 4 and Node 7 moisture transport patterns.

Winter. Areas of high contribution in winter months closely match areas of high moisture transport in each of the nodes (Figure 3.7D). The southern Atlantic coastline receives 20-25% of its winter precipitation from Node 7 alone. Much of the study region, apart from the coastal plain, receives at least 15% solely from the southwesterly fluxes of

the Node 8 pattern. The southwestern and western portions of the study region receive upwards of 20-25% solely from Gulf of Mexico fluxes associated with the Node 10 pattern. The Midwest and Great Lakes regions receive 20-25% from Node 12. While these regions receive large contributions with the occurrence of specific moisture transport patterns, New England receives winter precipitation under many of the water vapor transport patterns, particularly the patterns along the top left diagonal of the SOM characterized by offshore moisture transport.

Node 13 is associated with moderate contributions to winter precipitation (Figure 3.7D), demonstrating how a moisture transport pattern with relatively little water vapor but occurring frequently has a substantial effect on overall regional precipitation. Node 13 patterns, characterized by low IVT and zonal to northwesterly flow, occur twice as often as the next most frequent moisture pattern in winter months. Relatively high precipitation contributions around the Great Lakes with the Node 13 pattern indicates the relevance of this zonal to northwesterly flow in the lake effect precipitation regime in northern areas of the domain. The water vapor transport patterns distinguished by strong moisture transport over the Midwest and Great Lakes (Nodes 15 and 16), are uncommon, thus contribute little to winter precipitation. Similar to the fall months, none of the water vapor transport patterns showed trends in contributing significantly more or less precipitation to the winter precipitation regime during the course of the study period.

3.3.6. Relationship between precipitation average, pattern frequency, and contribution

The relationship between the frequency of a node and the total precipitation associated with the node is nonlinear (Figure 3.8). The high frequency and low

precipitation of Node 13 and the low frequency and high precipitation of Node 4 cause the relationship to more closely resemble a negative exponential function. Also notable is Node 13, distinguished by low IVT and high frequency, and Node 4, characterized by high IVT plume and rare frequency, each contribute similarly to annual precipitation across the eastern US. The patterns with the greatest average contributions to annual precipitation exhibit moderate frequency and moisture transport (Figure 3.8). Nodes 4, 5, and 15 have low to moderate contributions to average annual precipitation, though a Mann-Kendall trend test shows that the average annual contribution of these patterns increased significantly from 1981–2017 ($p < 0.05$).

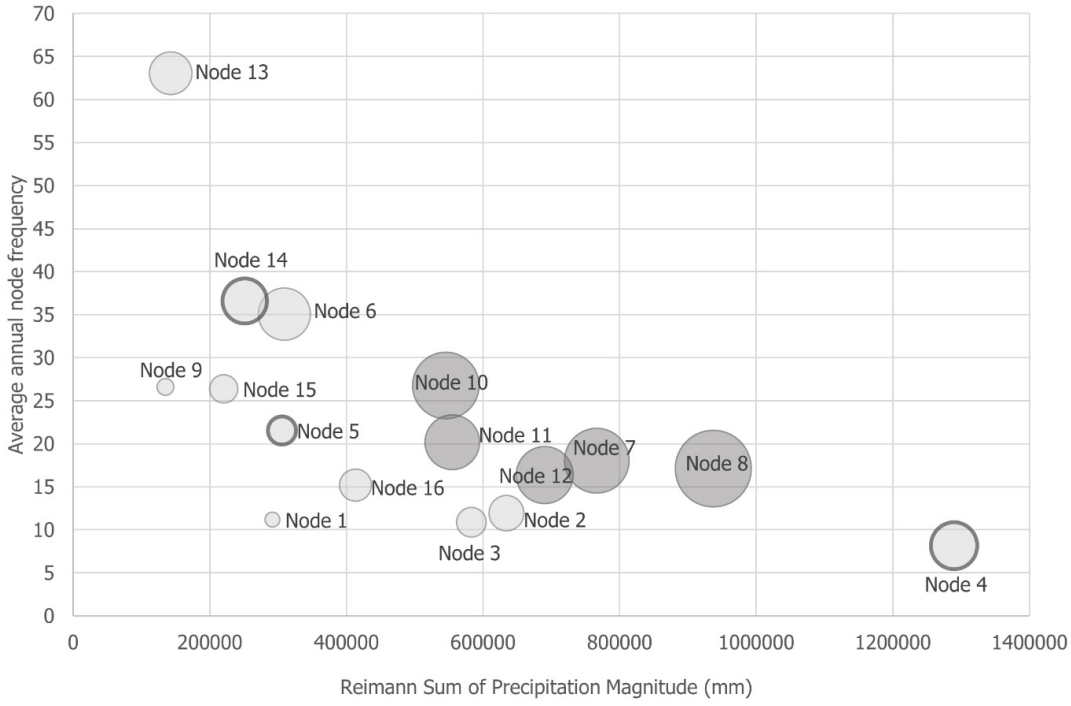

Figure 3.8. Reimann sum of average annual precipitation produced by each flux compared to average annual node frequency. Average contribution of each flux to annual precipitation is proportional to the diameter of the circular markers. The five fluxes with the largest average contributions to annual precipitation are shown in dark gray. Fluxes that exhibit increases in precipitation contribution during the 1981–2017 interval are indicated with bold outlines.

3.3.7. Precipitation magnitudes

Each water vapor transport pattern is associated with areas of light, moderate, and heavy precipitation (Figure 3.9). Node 9, the offshore pattern associated with the least daily precipitation, generates the smallest area of light precipitation (0 mm < x < 25 mm), with light precipitation extending over only 21% of the eastern US on average. A Mann-Kendall trend test detected a significant increase in the annual average size of this area from 1981 to 2017. Node 4 is associated with the largest area of light precipitation, observed over 56% of the study area on average. Node 4 days are also associated with the largest areas of moderate and heavy precipitation, with this area increasing significantly from 1981 to 2017. The smallest areas of moderate and heavy precipitation are again associated with Node 9, which is characterized by northwesterly flow and little IVT over land.

3.3.7.1. Seasonal precipitation magnitudes

The majority of moisture transport patterns are associated with significant increases in heavy precipitation in summer from 1981 to 2017 (Nodes 2, 5–7, 11, 12, 14–16; figure not shown). This suggests that the generation of precipitation became more efficient within many of the moisture transport patterns. The only pattern associated with significant declines in heavy precipitation in the summer is Node 1, which is characterized by strong moisture transport offshore. However, Node 1 transport patterns are associated with significant increases in heavy precipitation in the fall. This summertime decrease followed by an autumnal increase suggests a shift in the timing of heavy precipitation-generating mechanisms to later in the year. There are no statistically

significant changes in average annual area receiving heavy precipitation with these offshore Node 1 fluxes.

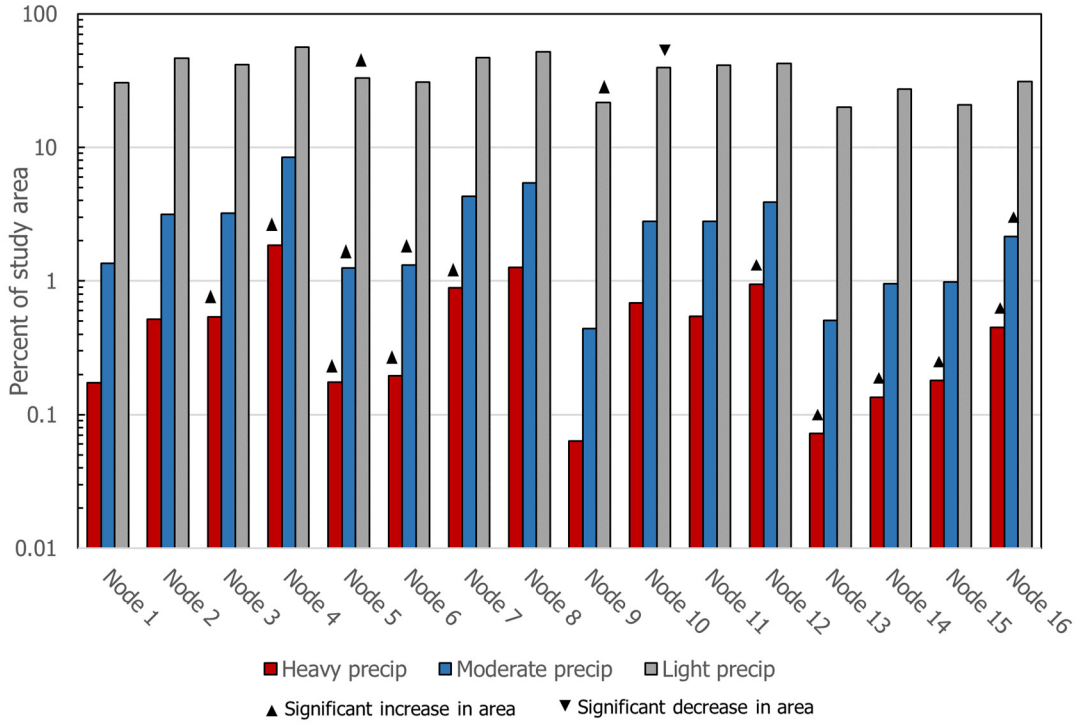

Figure 3.9. Average percent of study area receiving heavy precipitation ($x \geq 50$ mm; left bar; red), moderate precipitation ($25 \text{ mm} \leq x < 50$ mm; center bar; blue), and light precipitation ($0 \text{ mm} < x < 25$ mm; right bar; gray) for each node. Significant increases (decreases) in annual Reimann sums of these areas during the 1981–2017 interval are indicated by upward (downward) triangles.

3.4. Discussion and Conclusion

The investigation of regional precipitation through moisture supply patterns introduces a new perspective for understanding precipitation regimes. Many studies discuss how precipitation requires both a lifting mechanism as well as a moisture supply (e.g., Lavers et al. 2015; Kunkel et al. 2013). Several existing studies have considered

aspects of precipitation related to large-scale meteorological patterns in the eastern and northeastern US (e.g., Barlow et al. 2019; Agel et al. 2018, Roller et al. 2016) but not necessarily moisture delivery associated with precipitation events. To our knowledge, this study characterizing precipitation by moisture supply pathways is the first of its type. Therefore, our analysis of precipitation based on moisture delivery patterns—separate from pressure patterns, synoptic-scale or mesoscale storm systems, or frontal analysis—is a unique contribution to the framework for understanding precipitation variability. The six main findings from this study are summarized and discussed in sections 3.4.1-3.4.6.

We have confidence that the patterns identified in Teale and Robinson (under review; hereafter T&R) are robust for investigating precipitation in the eastern US because they are similar to patterns identified in recent research independent of this study. The T&R water vapor transport patterns associated with the most precipitation in the eastern US resemble the patterns that Agel et al. (2018) identified for extreme precipitation days in the northeastern US. While Agel et al. (2018) grouped extreme precipitation days in the northeastern US using tropopause height, we find that the IVT patterns associated with the most precipitation closely resemble the IVT composites of Agel et al. (2018)'s clusters. This overall agreement between clusters formed on pressure levels on extreme precipitation days (Agel et al. 2018) and patterns derived from nearly four decades of daily IVT (T&R) reinforces our confidence that water vapor transport patterns are robust indicators of regional precipitation patterns. We also find the T&R method to agree with other clustering studies on a seasonal timescale. For instance, the T&R water vapor transport patterns associated with the most precipitation in winter months closely resemble the winter weather patterns identified by Roller et al. (2016).

These agreements with other climate-typing studies shows that the use of IVT as a classification metric is successful in the eastern US. Main findings follow.

3.4.1. Vertical velocity aligns with precipitation

Areas of greatest upward motion aligned with areas of greater precipitation. The vertical lifting patterns associated with Nodes 4, 7, 8, 10, 12, 14, 15, and 16 produced the most precipitation over land. Areas of subsidence (Figure 3.2) coincide with areas of low precipitation (Figure 3.4). While Nodes 1-3 are characterized by high moisture transport offshore, these patterns are associated with subsidence over land, indicating that precipitation in the eastern US is unlikely with these patterns. Patterns of subsidence over the East Coast extend along the left column of the SOM-derived water vapor transport patterns (Figure 3.1), indicating that precipitation over land is unlikely with these patterns (Figure 3.2). The spatial resolution of the vertical velocity dataset used here excludes the impact of local to mesoscale systems, such as convective storms.

3.4.2. Precipitation frequency varies by node

The frequency of precipitation generated by each water vapor transport pattern varies spatially throughout the eastern US, with each transport pattern associated with occasional to frequent precipitation. This agrees with Agel et al. (2018)'s findings that extreme precipitation occurred in nearly each of the large-scale meteorological patterns they identified in the eastern US, as well as with Roller et al. (2016)'s findings that each of the Northeastern weather regimes they identified produced precipitation. While all patterns are associated with some precipitation, the frequency of precipitation varies substantially between the T&R water vapor transport patterns. For example, the strong moisture transport pattern along the Atlantic coastline (Node 4) produces precipitation for

nearly all of the eastern US at least 50% of the times it occurs, and above 80% of the times for the northeastern US as far south as North Carolina. Precipitation occurs less frequently with other patterns. The common moisture transport pattern characterized by zonal flow and low IVT (Node 13) is associated with infrequent precipitation across much of the eastern US. Heterogeneity in the frequency of precipitation associated with low-IVT patterns suggests the role of embedded mesoscale convective systems in producing precipitation rather than from synoptic-scale uplift (Kunkel et al. 2012, Murray and Cole 2011, Agel et al. 2015). These mesoscale dynamics, thermodynamics, and other precipitation-generating mechanisms are not resolvable at the spatial and temporal scales of this study.

3.4.3. Regional variation in precipitation

Highest precipitation averages occur with near-coastal and coastal fluxes, though relatively high precipitation magnitudes inland are associated with fluxes emanating from the Gulf of Mexico. The moisture transport pattern directly over the Atlantic coastline (Node 4) produces the highest daily precipitation magnitudes, exceeding 25 mm on average at some high elevations in the eastern US. Patterns of moisture transport through the Ohio River Valley and the Midwest (Nodes 8 and 12), are also associated with relatively high magnitudes of precipitation. This distinction between coastal and inland precipitation regimes aligns with Agel et al. (2015), who identify differences between the coastal and inland precipitation characteristics. We also find that the magnitude and spatial distribution of precipitation occurring with each water vapor transport pattern varies seasonally. A combination of these findings can be observed in Maine's apparent enhanced sensitivity to maritime fluxes in the summer months. This observation agrees

with previous findings. For instance, Douglas and Fairbanks (2011) identify the extreme precipitation regime of Maine as being distinct from that of the rest of New England.

3.4.4. Seasonal precipitation contributions

Each water vapor transport pattern has a spatially distinct contribution to annual and seasonal precipitation totals. Some of the patterns showed significant increases in their contribution to annual precipitation over the course of the 1981–2017 study period. Two of the three patterns with significant increases in precipitation contribution are associated with relatively low precipitation. The third transport pattern with an increasing contribution to the regional precipitation regime, however, produces the highest magnitudes of precipitation on average of all the water vapor transport patterns. While this pattern (Node 4) is relatively rare, the increasing magnitudes of precipitation by a transport pattern that already produces extreme precipitation may lead to an increase in hazardous flooding conditions through the eastern US. This node, along with a northeastern coastal pattern (Node 11), is strongly associated with flash flooding events in watersheds in the Catskill Mountains that are important for the fresh water supply for New York City (Teale et al. 2017).

The decreasing precipitation contribution by a moderate offshore pattern (Node 6) in spring and by two notably different patterns (far offshore Node 1 and low-IVT Node 13) in summer occurs with no significant changes in node frequency during these seasons. This indicates changes in either moisture content, the lifting mechanism producing precipitation such as convergence, or the spatiotemporal synchronism of these two variables associated with these water vapor transport patterns. In the instances of decreasing precipitation contribution associated with the offshore patterns (Nodes 1 and

6), the amount of precipitation received in the eastern US may decrease if these fluxes occurred further offshore, thus not impacting land precipitation. Because the patterns depicted in the SOM nodes are amalgams of the unique daily fluxes assigned to each pattern, slight shifts in location of the fluxes on any given day will not be recorded, provided that the daily flux still meets the criteria of that node better than any other pattern. However, the overall benefits of reducing the dimensionality of the IVT dataset through the SOM methodology outweigh the loss of detail for this type of study.

3.4.5. Importance of moderate transport patterns

The water vapor transport patterns of moderate frequency and moderate moisture content contribute greatest to annual precipitation in the eastern US. This differs from the western US, where the occurrence of a few strong IVT fluxes produce precipitation that drives the regional precipitation regime (Dettinger et al. 2011). This suggests that in the eastern US, attention should be paid to the moderate events as well as the extremes when examining variability in regional precipitation.

3.4.6. Increasing distribution of heavy precipitation

Each of the water vapor transport patterns is associated with some amount of heavy ($x \geq 50$ mm), moderate ($25 \text{ mm} \leq x < 50$ mm), and light ($0 \text{ mm} < x < 25$ mm) precipitation. Most of the transport patterns (10 of 16 patterns) are associated with statistically significant increases in areas of heavy precipitation from 1981 to 2017. Because there were no significant trends in the pattern frequency during the study period, these changes in the heavy precipitation delivered are likely related to the moisture richness and precipitation-generating mechanisms. This agrees with Thibeault and Seth (2014), who found relatively small changes in the number of wet days in model

simulations and attribute the increases in total precipitation in the Northeast to increased frequency of precipitation extremes.

The significant increases in heavy precipitation associated with the majority of the transport patterns agree with the significant increases in heavy precipitation throughout much of the contiguous US reported in several previous studies (Groisman et al. 2005; Easterling et al. 2017; Hoerling et al. 2016). Our finding that more significant changes in heavy precipitation are observed than changes in moderate to light precipitation agrees with Kunkel et al. (2013)'s finding that changes in extreme precipitation are occurring at a higher rate than increasing precipitation means.

We found that more than half of the moisture transport patterns through the eastern US produced significantly more heavy precipitation in the summer months than in fall. This finding agrees with the increases in warm-season precipitation reported in other studies (Easterling et al. 2017, Marquardt Collow et al. 2016). Because warm-season extreme precipitation is most often associated with mesoscale convective systems (Schumacher and Johnson 2006), this increase seemingly supports Tang et al. (2019)'s findings of increasing convective events in the Midwest and eastern US from 1979 to 2017.

The Fourth Assessment (Easterling et al. 2017), among other sources, indicates that increases in annual eastern precipitation are driven by increased precipitation in the fall. However, only one of the water vapor transport patterns from T&R produced significantly more heavy precipitation in the fall season, and that pattern (Node 1) has relatively little bearing on the precipitation regime. The lack of long-term trends in seasonal changes in heavy precipitation outside of the summer months could be related to

the presence of nonlinear signals. For example, Huang et al. (2017) found that increases in extreme precipitation in the Northeast from 1901–2014 were the compounded by a significant changepoint in fall and spring precipitation 1996.

3.4.7. Future work

This paper is the second of three that report on the role of variability in water vapor transport patterns in regional precipitation. It follows Teale and Robinson (under review), which developed and described the climatology of water vapor transport patterns of the eastern US. The final paper will assess the long-term variability of moisture transport patterns through the twentieth century. Additional future studies should investigate the frequency and moisture content of these transport patterns within projections of future climate. We also suggest that enhanced study of relationships between water vapor transport and precipitation cultivated in this study is warranted to better understand links between the Clausius-Clapeyron relationship, continental and global scale energy budgets, and precipitation variability.

3.5. References

Agel, L., M. Barlow, J. H. Qian, F. Colby, E. Douglas, and T. Eichler, 2015: Climatology of daily precipitation and extreme precipitation events in the Northeast United States. *J. Hydrometeorol.*, **16**, 2537–2557, https://doi.org/10.1175/JHM-D-14-0147.1.

——, ——, S. B. Feldstein, and W. J. Gutowski, 2018: Identification of large-scale meteorological patterns associated with extreme precipitation in the US northeast. *Clim. Dyn.*, **50**, 1819–1839, https://doi.org/10.1007/s00382-017-3724-8.

Barlow, M., and Coauthors, 2019: North American extreme precipitation events and related large-scale meteorological patterns: a review of statistical methods, dynamics, modeling, and trends. *Clim. Dyn.*, **53**, 6835–6875 pp., https://doi.org/10.1007/s00382-019-04958-z.

Colle, B. A., J. F. Booth, and E. K. M. Chang, 2015: A Review of Historical and Future Changes of Extratropical Cyclones and Associated Impacts Along the US East Coast. *Curr. Clim. Chang. Reports*, **1**, 125–143, https://doi.org/10.1007/s40641-015-0013-7.

Daly, C., R. Neilson, and D. L. Phillips, 1992: A statistical-topographic model for mapping climatological precipitation over mountainous terrain. *J. Appl. Meteorol.*, **33**, 140–158.

Dettinger, M. D., M. R. Ralph, T. Das, P. J. Neiman, D. R. Cayan, 2011: Atmospheric Rivers, Floods and the Water Resources of California. *Water*, **3**, 445–478, https://doi.org/10.3390/w3020445.

Douglas, E. M., and C. A. Fairbank, 2011: Is Precipitation in Northern New England Becoming More Extreme? Statistical Analysis of Extreme Rainfall in Massachusetts, New Hampshire, and Maine and Updated Estimates of the 100-Year Storm. *J. Hydrol. Eng.*, **16**, 203–217, https://doi.org/10.1061/(ASCE)HE.1943-5584.0000303.

Easterling, D. R., and Coauthors, 2017: Precipitation change in the United States. In: Climate Science Special Report: Fourth National Climate Assessment. *Forth Natioanl Clim. Assessment, Vol. I*, **I**, 207–230, https://doi.org/10.7930/J0H993CC.US

Griffiths, M. L., and R. S. Bradley, 2007: Variations of twentieth-century temperature and precipitation extreme indicators in the northeast United States. *J. Clim.*, **20**, 5401–5417, https://doi.org/10.1175/2007JCLI1594.1.

Groisman, P. Y., R. W. Knight, D. R. Easterling, T. R. Karl, G. C. Hegerl, and V. N. Razuvaev, 2005: Trends in intense precipitation in the climate record. *J. Clim.*, **18**, 1326–1350, https://doi.org/10.1175/JCLI3339.1.

Held, I. M., and B. J. Soden, 2006: Robust Responses of the Hydrological Cycle to Global Warming. *J. Clim.*, **19**, 5686–5699.

Hoerling, M., J. Eischeid, J. Perlwitz, X. W. Quan, K. Wolter, and L. Cheng, 2016: Characterizing recent trends in US heavy precipitation. *J. Clim.*, **29**, 2313–2332, https://doi.org/10.1175/JCLI-D-15-0441.1.

Huang, H., J. M. Winter, E. C. Osterberg, R. M. Horton, and B. Beckage, 2017: Total and extreme precipitation changes over the Northeastern United States. *J. Hydrometeorol.*, **18**, 1783–1798, https://doi.org/10.1175/JHM-D-16-0195.1.

Hughes-Hallett, Deborah; McCullum, William G.; et al. (2005). *Calculus* (4th ed.). Wiley. p. 751.

Huntington, T. G., 2006: Evidence for intensification of the global water cycle: Review and synthesis. *J. Hydrol.*, **319**, 83–95, https://doi.org/10.1016/j.jhydrol.2005.07.003.

Karl, T. R., J. M. Melillo, and T. C. Peterson, 2009: *Global Climate Change Impacts in the United States*. 196 pp.

Kunkel, K. E., D. R. Easterling, D. A. R. Kristovich, B. Gleason, L. Stoecker, and R. Smith, 2012: Meteorological causes of the secular variations in observed extreme precipitation events for the conterminous United States. *J. Hydrometeorol.*, **13**, 1131–1141, https://doi.org/10.1175/JHM-D-11-0108.1.

——, and Coauthors, 2013: Monitoring and understanding trends in extreme storms: State of knowledge. *Bull. Am. Meteorol. Soc.*, **94**, 499–514, https://doi.org/10.1175/BAMS-D-11-00262.1.

Lavers, D., M. Ralph, D. Waliser, A. Gershunov, and M. D. Dettinger, 2015: Climate change intensification of horizontal water vapor transport in CMIP5. *Geophys. Res. Lett.*, 1–9, https://doi.org/10.1002/2015GL064672.Received.

Marquardt Collow, A. B., M. G. Bosilovich, and R. D. Koster, 2016: Large-scale influences on summertime extreme precipitation in the Northeastern United States. *J. Hydrometeorol.*, **17**, 3045–3061, https://doi.org/10.1175/JHM-D-16-0091.1.

Murray, J. C., and B. A. Colle, 2011: The Spatial and Temporal Variability of Convective Storms over the Northeast United States during the Warm Season. *Mon. Weather Rev.*, **139**, 992–1012, https://doi.org/10.1175/2010MWR3316.1.

O'Gorman, P. A., and T. Schneider, 2009: The physical basis for increases in precipitation extremes in simulations of 21st-century climate change. *Proc. Natl. Acad. Sci. U. S. A.*, **106**, 14773–14777, https://doi.org/10.1073/pnas.0907610106.

Pall, P., M. R. Allen, and D. A. Stone, 2007: Testing the Clausius-Clapeyron constraint on changes in extreme precipitation under CO2 warming. *Clim. Dyn.*, **28**, 351–363, https://doi.org/10.1007/s00382-006-0180-2.

Peterson, T. C., and Coauthors, 2013: Monitoring and understanding changes in heat waves, cold waves, floods, and droughts in the United States: State of knowledge. *Bull. Am. Meteorol. Soc.*, **94**, 821–834, https://doi.org/10.1175/BAMS-D-12-00066.1.

Roller, C. D., J. H. Qian, L. Agel, M. Barlow, and V. Moron, 2016: Winter weather regimes in the northeast United States. *J. Clim.*, **29**, 2963–2980, https://doi.org/10.1175/JCLI-D-15-0274.1.

Schumacher, R. S., and R. H. Johnson, 2006: Characteristics of US extreme rain events during 1999-2003. *Weather Forecast*., **21**, 69–85, https://doi.org/10.1175/WAF900.1.

Sigrist, F., H. R. Künsch, and W. A. Stahel, 2012: A dynamic nonstationary spatio-temporal model for short term prediction of precipitation. *Ann. Appl. Stat.*, **6**, 1452–1477, https://doi.org/10.1214/12-AOAS564.

Tang, B. H., V. A. Gensini, and C. R. Homeyer, 2019: Trends in United States large hail environments and observations. *npj Clim. Atmos. Sci.,* **2**, 1–7, https://doi.org/10.1038/s41612-019-0103-7.

Teale, N. G., S. M. Quiring, and T. W. Ford, 2017: Association of synoptic-scale atmospheric patterns with flash flooding in watersheds of the New York City water

supply system. *Int. J. Climatol.*, **37**, 358–370, https://doi.org/10.1002/joc.4709.

Thibeault, J. M., and A. Seth, 2014: Changing climate extremes in the Northeast United States: observations and projections from CMIP5. *Clim. Change*, **127**, 273–287, https://doi.org/10.1007/s10584-014-1257-2.

Trenberth, K. E., 1999: Conceptual framework for changes of extremes of the hydrological cycles with climate change. *Clim. Change*, https://doi.org/10.1023/A:1005488920935.

——, 2011: Changes in precipitation with climate change. *Clim. Res.*, **47**, 123–138, https://doi.org/10.3354/cr00953.

——, A. Dai, R. M. Rasmussen, and D. B. Parsons, 2003: The changing character of precipitation. *Bull. Am. Meteorol. Soc.*, **84**, 1205-1217+1161, https://doi.org/10.1175/BAMS-84-9-1205.

——, J. Fasullo, and L. Smith, 2005: Trends and variability in column-integrated atmospheric water vapor. *Clim. Dyn.*, **24**, 741–758, https://doi.org/10.1007/s00382-005-0017-4.

4. LONG-TERM VARIABILITY IN ATMOSPHERIC MOISTURE TRANSPORT AND RELATIONSHIP WITH HEAVY PRECIPITATION IN THE EASTERN US

Abstract

This study investigates variability in moisture transport patterns within the eastern United States and adjacent Atlantic Ocean during the twentieth and early twenty-first centuries and relates these patterns to heavy precipitation. Daily water vapor transport from the European Centre for Medium-Range Weather Forecasts ERA-20C reanalysis for the eastern US (30°–50°N × 60°–90°W) from 1900–2010 are classified into previously defined moisture transport patterns. Over the 111-year study period, annual counts of the high-IVT patterns increase at the expense of low-IVT pattern counts, with the rates of these changes varying by pattern and by season. The frequency of intense IVT patterns persisting for consecutive days increases, weak IVT patterns are interrupted more frequently, and moisture transport in each of the patterns increases over the study period. Furthermore, the enhanced rate of increase in the highest percentiles of the patterns characterized by highest IVT indicates an intensification of IVT in the eastern US. This intensification is expressed in the moisture transport patterns with spatial and seasonal variability. Heavy precipitation days from eleven stations are related to the water vapor transport patterns. Several patterns emerge as major contributors to the regional heavy precipitation regimes within the study area. Over the twentieth and early twenty-first centuries, the occurrence of heavy precipitation decreases with frequent, zonal patterns and increases with meridional, high-IVT patterns. This indicates an increasing influence of synoptic-scale meridional moisture transport on heavy precipitation across the eastern

US. This study demonstrates the utility of a moisture transport approach to contextualize regional precipitation shifts within the changing global hydroclimatic system.

4.1. Introduction

Intensification of the water cycle is a widely recognized impact of a warmer climate system (Huntington 2006; Allen and Ingram 2002; Held and Soden 2006). This intensified hydrologic system includes a theoretical increase in total atmospheric water content of 7% per Kelvin increase in temperature (Held and Soden 2006). This added moisture content has potential varied impacts on precipitation (Wentz et al. 2007; Byrne and O'Gorman 2015). Such impacts have been observed in the northeastern US, where increases in both annual totals and extreme precipitation have been observed over the past several decades (Douglas and Fairbank 2011; Hayhoe et al. 2007; Hoerling et al. 2016; Huang et al. 2017; Groisman et al. 2005). Trends are variable in the southeastern US, with decreases in annual precipitation and increases in the frequency of heavy precipitation (Easterling et al. 2017). However, few studies link these changes with water vapor transport—arguably the most important variable for precipitation. Agel et al. (2018) show how several large-scale meteorological patterns frequently associated with extreme precipitation in the northeastern US are closely linked to atmospheric moisture transport patterns. Lavers and Villarini (2013) show that atmospheric rivers are frequently related to heavy rainfall events in the central US. For the southeastern US, Mahoney et al. (2016) also show the regional importance of atmospheric rivers in the extreme precipitation regime. Despite these useful studies demonstrating the importance

of moisture transport in eastern US hydroclimatology, it has remained unclear how such transport has varied over multidecadal timescales, or how variability in synoptic-scale water vapor transport is related to changes in heavy precipitation across the eastern US.

This paper is the third in a series of contributions that provide new insights into the relationship between water vapor transport and precipitation in the eastern US. In the first study, a comprehensive climatology of water vapor transport was generated and characterized. This included defining a set of water vapor transport patterns accounting for all manners of moisture delivery through the eastern US. The second study related the transport patterns to the overall regional precipitation regime using high resolution precipitation data from 1981 to 2017. This third study explores two primary research goals: (1) furthering understanding of the eastern US climatology of water vapor transport (and variability therein) by extending analysis back through the twentieth century, and (2) relating primary modes of water vapor transport to heavy precipitation. The first goal relates to variability in the dynamics and thermodynamics of water vapor in the eastern US, interrogating both the variability in the moisture transport pattern frequency as well as the intensity of the patterns over the past century. The second investigates if or how the relationship between water vapor transport patterns and heavy precipitation in the region may reflect the observed changes in precipitation.

The data and methods employed in this study are described in Section 4.2. Results of both objectives are presented in Section 4.3, with node variability presented in Section 4.3.1 and precipitation associations in Section 4.3.2. The results are summarized and discussed in Section 4.4.

4.2. Data & Methods

4.2.1. Data

Patterns of water vapor transport were previously identified in Teale and Robinson (in review; hereafter "T&R"). In T&R, a self-organizing map methodology was applied to daily vertically integrated water vapor transport (IVT) data from the European Centre for Medium-Range Weather Forecasts (ECMWF) ERA-Interim dataset. This unsupervised, machine-learning methodology ingested 39 years of daily IVT data (1979–2017) to form sixteen distinct nodes, or patterns, describing moisture transport over the eastern US (Figure 4.1). These nodes are amalgams of the data comprising the patterns. That is, while each day is better represented by its assigned pattern than any other pattern, slight variations between the daily data and the node pattern are to be expected. The node patterns developed in T&R, as well as the corresponding dates assigned to each pattern, are employed directly in the present study.

Daily historical IVT data are obtained from the ECMWF ERA-20C reanalysis dataset for the spatial domain of 30°–50°N × 60°–90°W at 2.5° × 2.5° spatial resolution (Poli et al. 2016). These parameters match those of the IVT employed in T&R to identify the major patterns of water vapor transport across the eastern US. These daily data are acquired from 1900–2010. As in T&R, IVT is calculated from vertical integrals of zonal and meridional moisture transport, as:

$$IVT = \sqrt{(IVT_v)^2 + (IVT_u)^2}$$

In this calculation, IVT_v and IVT_u are daily vertical integrals of northward and eastward water vapor fluxes, respectively. These integrals are calculated as described in T&R.

These vertical integrals are provided directly from the ECMWF ERA-20C data portal (Poli et al. 2016).

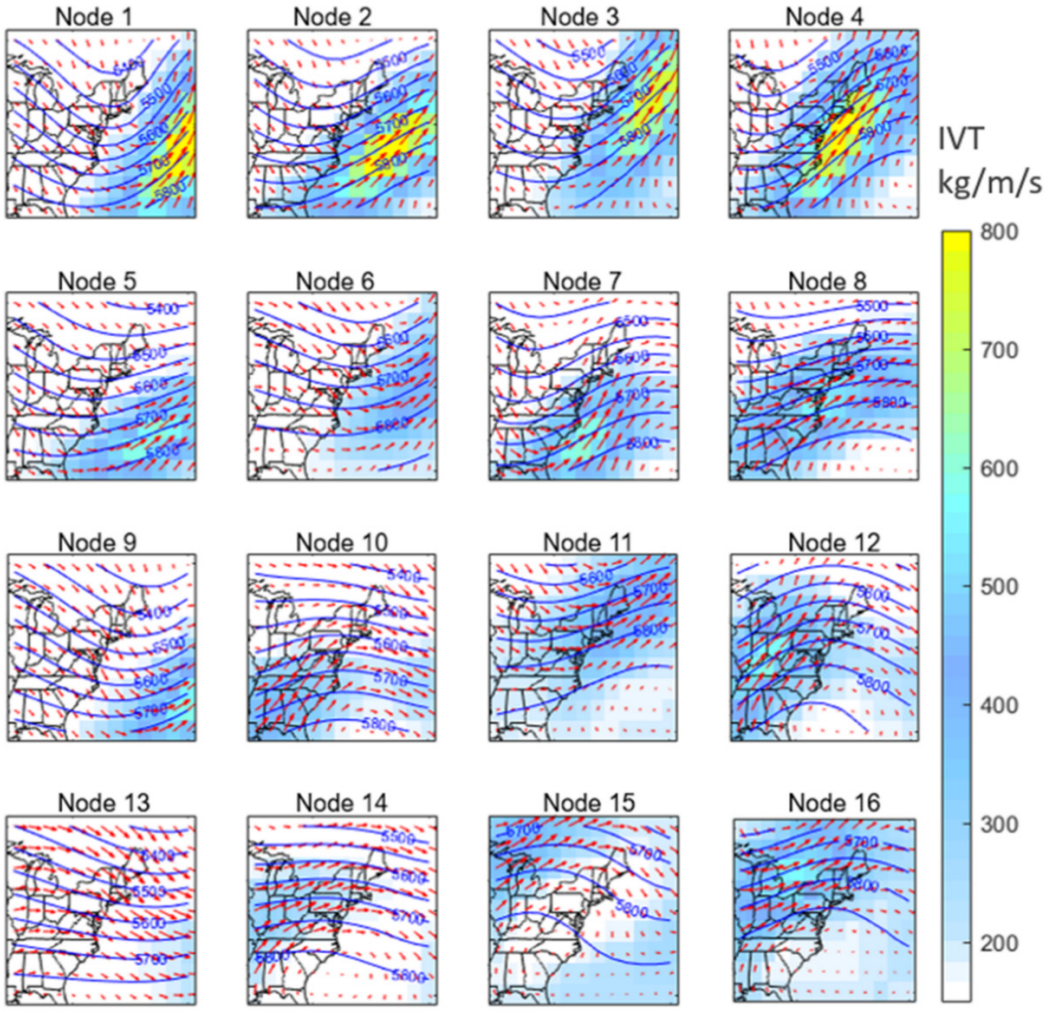

Figure 4.1. Water vapor fluxes identified by Teale and Robinson (under review). Integrated vapor transport (shading) is shown for the study area. 500 mb wind vectors (arrows) and 500 mb geopotential height (contours) shown for reference.

Precipitation data used in this study are daily observations from stations within the NOAA National Centers for Environmental Information Global Historical Climatology Network-Daily dataset (GHCN-Daily; Menne et al. 2012a). This official US archive of daily climate data is comprised of temperature, precipitation, and snow records from 80,000 stations globally (Menne et al. 2012b). This dataset is the optimal choice for this study because of the length of records as well as the quality control of the data. We identified eleven stations distributed throughout the eastern US with ≥ 85% coverage during the 1900–2010 study period. These stations are described in Table 4.1 and shown in Figure 4.2. They are selected to provide a distribution across the northern and central states included in study region.

Table 4.1. GHCN stations with ≥ 85% coverage of daily data between 1900–2010.

Station	Lat (N)	Lon (W)	State	Description
USC00176937	46.7°	68.0°	ME	Presque Isle
USC00274399	42.9°	72.3°	NH	Keene
USW00094728	40.8°	74.0°	NY	New York City Central Park
USC00304174	42.4°	76.4°	NY	Ithaca Cornell University
USC00366233	41.0°	80.4°	PA	New Castle 1 N
USC00200230	42.3°	83.7°	MI	Ann Arbor U of Michigan
USC00441593	38.0°	78.5°	VA	Charlottesville 2 W
USC00314684	35.2°	77.5°	NC	Kinston 7 SE
USC00120784	39.2°	86.5°	IN	Bloomington Indiana University
USW00013872	35.6°	82.6°	NC	Asheville
USC00404561	35.6°	88.8°	TN	Jackson Experimental Station

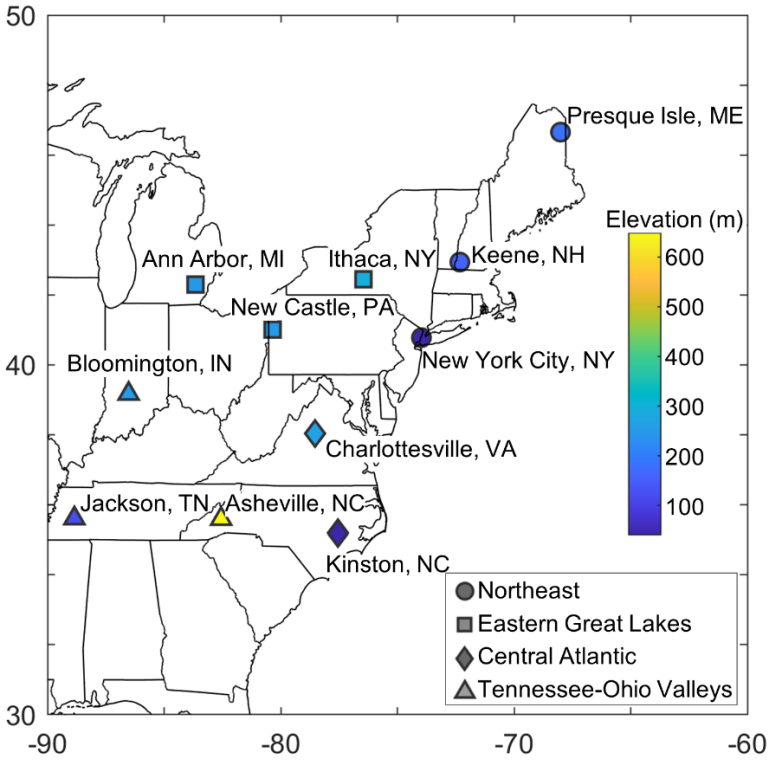

Figure 4.2. Locations of GHCN-Daily stations employed in this study. Regions are indicated by marker shape. Station elevation is indicated by color.

4.2.2. Methods

4.2.2.1. Model training

To sort historical IVT data into the patterns identified in T&R, a model is trained to classify daily IVT patterns. We employ the daily IVT from 1979–2017 from ERA-Interim (Dee et al. 2011) to initialize this procedure; the same used to identify patterns in T&R. The training data are the first 10,000 days of the time period (01 January 1979–18 May 2006); the testing data are the remaining 4,245 days (18 May 2006–12 December 2017). Each of the 10,000 samples of training data are comprised of 117 predictor

variables each (the 117 2.5° × 2.5° grid cells filling the study area for each sample day) and one response value (the SOM node to which each sample day was assigned in T&R).

The MATLAB Classification Learner is employed to analyze this 10,000 × 118 training dataset and develop models describing and predicting the patterns. We initialize the application to train a model on our training dataset with 25% of the data held out for model validation. Through trial and error with each of the model types available in the application, a linear support vector machine (SVM) model emerges as the optimal classification method for predicting IVT patterns in this case, with 92.9% accuracy.

SVM is a non-parametric supervised machine-learning procedure in which the training algorithm develops a hyperplane that separates data into distinct pre-defined patterns (Mountrakis et al. 2011; Karamizadeh et al. 2014; Cortes and Vapnik 1995). Since its introduction in the 1990s (Cortes and Vapnik 1995), SVM has been recognized for its skill in image and pattern classification (Zhan and Shen 2005; Karamizadeh et al. 2014) and as such is frequently used in remote sensing contexts (Mountrakis et al. 2011). For example, SVM has been widely used in classification of vegetation, including savanna tree species from hyperspectral data (Colgan et al. 2012; 76% prediction accuracy) and dominant vegetation cover in Iraq from satellite data (Qader et al. 2016, > 85% prediction accuracy). Classification of other types of land cover is also commonly carried out using SVM: Yan et al. (2015) reviewed the literature on SVM methods in classifying urban land cover, and Devadas et al. (2012) show that SVM has advantages over traditional pixel-based classification methods in predicting agricultural land use/land cover classes. SVM has also been used in classifying glacial snowmelt from satellite data (Wang et al. 2019) and is an emerging machine-learning classification method in digital

soil mapping (Heung et al. 2016). Though it is comparatively less common in hydroclimatological contexts, SVM has been used to downscale precipitation in climate model projections (Tripathi et al. 2006) as well as in drought monitoring (Feng et al. 2019).

The linear SVM model developed on the training data is then applied to the testing data. The predicted nodes for each day of testing data are compared to the nodes assigned by the SOM in T&R to provide an additional accuracy metric for the classification model. On this dataset, the linear SVM again predicts the correct node assignment with 92.9% accuracy.

A confusion matrix from the model training in the Classification Learner application shows that the majority of nodes are predicted with >90% accuracy (Supplemental Figure 4.1). The lowest accuracies are associated with Node 3 days, 23% of which are misclassified as Node 6 patterns. These patterns are similar spatially, but Node 3 patterns contain stronger IVT than Node 6 patterns. This suggests that predicted patterns may have a slight tendency to be sorted into the less-extreme pattern. Most of the nodes have occasional misclassifications as Node 6 patterns (50% of nodes are misclassified as Node 6 at a rate of 1% or less), indicating that predicted Node 6 counts may be slightly overestimated.

The classification model is run on daily IVT from ERA-20C to sort each day of historical data into the best-matching SOM node. Daily node assignments for the overlap period, 1979–2010, have a 73.7% match rate; that is, node classifications between daily IVT patterns from ERA-Interim and ERA-20C are in agreement about three quarters of the time. This modest relationship is the result of differences between the two reanalysis

products. To investigate the mismatched classifications, we construct another confusion matrix, this time comparing the assigned nodes in T&R with the node classifications in the daily ERA-20C predicted by our classification model. This confusion matrix shows some similarities to the model misclassifications. For instance, there is still a tendency for Node 3 patterns to be classified as Node 6 patterns (Supplemental Figure 4.2). Overall, while there is some disagreement, we find that the model sorts daily ERA-20C patterns into more conservative nodes. Therefore, by implementing ERA-20C with this classification model, we minimize biases associated with overestimating the frequency of extreme nodes.

The higher counts of mismatched-classifications between reanalysis datasets than with the model training misclassifications follow the same general patterns as the model training confusion matrix. This indicates that the model is classifying consistently, and that the mismatching pattern classifications arise from differences between the historical dataset and the ERA-Interim dataset. Investigation into these differently assigned values reveals that more of the assignment mismatches occur in the warm season than in the cool season (Supplemental Figure 4.3) and that the rate of misclassifications is relatively stable throughout the overlap period (Supplemental Figure 4.4).

4.2.2.2. Analyses

Trends in annual and seasonal node counts are detected using a Mann-Kendall test ($p<0.05$; Mann 1945; Kendall 1938). This test is also used to detect trends in the persistence of each node. Because many of the patterns are transient, here we consider persistence as the number of times a node occurs for two or more consecutive days and assess these values on annual, pentad, and decadal timescales.

Annual IVT is assessed for trends by examining the 50th, 85th, 95th, and 99th percentiles of IVT over the study area for each year, employing a Mann-Kendall trend test to detect trends ($p<0.05$). We also test for trends in the IVT for each node. Because some of the infrequent nodes did not occur each year, we do not examine annual IVT percentiles for each node as we do for overall IVT. Instead, the 50th, 85th, 95th, and 99th percentiles of IVT for each day each node occurs is calculated, and these values are tested for trends.

Trends in IVT for each node are investigated by each grid cell to determine how variability in moisture transport is distributed spatially across the study domain. For each of the days assigned to each node, a Mann-Kendall trend test ($p<0.05$) is used to identify significant IVT trends. For grid cell exhibiting a trend in IVT from 1900–2010, the slope of the function is estimated using Thiel-Sen regression (Harynuk 2020). The Theil-Sen regression is a robust nonparametric method for estimating linear functions (Theil 1950; Sen 1968). The Mann-Kendall trend test and Theil Sen robust linear regression are methods commonly used for trend detection and slope estimation in hydroclimatology (e.g., Kunkel et al. 2010; Huang et al. 2017).

Historical precipitation data are analyzed for each station as well as within four regions based on latitude and proximity to the Atlantic coast. The geographic division between inland and coastal regions is based on climatologies developed in Agel et al. (2015). The Northeast region includes stations in the northern Mid-Atlantic and New England. Stations in the northeastern Midwest, Upstate New York, and western Pennsylvania are assigned to the Eastern Great Lakes region. The Tennessee-Ohio Valleys region includes the stations in the southern Midwest and Tennessee Valley.

Stations in Virginia and eastern North Carolina fall within the Central Atlantic region. For each year, a subset of heavy precipitation days at each station is extracted. To determine these heavy precipitation days throughout the 111-year study period, the 95th percentile of measurable precipitation (P_{95}) at each station is determined on an annual timescale. Daily precipitation meeting or exceeding each of these thresholds is included in the subset of historical heavy precipitation ("$\geq P_{95}$ days"). By calculating heavy precipitation relative to each year, we ensure that the sample population represents each year of the 1900–2010 study interval. Mann-Kendall tests and Theil-Sen linear regression are employed to detect and estimate trends in the magnitude of precipitation falling in daily heavy precipitation events from 1900–2010.

The days on which heavy precipitation occurred are compared with the T&R nodes to describe the patterns of water vapor transport associated with heavy precipitation at each station, in each region, and within the entire eastern US. The frequency with which each node produces $\geq P_{95}$ precipitation is assessed. Nodes frequently preceding $\geq P_{95}$ days are evaluated to identify major transitions in moisture transport patterns associated with heavy precipitation.

4.3.Results

4.3.1. Node variability

The sixteen nodes that distinguish patterns of water vapor transport (Figure 4.1) are described in Chapter 2. This earlier chapter describes how in addition to each node exhibiting a distinct spatial pattern, they also vary in their frequency and intensity.

4.3.1.1. Node counts

Twelve of the sixteen node patterns have significant positive trends in annual counts from 1900–2010, and two show negative trends (Figure 4.3). Positive trends in annual frequency occur in patterns with comparatively higher moisture transport. The pattern with the largest increasing trend is Node 15, with a trend of +0.99 counts per decade, meaning approximately one additional occurrence per decade, or eleven additional occurrences per decade by the end of the study period (Table 4.2). This pattern is characterized by moisture transport over the Great Lakes west of a high-pressure ridge over the eastern seaboard. From 1900–2010, the greatest overall count increases occur with Node 16, also characterized by widespread moisture transport that is strongest over the Great Lakes. This 351% increase in occurrences coupled with a moderate increasing trend reflects the relatively low frequency of this pattern. Negative trends are observed in Nodes 13 and 14, patterns with little water vapor transport, which decline by 34% and 40%, respectively, from 1900–2010 (Table 4.2).

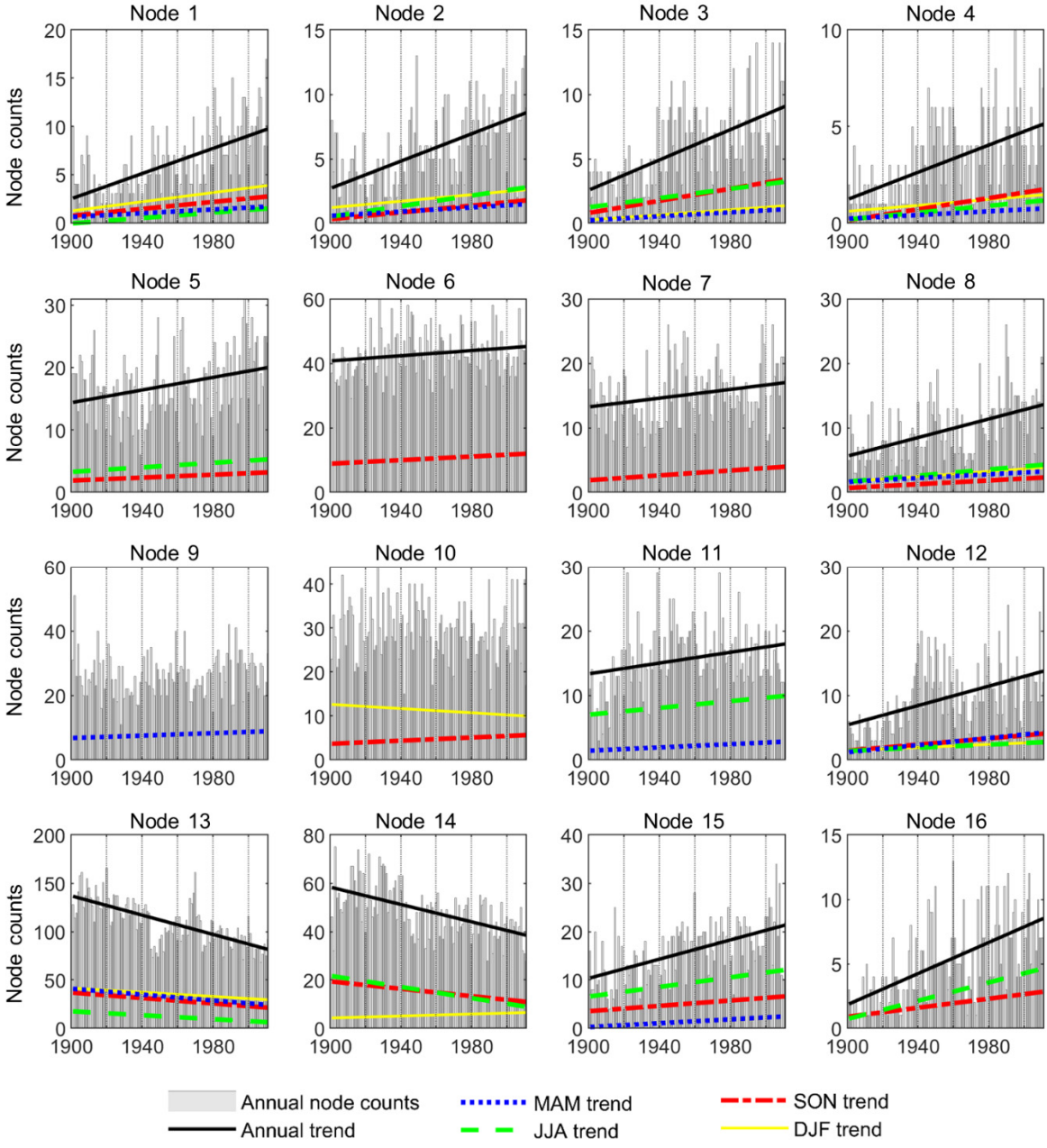

Figure 4.3. Annual node counts, 1900–2010. Lines indicate significant trends in annual (solid black), spring (dotted blue), summer (dashed green), fall (dot-dashed red), and winter (solid, yellow) counts.

Table 4.2. Changes in node counts between 01-01-1900 and 31-12-2010. Changes that are not significant at $p<0.05$ (Mann-Kendall) are not shown.

	Percent increase	Trends per decade				
	Overall	Annual	Spring	Summer	Fall	Winter
Node 1	282%	0.65	0.10	0.14	0.18	0.24
Node 2	212%	0.53	0.08	0.20	0.13	0.13
Node 3	247%	0.59	0.08	0.18	0.24	0.10
Node 4	307%	0.35	0.05	0.09	0.14	0.08
Node 5	39%	0.51	—	0.18	0.12	—
Node 6	11%	0.40	—	—	0.28	—
Node 7	28%	0.34	—	—	0.19	—
Node 8	140%	0.72	0.15	0.24	0.15	0.19
Node 9	—	—	0.19	—	—	—
Node 10	—	—	—	—	0.18	-0.24
Node 11	34%	0.42	0.13	0.26	—	—
Node 12	151%	0.75	0.27	0.12	0.24	0.12
Node 13	-40%	-4.99	-1.52	-1.02	-1.41	-1.08
Node 14	-34%	-1.80	—	-1.15	-0.76	0.20
Node 15	105%	0.99	0.20	0.50	0.28	—
Node 16	351%	0.60	—	0.35	0.18	—

There are more significant trends in seasonal node counts in summer and fall than in spring and winter, though in the latter more than half of the nodes exhibit trends. During the fall, fourteen of the sixteen patterns show trends in node counts; twelve show trends in the summer. Both positive and negative trends in annual and seasonal node counts are present from 1900–2010, and trends in seasonal counts are not necessarily consistent within each node. Most patterns show seasonal trends that are either all positive (e.g., the strong offshore and coastal moisture transport patterns of Nodes 1–4 and strong inland moisture transport patterns of Nodes 8 and 12) or all negative (e.g., the low-IVT Node 13 patterns). Other node patterns show significant trends in some seasons but not others. For

example, Node 11 moisture transport patterns over New England show increasing trends in spring and summer frequency, but not in fall or winter. The Great Lakes moisture patterns of Nodes 15 and 16 show increasing trends in the warm seasons, but not in winter; this is likely due to the very low frequency of these patterns in the winter months. This may also be related to irrigation during the agricultural season (Alter et al. 2015). Some patterns have conflicting seasonal trends. For example, the Gulf of Mexico moisture transport influencing the southeastern US (Node 10) is increasing in frequency in the fall but decreasing in the winter, while exhibiting no significant annual trend. Node 14, defined by moisture transport through the Midwest along the Ohio River Valley, shows decreasing frequency annually and in the summer and fall but an increasing frequency in winter.

4.3.1.2. Node persistence

Several nodes show trends in the frequency of their persistence over two or more days. These trends are detectable on 1-year, 5-year, and 10-year timescales (Figure 4.4), with low-IVT (Nodes 13 and 14) and Great Lakes pattern (Node 16) trending most often. Consecutive occurrences of Nodes 13 and 14 decline the most over the study period, indicative of Node 13 or Node 14 patterns becoming interrupted more frequently in recent decades. The high moisture transport of Nodes 1 and 16 have occurred more persistently over time. Node 1, a strong offshore moisture transport pattern, has positive trends in persistence on decadal and pentadic timescales, but not annual timescales. Node 10, characterized by moisture transport from the Gulf of Mexico through the Southeast, shows increasing trends in pattern persistence at the annual timescale, but not at longer timescales. Overall, trends in persistence show that zonal patterns have become disrupted

more frequently during the past century, while meridional patterns have exhibited an increasing tendency to stall over the eastern US.

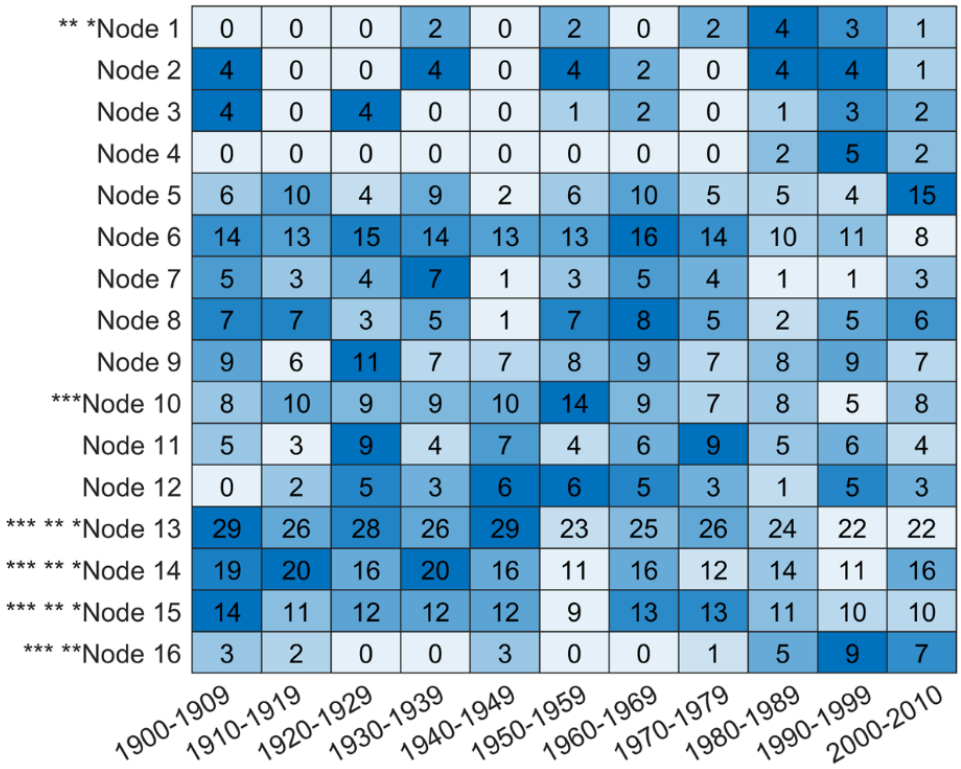

Figure 4.4. Percent of node occurrences that persisted for two or more days per decade. Significant trends in the number of node occurrences persisting two or more days is indicated for annual (***), 5-year (**), and decadal (*) timescales.

4.3.1.3. IVT percentiles

This highest IVT values increased from 1900–2010, indicating an intensification of water vapor transport throughout the eastern US. These increases are present in each node pattern (Figure 4.5, Supplemental Table 4.1). There are no negative trends in IVT at any percentile or within any node. Trends in the 95th and 99th percentile of IVT are stronger and more prevalent than in the 85th and 50th percentiles; that is, the most intense

IVT is increasing faster than the more moderate ranges of the distribution. The rate of increase was greatest in the 99th percentile for all nodes. These significant trends in the 95th and 99th percentiles occur in every node, while trends in the 85th and 50th percentiles are common but do not appear in every node (Supplemental Table 4.1).

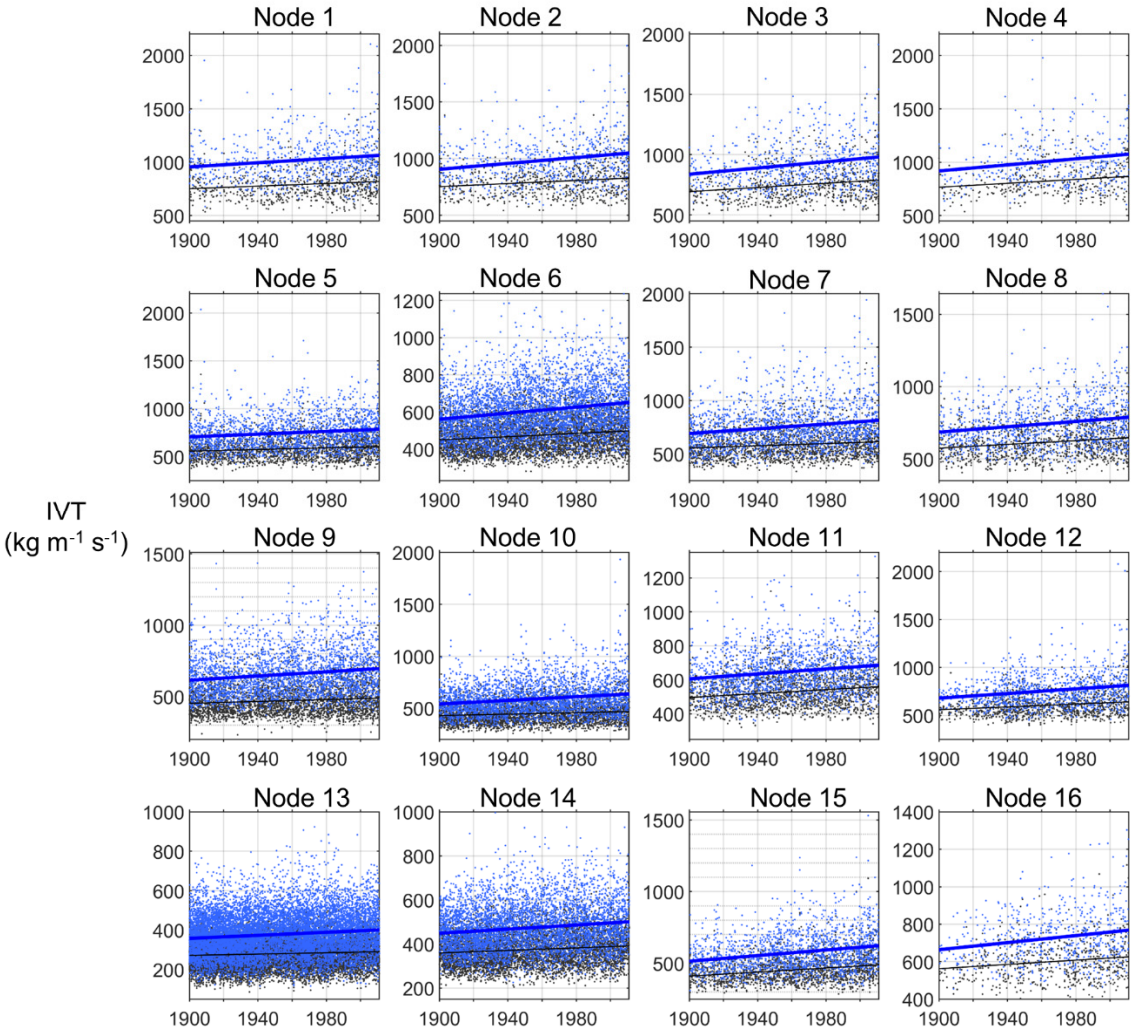

Figure 4.5. 95th (black) and 99th (blue) percentiles of IVT shown for each node occurrence. Significant trends in percentiles from 1900–2010 are shown.

Additionally, the highest IVT values of the strongest moisture transport patterns are increasing faster than those of moderate and weak moisture transport patterns. This is evident as trends in the 99th percentile are strongest in the nodes characterized by the strongest moisture transport (Nodes 1-4, 7, 12, 15). These two findings together show a strengthening of the highest IVT values through the twentieth and earth twenty-first centuries.

The patterns of IVT intensification in each node are also visible in the water vapor transport regime as a whole. Significant increases in annual IVT occur from 1900–2010 for the 50th, 85th, 95th, and 99th percentiles (Supplemental Figure 4.5). The rates of increase rise with each percentile, with the 50th percentile of IVT increasing by 13% and the 85th, 95th, and 99th percentiles by 22%, 24% and 30%, respectively.

4.3.1.4. IVT spatial distribution

While the percentiles of IVT demonstrate that most nodes experience an increase in IVT during the study period at multiple levels, an examination of IVT trends by grid cell reveals that these trends are not equally distributed across the study area (Figure 4.6). Most nodes experience both significant increasing and decreasing local trends (Figure 4.6). The decreasing trends correspond with low IVT values and convergence at the 500 mb height (Figure 4.1). The strongest positive trends tend to correspond with areas of high IVT. The strongest increase in IVT manifests in Node 4, stretching northward along the Mid-Atlantic coastline into eastern NY and western New England. This node contains the highest IVT values impacting land as well as the highest and most consistent precipitation (Chapter 2). Therefore, continued increases in IVT in this pattern of

moisture transport would likely enhanced flooding to these areas beyond the major events that have already occurred in this situation.

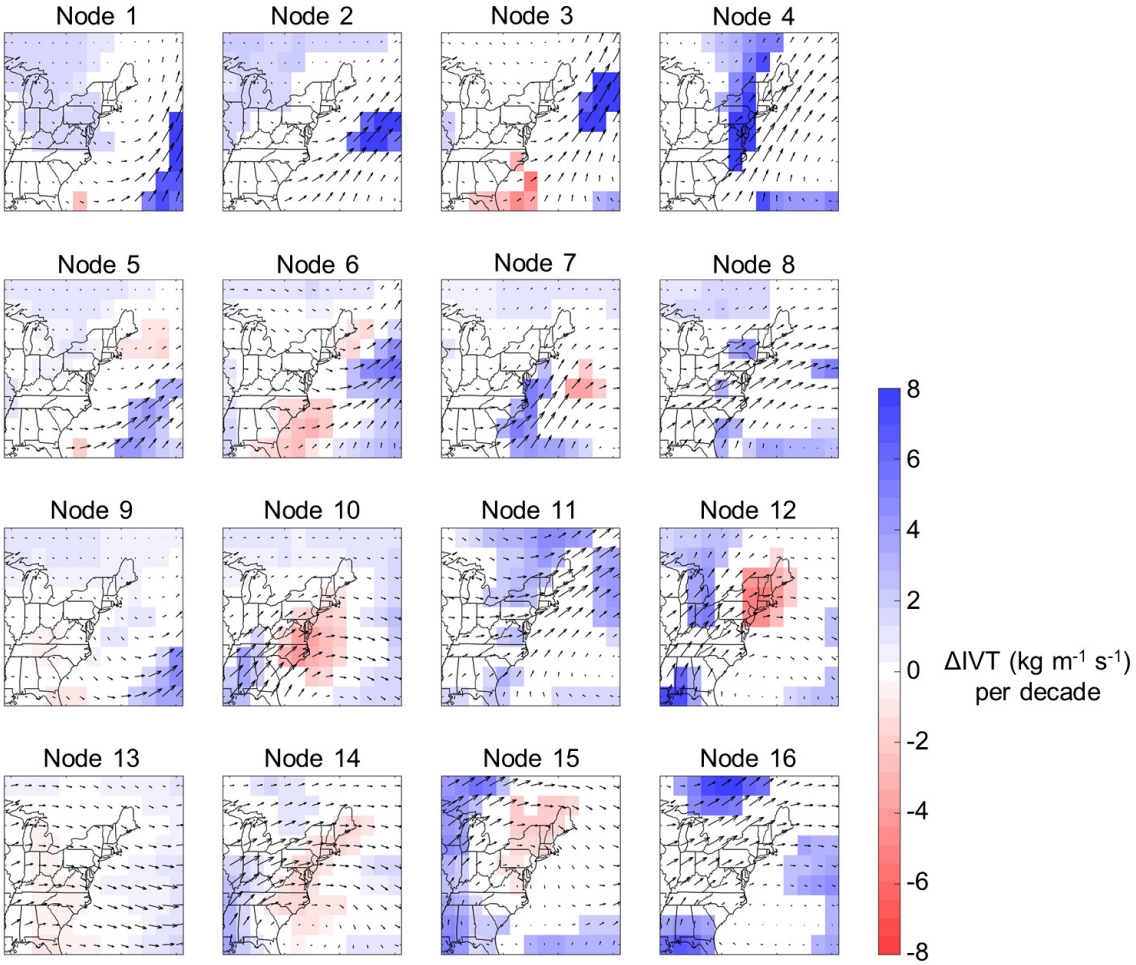

Figure 4.6. Spatial distribution of daily trends in IVT per decade from 1900 through 2010. Trends are indicated by shading. The IVT pattern characterizing each node is shown as vectors.

Seasonal trends in daily IVT are stronger than annual trends during the study period. Among the strongest positive trends over land includes a strong increase in IVT from the Appalachians through the Mid-Atlantic in the spring with Node 4 (Figure 4.7A).

This regional intensification is coupled with decreased IVT for the same area within Node 10. The latter suggests that the high moisture transport extending from the Gulf of Mexico to offshore the Carolinas (Node 10) was stronger in the spring in the early 20th century than at the end of the study interval. The increase in IVT in Node 4 indicates that in addition to becoming more frequent, this node also strengthened in its spring moisture transport during the 20th century.

Several nodes exhibit significant increases in summer IVT that do not impact land (Figure 4.7B). Others show considerable increases or decreases in moisture transport over the eastern US. For example, positive trends in Node 8 IVT for the southern US demonstrate increases in southwesterly moisture transport from the Gulf of Mexico. Negative trends in Node 2 IVT for the same area demonstrate that this offshore southwesterly moisture transport pattern was either stronger or closer to the southern US early in the 20th century than later. The simultaneous strengthening and weakening of IVT associated with Node 12 at different areas suggest that this strong southwesterly moisture transport through the Midwest shifted westward during the study interval.

The strongest increases in IVT in fall occur from the southern US through the Ohio River Valley within Node 12 (Figure 4.7C). This node also shows the strongest deceases in fall moisture transport over land of all the nodes occurring in New England. The positioning of these positive and negative trends suggests that southwesterly moisture transport from the western Gulf of Mexico through New England was either more zonal in the early 20th century than at the end of the study interval, has shifted southward, or a combination of the two.

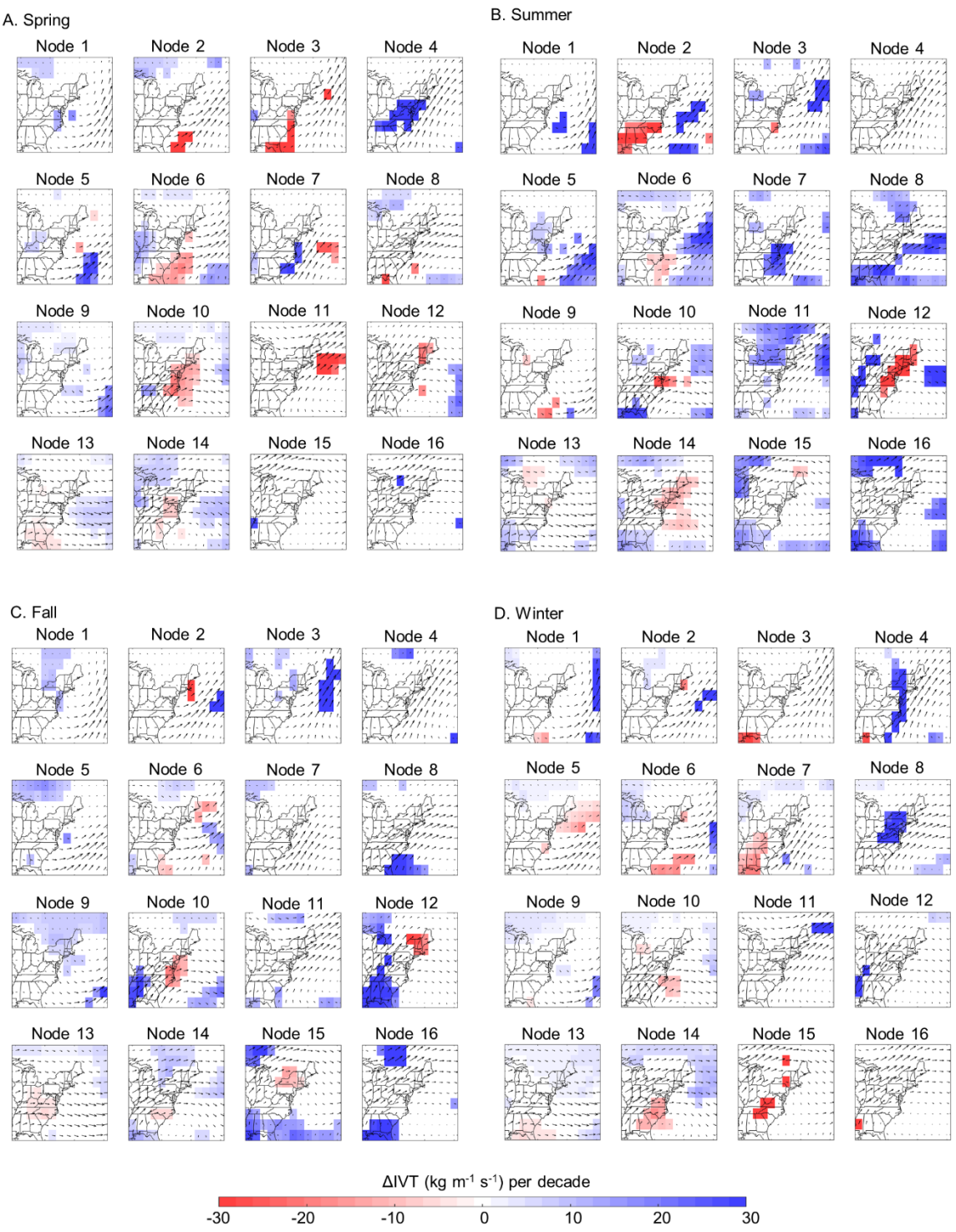

Figure 4.7. Spatial distribution of daily trends in IVT per decade in (A) spring, (B) summer, (C) fall, (D) winter from 1900 through 2010. Shading applies to each subfigure.

The center of the study region shows the strongest increases in winter moisture transport, with Node 4 and Node 8 showing strong increases in IVT from the Mid-Atlantic northward (Figure 4.7D). In particular, the filamentary structure of the IVT associated with Node 4 suggests that this moisture transport pattern may be related to an increase in atmospheric river strength in the eastern US. These increases in winter Node 4 and Node 8 IVT drive the increase in IVT in the northeastern US overall (Figure 4.6).

4.3.2. Heavy precipitation associations with nodes

Of the eleven stations included in this study, the 95th percentiles (P_{95}) of precipitation from 1900–2010 are highest in the central regions (Table 4.3). The Central Atlantic stations have the highest P_{95} as a region, though the P_{95} value is highest overall at Jackson, TN. The long-term P_{95} value at Asheville, NC is lower than that of other center stations due to Asheville's valley location being impacted by rain shadows in several directions. New York City, NY has a P_{95} value that is comparable to those of the southern regions. Four of the stations in the northern portion of the study region show significant increases in the amount of precipitation falling at or above the 95th percentile of annual precipitation during the study period (Figure 4.8).

Several node patterns emerge as frequent contributors to heavy precipitation in the eastern US (Table 4.3). Heavy precipitation in the two northern regions is frequently associated with enhanced moisture transport off the northeastern coastline (Node 6) and over New England (Node 11). The $\geq P_{95}$ precipitation days of the Northeast are also frequently associated with moisture transport centered on the southeastern and Mid-Atlantic coastline (Node 7). At the northern stations in the Northeast (Keene, NH and Presque Isle, ME), heavy precipitation is also associated with the strong moisture

transport of Node 3. The heavy precipitation in the Eastern Great Lakes is distinguished from the Northeast by strong association of Node 14 on ≥P_{95} days. Node 14 is characterized by moderate moisture transport from the southwest through the Midwest and Ohio Valley. This pattern is also frequently associated with ≥P_{95} days in the Tennessee-Ohio Valleys region. The other main nodes associated with heavy precipitation in the Tennessee-Ohio Valleys (Nodes 10 and 12) emanate from the Gulf of Mexico, with Node 12 moisture transport extending through the Midwest and Node 10 transport moving off the Atlantic coastline with Node 10. The heavy precipitation days of the Central Atlantic have similar associations with the Northeast, though they are impacted by systems entrained in the frequent, zonal Node 13 pattern rather than the far northeastern pattern of Node 11.

Table 4.3. For each station or region: the 95th percentile of precipitation (1900–2010), and the percentage of heavy precipitation days associated with the three nodes most frequently associated with ≥P_{95} precipitation days. Percentiles not calculated for regions.

Region or Station	P_{95} 1900-2010 (mm)	Nodes most frequently associated with ≥P_{95}		
Northeast		Node 6: 16.8%	Node 7: 12.0%	Node 11: 10.8%
Presque Isle, ME	23.4	Node 6: 26.9%	Node 11: 13.8%	Node 3: 12.8%
Keene, NH	27.4	Node 6: 17.8%	Node 3: 12.1%	Node 11: 10.1%
NY City, NY	35.4	Node 7: 23.6%	Node 10: 12.6%	Node 14: 11.3%
Eastern Great Lakes		Node 14: 17.5%	Node 11: 12.0%	Node 6: 10.0%
Ithaca, NY	21.8	Node 14: 13.8%	Node 6: 13.1%	Node 11: 12.9%
New Castle, PA	23.6	Node 14: 15.2%	Node 11:14.5%	Node 8: 14.2%
Ann Arbor, MI	23.2	Node 14: 24.2%	Node 12: 20.6%	Node 10: 10.1%
Tennessee-Ohio Valleys		Node 10: 23.8%	Node 14: 14.2%	Node 12: 13.9%
Bloomington, IN	34.8	Node 12: 19.7%	Node 14: 19.1%	Node 10: 14.6%
Asheville, NC	27.4	Node 10: 31.1%	Node 13: 14.6%	Node 14: 10.9%
Jackson, TN	43.7	Node 10: 24.6%	Node 12: 16.2%	Node 8: 13.4%
Central Atlantic		Node 7: 18.5%	Node 13: 17.9%	Node 6: 11.5%
Charlottesville, VA	36.8	Node 7: 20.2%	Node 13: 17.0%	Node 10: 11.9%
Kinston, NC	42.0	Node 10: 24.6%	Node 12: 16.2%	Node 8:13.4%

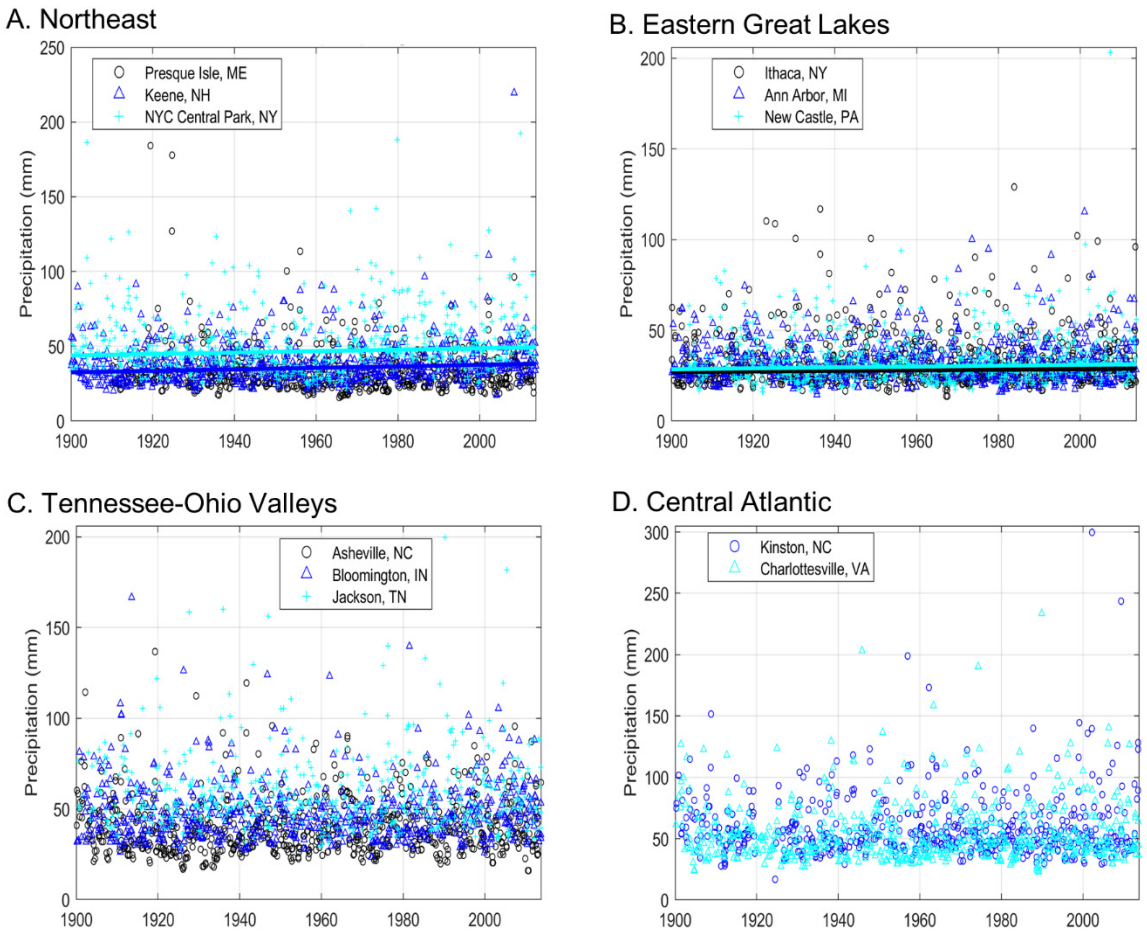

Figure 4.8. Precipitation magnitudes ≥P_{95} observed within the (A) Northeast, (B) Eastern Great Lakes, (C) Tennessee-Ohio Valleys, and (D) Central Atlantic regions. For each station, any significant trends in heavy precipitation magnitude are displayed.

4.3.2.1. Shifts in node associations with heavy precipitation

Over the twentieth century, the proportion of ≥P_{95} days associated with frequent IVT nodes with relatively low and/or zonal IVT decreases while the proportion of heavy precipitation days associated with stronger and more meridional nodes increases (Figure 4.9). This shift in the prominent contributors to heavy precipitation is visible in several regions. In the Northeast, the decreasing proportion of ≥P_{95} days associated with Nodes 13 and 14 from 1900–2010 is coupled with a lack of substantial increases in the other

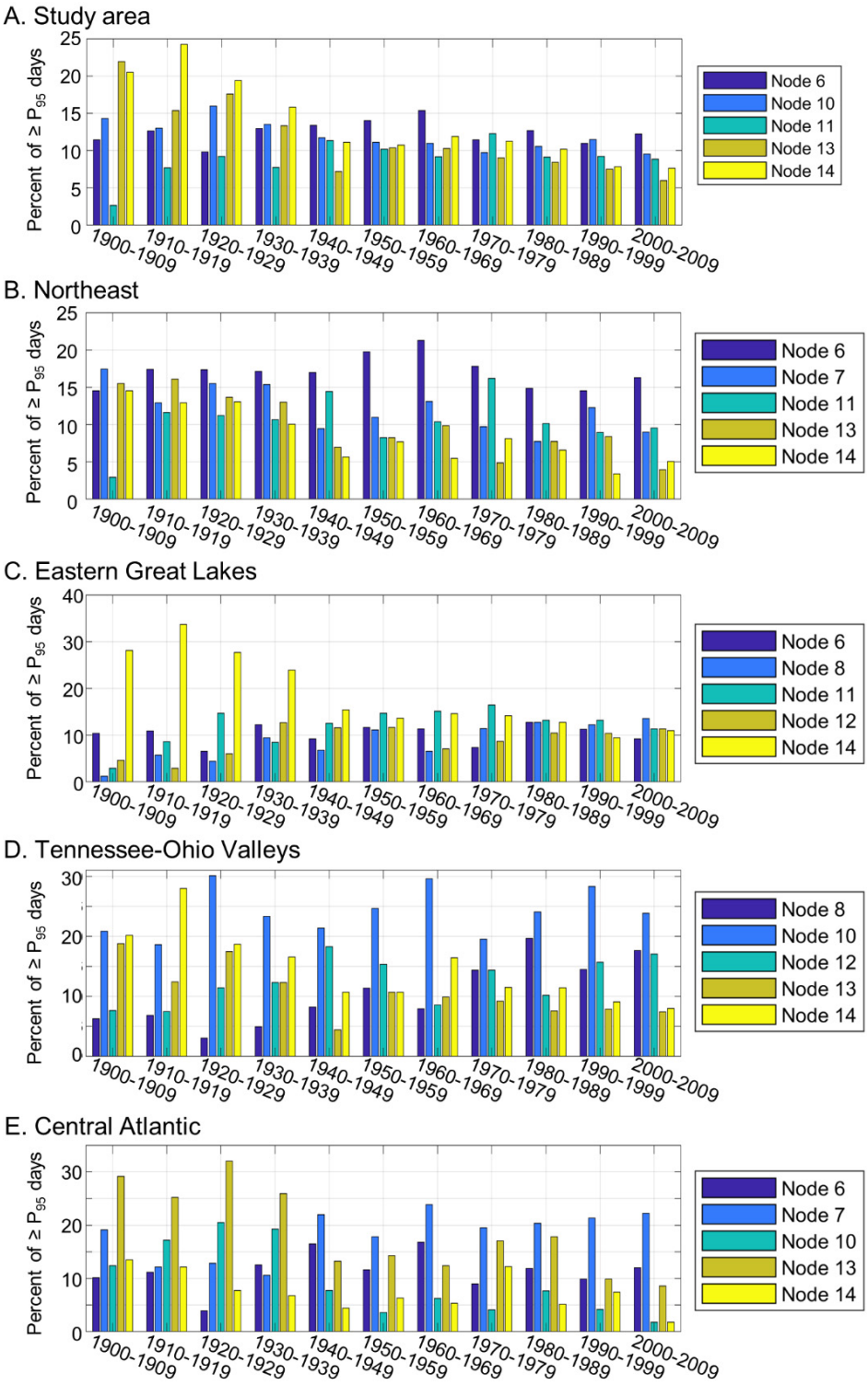

Figure 4.9. The percent of ≥P_{95} days associated with the five nodes of highest recurrence with heavy precipitation for the (A) entire study area, (B) Northeast, (C) Eastern Great Lakes, (D) Tennessee-Ohio Valleys, and (E) Central Atlantic regions. Node colors vary by region.

prominent nodes associated with heavy precipitation. This indicates that moisture transport associated with heavy precipitation in the region is becoming more varied (Figure 4.9B). In the Eastern Great Lakes, the decreased association between Node 14 and heavy precipitation is coupled with an increase in the strong Node 8 moisture transport (Figure 4.9C). The percent of $\geq P_{95}$ days associated with the strong, southwesterly Node 8 pattern also increases by decade in the Tennessee-Ohio Valleys region (Figure 4.9D). In the Central Atlantic, a higher proportion of heavy precipitation is becoming associated with Atlantic as opposed to Gulf of Mexico fluxes (Figure 4.9E). During the study interval, associations between $\geq P_{95}$ days and the strong Gulf of Mexico Node 10 decrease in this region (Figure 4.9E). Beginning in the 1940s, this decrease in Gulf moisture transport is offset by increases in the proportion of heavy precipitation associated with the Atlantic Node 7 pattern.

4.3.2.2. Frequency of heavy precipitation per node

The nodes that are most frequently associated with $\geq P_{95}$ days in the eastern US are among the region's most commonly occurring moisture transport patterns (Supplemental Figure 4.6). Node 13, for instance, accounts for nearly 30% of days between 1900 and 2010 (Supplemental Figure 4.6), though the annual frequency of this node declines during the study interval (Figure 4.3). Heavy precipitation occurs with this zonal, low-IVT node less than 5% of the time this node occurs (Figure 4.10A). The other nodes frequently associated with $\geq P_{95}$ days coincide with heavy precipitation 5%-31% of the times they occur. Other nodes that are less frequent overall are associated with heavy precipitation more frequently (Figure 4.10). For instance, heavy precipitation occurs with

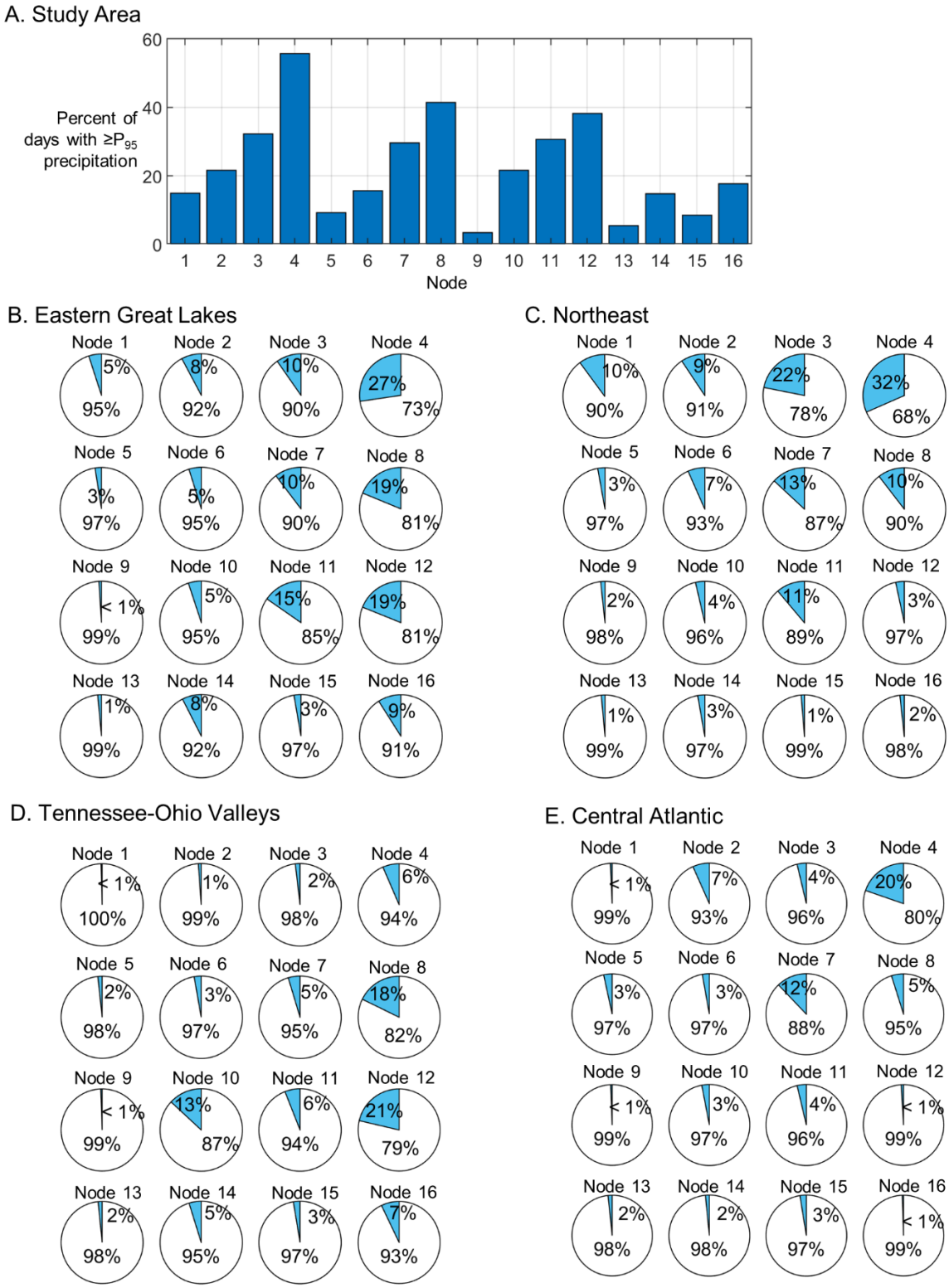

Figure 4.10. The percent of node days on which ≥P_{95} precipitation occurs for the (A) entire study area, (B) Northeast, (C) Eastern Great Lakes, (D) Tennessee-Ohio Valleys, and (E) Central Atlantic regions.

Node 4 56% of the time this node occurs (Figure 4.10A). This pattern of strong moisture transport along the eastern seaboard is associated with heavy precipitation most consistently of all the nodes in the Northeast, Eastern Great Lakes, and Central Atlantic regions (Figure 4.10B, C, E). Despite the reliability of this node in producing heavy precipitation, its low frequency prevents it from being a prominent contributor to overall heavy precipitation occurrences in the eastern US. In the Tennessee-Ohio Valleys region, $\geq P_{95}$ precipitation occurs consistently with Node 12, which is characterized by strong southwesterly moisture transport from the Gulf of Mexico through the northeastern US (Figure 4.10D). The moderate frequency of Node 12 coupled with its relatively consistent occurrence with heavy precipitation makes this a major contributor to the heavy precipitation regime of the inland regions.

4.3.2.3. Recurring node sequences with heavy precipitation

Heavy precipitation in the eastern US occurs with a variety of moisture transport sequences (Figure 4.11). These sequences depict the antecedent atmospheric conditions that portend heavy precipitation associated with each node. Nodes 10, 13, and 14 most frequently precede heavy daily precipitation events. These nodes are characterized by low synoptic-scale moisture transport (Node 13) and moisture transport along the southern and western boundaries of the study region (Nodes 10 and 14). The prevalence of these patterns before many $\geq P_{95}$ precipitation days reveals two scenarios resulting in heavy precipitation.

In the first scenario, transient moisture systems associated with heavy precipitation develop or migrate eastward across the study region on daily to sub-daily timescales. For instance, the occurrence of zonal, low-IVT Node 13 before southwesterly, high-IVT

Node 7 ≥P_{95} precipitation days demonstrates the potential for this moisture stream to develop along the Atlantic coastline on sub-daily timescales. This first scenario describes the antecedent conditions frequently associated with ≥P_{95} precipitation occurring on Node 4, 7, 8, and 12 days.

The second scenario involves the entrainment of mesoscale or local scale heavy precipitation mechanisms within relatively zonal or low-IVT nodes impacting the study region for multiple days. This could represent the system either migrating across the study region or being stalled for consecutive days. This explains the relatively high frequency with which Nodes 6, 10, 13, and 14 ≥P_{95} precipitation days are preceded by a day of the same node (Figure 4.11). The decreasing frequency and persistence of several of these nodes from 1900–2010 (Figures 4.3 and 4.4) indicate a decrease in the frequency of systems which produce heavy precipitation at sequential locations across the eastern US, possibly due to an increasing influence of short-lived, meridional, moisture-rich circulation patterns.

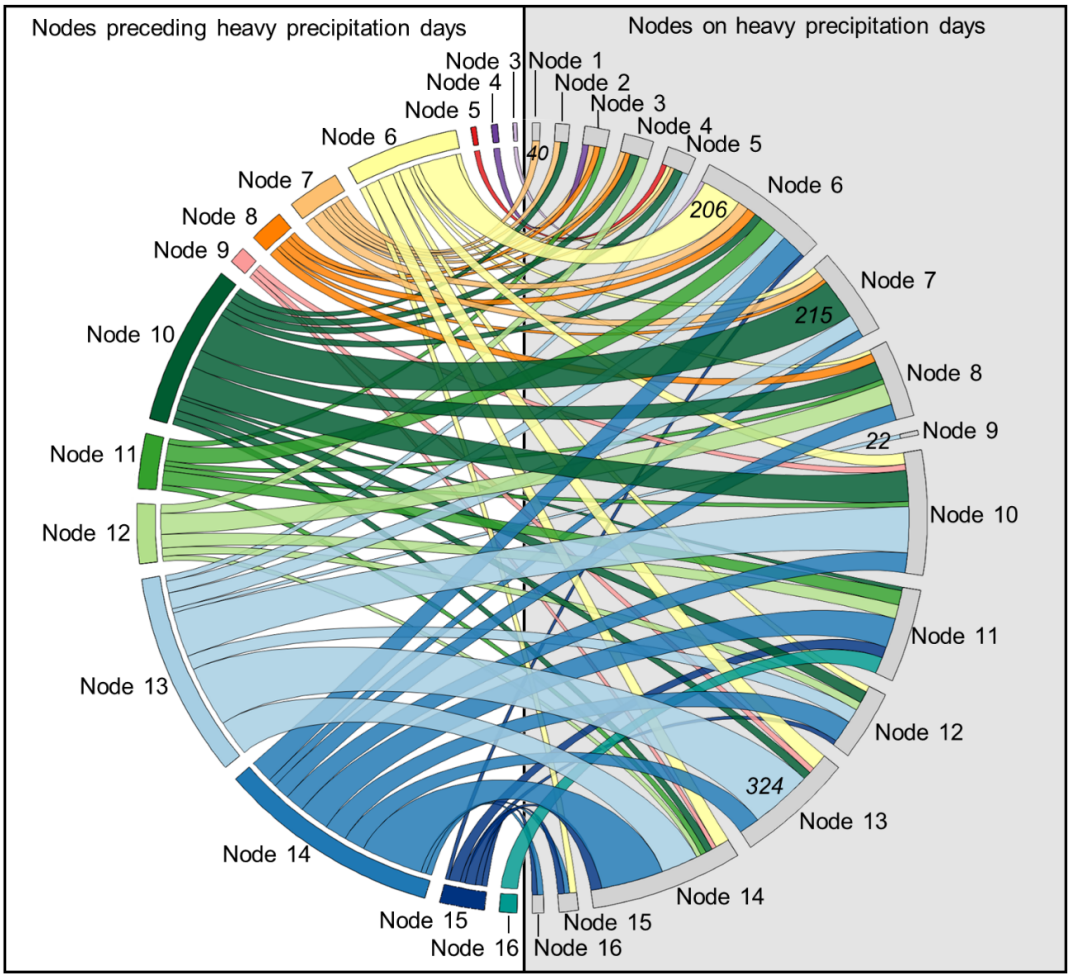

Figure 4.11. Left: The relative number of times each node precedes ≥P_{95} days. Right (shaded): The relative number of ≥P_{95} days associated with each node. Width of the colored bands indicates the frequency with which each node precedes the nodes of ≥P_{95} days. Node transitions occurring < 20 times during the 1900–2010 interval are omitted. Select counts of each transition are indicated (italicized) over the ribbon. Data visualized using Circos Table Viewer (Krzywinski et al. 2009; http://mkweb.bcgsc.ca/tableviewer/).

4.4. Discussion and Conclusions

This study of the relationship of moisture transport, precipitation, and their variability across the eastern US over the past century is the third in a series that broadly examines moisture transport within this region. Here, we examine the long-term climatology of

water vapor transport in the eastern US and its relationship with occurrences of heavy precipitation. By incorporating data from reanalysis products and long-term station observations, previous understanding of variability and relationships seen over short intervals is extended throughout the 20th and early 21st centuries. This expanded scope best informs future research regarding major drivers and the overall variability of the hydroclimatic regime of the eastern US and, likely, other temperate regions across the globe.

Distinct patterns of water vapor transport, expressed here as nodes, show increases in integrated vapor transport over the 111-year study period. The largest increases in integrated vapor transport are in the highest percentiles of the strongest moisture transport patterns, showing that the strongest moisture transport patterns are becoming stronger. The substantial increases in the 95th and 99th percentiles of IVT agree with projections of increases in the upper bounds of IVT by the end of the twenty-first century (Lavers et al. 2015; Warner et al. 2015) associated with increases in temperature as shown by the Clausius-Clapeyron equation (Held and Soden 2006).

Increases in moisture transport are inhomogeneous across temporal and spatial scales. Node frequency and intensity are shifting at annual and seasonal timescales, and multiple shifts in moisture transport throughout the eastern US occur throughout the study period. In particular, the meridional, high-IVT patterns increase in frequency at the expense of zonal and low-IVT patterns. This seemingly agrees with findings of increased precipitation days and decreased consecutive dry days observed in the study region (Bartels et al. 2020; Trepanier et al. 2015; Diem 2013), as well as with increases in heavy precipitation days (Groisman et al. 2005b; Diem 2013). Over the course of the study

period, IVT in each moisture transport pattern intensifies and weakens at regional and sub-regional scales. This is much like the findings of Bordi et al. (2015), which show trends in South American total column water vapor varying by region from 1979–2012. Therefore, our findings confirm that while widespread increases in IVT are frequently discussed as homogenous increases, they contain non-negligible components of spatial heterogeneity.

We find that nodes with the greatest coincidence with heavy precipitation occur with moderate frequency. This differs from the western US, where fewer events largely determine annual precipitation totals (Dettinger 2013). This demonstrates the importance of assessing the moisture flux climatology as a whole as opposed to focusing solely on the extremes of moisture transport when considering the hydroclimatology of the eastern US. We also find that many of the heavy precipitation days in the eastern US are preceded by days with the same moisture transport pattern, particularly when there is a relatively zonal flow. These consecutive days of the same moisture pattern may represent a precipitation-generating system tracking across the eastern US over multiple days. Such systems would have implications in compound extremes (i.e., extreme events occurring simultaneously or in quick succession, spatially or temporally), resulting in enhanced impacts, costs, and damages than if the event were isolated (Hao et al. 2018). There is significant potential for this type of situation, considering that mesoscale processes (possibly too small to be captured by the resolution of this study) entrained within synoptic-scale patterns are frequent contributors to heavy and extreme precipitation in the eastern US (Barlow et al. 2019, Schumacher and Johnson 2005).

Several of the nodes are infrequent but are strongly associated with heavy precipitation. These nodes are generally characterized by strong, confined corridors of moisture transport. Across these nodes, rates of multi-day occurrences increase throughout the study period. This has implications for flooding, particularly if heavy precipitation is delivered through these slower moving systems (Hao et al. 2018). The increasing frequency and persistence of synoptic-scale meridional moisture transport patterns also suggest a link to changes in jet stream behavior. Francis and Vavrus (2015) show that the decreased poleward temperature gradient from global warming weakens zonal flow, which results in increased meridional flow and a wavier jet stream. This meridional flow favors persistent weather patterns (Coumou et al. 2014). The increase in frequency and persistence of meridional transport patterns in our study resembles this increase in persistent meridional circulation patterns. Consequently, this shift may have implications regarding poleward moisture and energy exports (Knippertz et al. 2013; Gimeno et al. 2014).

Over the course of the study period, nodes most consistently associated with heavy precipitation increased in frequency, persistence, and IVT. Though these nodes are too rare to greatly influence the regional heavy precipitation regime during this study period, they suggest the potential for the future intensification of heavy precipitation. This demonstrates the need to pay special attention to rare, impactful events that may lead to deadly and catastrophic flooding.

This study demonstrates how examination of all aspects of moisture transport in the eastern US is necessary to understand variability in the hydroclimatological regime. Our study also contributes to the knowledge of hydroclimatic variability in the context of

climate change. While providing a great deal of information on precipitation variability, the growing body of literature investigating precipitation changes through pressure patterns and storm systems generally overlooks moisture content. Our study enhances this literature by investigating variability in synoptic-scale moisture transport and its relationship with precipitation. This moisture transport approach synthesizes changes in circulation with increases in atmospheric moisture content, providing a more direct link between global warming and precipitation variability than can be achieved through circulation patterns alone. We recommend that future work combine these approaches to investigate how the moisture transport involved in specific systems, such as extratropical cyclones and other frontal activity, impacts the precipitation regime. Future examination of regional precipitation regimes, using both this moisture transport approach and the classic storm systems approach in concert, would likely shed new light on historical climate records as well as future climate projections.

4.5. References

Agel, L., M. Barlow, J. H. Qian, F. Colby, E. Douglas, and T. Eichler, 2015: Climatology of daily precipitation and extreme precipitation events in the Northeast United States. *J. Hydrometeorol.*, **16**, 2537–2557, https://doi.org/10.1175/JHM-D-14-0147.1.

——, ——, S. B. Feldstein, and W. J. Gutowski, 2018: Identification of large-scale meteorological patterns associated with extreme precipitation in the US northeast. *Clim. Dyn.*, **50**, 1819–1839, https://doi.org/10.1007/s00382-017-3724-8.

Allen, M. R., and W. J. Ingram, 2002: Constraints on future changes in climate and the hydrologic cycle. *Nature*, **419**, 224–232, https://doi.org/10.1038/nature01092.

Alter, R. E., Y. Fan, B. R. Lintner, C. P. Weaver, R. E. Alter, Y. Fan, B. R. Lintner, and C. P. Weaver, 2015: Observational Evidence that Great Plains Irrigation Has Enhanced Summer Precipitation Intensity and Totals in the Midwestern United

States. *J. Hydrometeorol.*, **16**, 1717–1735, https://doi.org/10.1175/JHM-D-14-0115.1.

Barlow, M., and Coauthors, 2019: *North American extreme precipitation events and related large-scale meteorological patterns: a review of statistical methods, dynamics, modeling, and trends*. Springer Berlin Heidelberg, 6835–6875 pp.

Bartels, R. J., A. W. Black, and B. D. Keim, 2020: Trends in precipitation days in the United States. *Int. J. Climatol.*, **40**, 1038–1048, https://doi.org/10.1002/joc.6254.

Bordi, I., R. De Bonis, K. Fraedrich, and A. Sutera, 2015: Interannual variability patterns of the world's total column water content: Amazon River basin. *Theor. Appl. Climatol.*, **122**, 441–455, https://doi.org/10.1007/s00704-014-1304-y.

Byrne, M. P., and P. A. O'Gorman, 2015: The response of precipitation minus evapotranspiration to climate warming: Why the "Wet-get-wetter, dry-get-drier" scaling does not hold over land. *J. Clim.*, **28**, 8078–8092, https://doi.org/10.1175/JCLI-D-15-0369.1.

Colgan, M. S., C. A. Baldeck, J. baptiste Féret, and G. P. Asner, 2012: Mapping savanna tree species at ecosystem scales using support vector machine classification and BRDF correction on airborne hyperspectral and LiDAR data. *Remote Sens.*, **4**, 3462–3480, https://doi.org/10.3390/rs4113462.

Cortes, C., and V. Vapnik, 1995: Support-Vector Networks. *Mach. Learn.*, **20**, 273–297, https://doi.org/10.1109/64.163674.

Coumou D, V. Petoukhov, S. Rahmstorf, S. Petri, and H. J. Schellnguber, 2014: Quasi-resonant circulation regimes and hemispheric synchronization of extreme weather in boreal summer *Proc. Nat. Acad. Sci.*, **111** (34) 12331-12336.

Dee, D., and Coauthors, 2011: The ERA - Interim reanalysis: Configuration and performance of the data assimilation system. *Quaterly J. R. Meteorol. Soc.*, **137**, 553–597, https://doi.org/10.1002/qj.828.

Dettinger, M. D., 2013: Atmospheric Rivers as Drought Busters on the US West Coast. *J. Hydrometeorol.*, **14**, https://doi.org/10.1175/JHM-D-13-02.1.

Devadas, R., R. J. Denham, and M. Pringle, 2012: Support Vector Machine Classification of Object-Based Data for Crop Mapping, Using Multi-Temporal Landsat Imagery. *ISPRS - Int. Arch. Photogramm. Remote Sens. Spat. Inf. Sci.*, **XXXIX-B7**, 185–190, https://doi.org/10.5194/isprsarchives-xxxix-b7-185-2012.

Diem, J. E., 2013: Influences of the Bermuda High and atmospheric moistening on changes in summer rainfall in the Atlanta, Georgia region, USA. *Int. J. Climatol.*, **33**, 160–172, https://doi.org/10.1002/joc.3421.

Douglas, E. M., and C. A. Fairbank, 2011: Is Precipitation in Northern New England Becoming More Extreme? Statistical Analysis of Extreme Rainfall in Massachusetts, New Hampshire, and Maine and Updated Estimates of the 100-Year Storm. *J. Hydrol. Eng.*, **16**, 203–217, https://doi.org/10.1061/(ASCE)HE.1943-5584.0000303.

Easterling, D. R., and Coauthors, 2017: Precipitation change in the United States. In: Climate Science Special Report: Fourth National Climate Assessment. *Fourth Natl. Clim. Assessment, Vol. I*, **I**, 207–230, https://doi.org/10.7930/J0H993CC.US

Feng, P., B. Wang, D. L. Liu, and Q. Yu, 2019: Machine learning-based integration of remotely-sensed drought factors can improve the estimation of agricultural drought in South-Eastern Australia. *Agric. Syst.*, **173**, 303–316, https://doi.org/10.1016/j.agsy.2019.03.015.

Francis, J. A., and S. J. Vavrus, 2015: Evidence for a wavier jet stream in response to rapid Arctic warming. *Environ. Res. Lett.*, **10**, https://doi.org/10.1088/1748-9326/10/1/014005.

Gimeno, L., R. Nieto, M. Vazquez, and D. A. Lavers, 2014: Atmospheric rivers: a mini-review. *Front. Earth Sci.*, **2**, https://doi.org/10.3389/feart.2014.00002.

Groisman, P. Y., R. W. Knight, D. R. Easterling, T. R. Karl, G. C. Hegerl, and V. N. Razuvaev, 2005a: Trends in intense precipitation in the climate record. *J. Clim.*, **18**, 1326–1350, https://doi.org/10.1175/JCLI3339.1.

Harynuk, J. 2020. Theil-Sen Regression with intercept (https://www.mathworks.com/matlabcentral/fileexchange/71205-theil-sen-regression-with-intercept), MATLAB Central File Exchange. Retrieved March 24, 2020.

Hao, Z., V. P. Singh, and F. Hao, 2018: Compound extremes in hydroclimatology: A review. *Water (Switzerland)*, **10**, 16–21, https://doi.org/10.3390/w10060718.

Hayhoe, K., and Coauthors, 2007: Past and future changes in climate and hydrological indicators in the US Northeast. *Clim. Dyn.*, **28**, 381–407, https://doi.org/10.1007/s00382-006-0187-8.

Held, I. M., and B. J. Soden, 2006: Robust Responses of the Hydrological Cycle to Global Warming. *J. Clim.*, **19**, 5686–5699.

Heung, B., H. C. Ho, J. Zhang, A. Knudby, C. E. Bulmer, and M. G. Schmidt, 2016: An overview and comparison of machine-learning techniques for classification purposes in digital soil mapping. *Geoderma*, **265**, 62–77, https://doi.org/10.1016/j.geoderma.2015.11.014.

Hoerling, M., J. Eischeid, J. Perlwitz, X. W. Quan, K. Wolter, and L. Cheng, 2016: Characterizing recent trends in US heavy precipitation. *J. Clim.*, **29**, 2313–2332, https://doi.org/10.1175/JCLI-D-15-0441.1.

Huang, H., J. M. Winter, E. C. Osterberg, R. M. Horton, and B. Beckage, 2017: Total and Extreme Precipitation Changes over the Northeastern United States. *J. Hydromete*, **18**, 1783–1799, https://doi.org/10.1175/JHM-D-16-0195.1.

Huntington, T. G., 2006: Evidence for intensification of the global water cycle: Review and synthesis. *J. Hydrol.*, **319**, 83–95, https://doi.org/10.1016/j.jhydrol.2005.07.003.

Karamizadeh, S., S. M. Abdullah, M. Halimi, J. Shayan, and M. J. Rajabi, 2014:

Advantage and drawback of support vector machine functionality. *I4CT 2014 - 1st Int. Conf. Comput. Commun. Control Technol. Proc.*, 63–65, https://doi.org/10.1109/I4CT.2014.6914146.

Kendall, M. G., 1938: A New Measure of Rank Correlation. *Biometrika*, https://doi.org/10.2307/2332226.

Knippertz, P., H. Wernli, and G. Glaser, 2013: A Global Climatology of Tropical Moisture Exports. *J. Clim.*, **26**, 3031–3045, https://doi.org/10.1175/JCLI-D-12-00401.1.

Krzywinski, M., J. Schein, I. Birol, J. Connors, R. Gascoyne, D. Horsman, S. J. Jones, and M. A. Marra, 2009: Circos: An information aesthetic for comparative genomics. *Genome Res.*, **19**, 1639–1645, https://doi.org/10.1101/gr.092759.109.

Kunkel, K. E., D. R. Easterling, D. A. R. Kristovich, B. Gleason, L. Stoecker, and R. Smith, 2010: Recent increases in US heavy precipitation associated with tropical cyclones. *Geophys. Res. Lett.*, **37**, 2–5, https://doi.org/10.1029/2010GL045164.

Lavers, D., M. Ralph, D. Waliser, A. Gershunov, and M. D. Dettinger, 2015: Climate change intensification of horizontal water vapor transport in CMIP5. *Geophys. Res. Lett.*, 1–9, https://doi.org/10.1002/2015GL064672.Received.

——, and G. Villarini, 2013: Atmospheric Rivers and Flooding over the Central United States. *J. Clim.*, **26**, 7829–7836, https://doi.org/10.1175/JCLI-D-13-00212.1.

Mahoney, K., and Coauthors, 2016: Understanding the Role of Atmospheric Rivers in Heavy Precipitation in the Southeast United States. *Mon. Weather Rev.*, **144**, 1617–1632, https://doi.org/10.1175/MWR-D-15-0279.1.

Mann, H. B., 1945: Nonparametric Tests Against Trend. *Econometrica*, https://doi.org/10.2307/1907187.

Menne, M. J., and Coauthors, 2012a: Global Historical Climatology Network-Daily (GHCN-Daily), version 3. NOAA National Climatic Data Center. doi:10.7289/V5D21VHZ [accessed 30 March 2020].

——, I. Durre, R. S. Vose, B. E. Gleason, and T. G. Houston, 2012b: An overview of the global historical climatology network-daily database. *J. Atmos. Ocean. Technol.*, **29**, 897–910, https://doi.org/10.1175/JTECH-D-11-00103.1.

Mountrakis, G., J. Im, and C. Ogole, 2011: Support vector machines in remote sensing: A review. *ISPRS J. Photogramm. Remote Sens.*, **66**, 247–259, https://doi.org/10.1016/j.isprsjprs.2010.11.001.

Poli, P., and Coauthors, 2016: ERA-20C: An Atmospheric Reanalysis of the Twentieth Century. *J. Clim.*, **29**, 4083–4097, https://doi.org/10.1175/JCLI-D-15-0556.1.

Qader, S. H., J. Dash, P. M. Atkinson, and V. Rodriguez-Galiano, 2016: Classification of Vegetation Type in Iraq Using Satellite-Based Phenological Parameters. *IEEE J. Sel. Top. Appl. Earth Obs. Remote Sens.*, **9**, 414–424, https://doi.org/10.1109/JSTARS.2015.2508639.

Schumacher, R. S., and R. H. Johnson, 2006: Characteristics of US extreme rain events during 1999-2003. *Weather Forecast.,* **21**, 69–85, https://doi.org/10.1175/WAF900.1.

Sen, P. K., 1968: Estimates of the Regression Coefficient Based on Kendall ' s Tau Author (s): Pranab Kumar Sen Source : Journal of the American Statistical Association , Vol . 63 , No . 324 (Dec ., 1968), pp . Published by : Taylor & Francis , Ltd . on behalf of the A. *J. Am. Stat. Assoc.*, **63**, 1379–1389.

Theil, H., 1950: A rank-invariant method of linear and polynomial. *Mathematics*, **392**, 387–392.

Trepanier, J. C., M. J. Roberts, and B. D. Keim, 2015: Trends and spatial variability in dry spells across the south-central United States. *J. Appl. Meteorol. Climatol.*, **54**, 2261–2272, https://doi.org/10.1175/JAMC-D-14-0319.1.

Tripathi, S., V. V. Srinivas, and R. S. Nanjundiah, 2006: Downscaling of precipitation for climate change scenarios: A support vector machine approach. *J. Hydrol.*, **330**, 621–640, https://doi.org/10.1016/j.jhydrol.2006.04.030.

Wang, X., Z. Wu, and X. Li, 2019: Near-surface snowmelt detection on the Greenland ice sheet from FengYun-3 MWRI data. *Cluster Comput.*, **22**, 8301–8308, https://doi.org/10.1007/s10586-018-1743-9.

Warner, M. D., C. F. Mass, and E. P. Salathé, 2015: Changes in Winter Atmospheric Rivers along the North American West Coast in CMIP5 Climate Models. *J. Hydrometeorol.*, **16**, 118–128, https://doi.org/10.1175/JHM-D-14-0080.1.

Wentz, F. J., L. Ricciardulli, K. Hilburn, and C. Mears, 2007: How much more rain will global warming bring? *Science (80-.).*, **317**, 233–235, https://doi.org/10.1126/science.1140746.

Yan, W. Y., A. Shaker, and N. El-Ashmawy, 2015: Urban land cover classification using airborne LiDAR data: A review. *Remote Sens. Environ.*, **158**, 295–310, https://doi.org/10.1016/j.rse.2014.11.001.

Zhan, Y., and D. Shen, 2005: Design efficient support vector machine for fast classification. *Pattern Recognit.*, **38**, 157–161, https://doi.org/10.1016/j.patcog.2004.06.001.

5. CONCLUSIONS

This dissertation identifies patterns of moisture transport impacting the eastern US and the adjacent Atlantic and relates these patterns to regional precipitation. Despite a growing body of literature relating variability in precipitation—particularly heavy precipitation—to storm systems and weather patterns, this link between precipitation and its supplied moisture had not yet been established for this region. By assessing precipitation variability through patterns of moisture delivery, as opposed to the moisture delivery sourcing precipitation of a certain magnitude, we develop a novel climatology of water vapor transport for the eastern US and assess its impacts on the entire regional precipitation regime. Furthermore, this approach directly links variability in eastern US precipitation with global climate change due to atmospheric moisture's sensitivity to temperature.

The objectives of this dissertation are to: (1) develop a climatology of water vapor transport accounting for all manners of moisture delivery through the eastern US and adjacent Atlantic, and (2) relate moisture transport to regional precipitation. These objectives are met through a series of three studies.

The first study in this dissertation, Chapter 2, develops a climatology of moisture transport patterns influencing the eastern US and adjacent Atlantic. This is achieved using a self-organizing map methodology ingesting integrated water vapor transport (IVT), capturing both primary patterns of integrated vapor transport as well as patterns that are comparatively rare. In this way, the resulting sixteen patterns ("nodes") reflect all manners of moisture delivery through the 30°–50°N × 60°–90°W study domain. These

sixteen patterns are unique, each with a distinct frequency, seasonality, and spatial distribution of moisture transport across the study area. The warm season water vapor delivery is comprised of a wide variety of transport patterns, reflecting various moisture sources and flux trajectories. In contrast, one zonal, low-IVT node dominates the winter months, with occasional occurrences of other water vapor transport patterns.

Within the first study, we establish the relationship between moisture transport and frequency, and the impact of this relationship on the water vapor fluxes influencing the study area. Overall, nodes depicting the highest instantaneous moisture transport over the study area are relatively infrequent; nodes with low to moderate moisture transport are relatively common. This demonstrates that because of their high frequency, moderate moisture transport patterns are major contributors to regional water vapor delivery. This study also shows that most confined moisture transport corridors are the most ephemeral, while the patterns containing the most even distributions of moisture transport are more likely to persist for multiple consecutive days.

The high frequency with which broad definitions of atmospheric rivers are met is demonstrated in the first study. Occurring across a variety of water vapor transport patterns, this reveals the multifaceted appearance of so-called atmospheric rivers in the eastern US, and also the need for more restrictive definitions of atmospheric rivers to be used in this study region for the term to be useful. This sets the eastern US apart from regions in which atmospheric rivers are frequently studied using moisture transport thresholds alone.

This first study contributes to the literature of the hydroclimatology of the eastern US, as well as to the subsequent studies of this dissertation. This novel climatology

directly depicts the pathways through which water vapor is transported through the region: an enhancement to inferring moisture transport solely through pressure patterns. This new information enables the hydroclimatology of the eastern US to be better understood. The understanding of moisture transport cultivated in the first study provides a baseline from which deviations can be measured, thereby providing a foundation for investigating variability in moisture transport as well as situating the regional climatology within the context of global climate change. This foundation provides the necessary understanding of moisture transport utilized in subsequent chapters of this dissertation. However, even high magnitudes of water vapor transport do not guarantee precipitation. To understand the impact exerted by different patterns of this comprehensive moisture transport climatology, these patterns must be related to regional precipitation.

In the second study (Chapter 3), the climatology of water vapor transport developed in the first study is related to precipitation in the eastern US. This study is the first of its kind linking precipitation to water vapor transport for this region. High-resolution, gridded precipitation data for the eastern US captures the variability of precipitation associated with each node. Precipitation generally follows the same spatial patterns as both IVT and vertical velocity, though impacts of elevation can be discerned.

The highest precipitation averages occur with moisture transport patterns defined by high magnitudes of water vapor transport. Precipitation also occurs with these IVT-rich patterns more consistently than with low-IVT patterns. However, while IVT-rich patterns are associated with both consistent precipitation and relatively high average precipitation, the low frequency of these patterns abates their overall impact in the annual hydroclimatology. Instead, patterns of moderate frequency and moderate intensity exert

the greatest contribution to the annual precipitation of the study domain. This finding illustrates the importance of assessing the moisture delivery regime of the eastern US as a whole, as focusing on only the most extreme moisture fluxes would overlook much of the regional moisture transport and precipitation.

Examining precipitation by the pattern of moisture delivery reveals how changes in atmospheric moisture and circulation are manifested in precipitation patterns. Our second study shows that the majority of water vapor transport patterns are linked with increases in precipitation—particularly heavy precipitation—from 1981–2017. This agrees with the state of the literature in that heavy precipitation is increasing faster than moderate precipitation. Furthermore, this second study expands such information by identifying which specific moisture transport patterns are associated with these increases.

The link between water vapor transport and heavy precipitation identified in the second study is investigated further in the third (Chapter 4). This final study extends both the variability in moisture transport patterns as well as their relationship with heavy precipitation back through the 20th century. This is done by training a model to classify historical IVT fluxes into the IVT patterns developed in Chapter 2 and by introducing long-term precipitation data from stations with records from 1900–2010.

In this third study, long-term changes in the frequency, persistence, and intensity of the moisture transport patterns are identified. These analyses reveal that the frequency and persistence of meridional, strong-IVT patterns increase from 1900–2010, indicating a shift to more frequent meridional circulation and moisture advection in the eastern US. This is coupled by a decreased frequency and persistence of the low-IVT, zonal patterns,

which have been shown in earlier studies to contribute substantially to annual precipitation totals through moderate daily precipitation averages.

The intensification of water vapor transport in the eastern US, as shown through the strengthening of the highest percentiles of moisture transport, agrees with the current knowledge of hydroclimatic impacts of climate change. The third paper furthers this knowledge by showing how these changes are distributed across the eastern US, identifying where moisture transport patterns are increasing in IVT and where decreases are evidenced. This investigation shows how the moisture transport patterns have changed, dynamically and thermodynamically, since the beginning of the 20th century.

The third study also expands upon findings from previous studies to investigate how the frequency of the moisture transport pattern overall influences its contribution to the heavy precipitation regime. We find that through the 20th and early 21st centuries, nodes of moderate moisture transport and frequency are replacing the frequent, low-IVT systems as the patterns most associated with heavy precipitation in the eastern US. Some moisture rich IVT patterns, though consistently associated with heavy precipitation, are not prominent patterns in the overall heavy precipitation regime due to their low frequency. However, over the course of the study period these patterns have increased in frequency, persistence, and vapor transport, and have been associated with notable excessive precipitation events.

This third study synthesizes and expands upon the first two to demonstrate the value in utilizing a moisture-transport approach to investigating variability in precipitation. This approach enables observed changes in precipitation to be linked to variability in water vapor transport; a direction which had yet to be pursued for the

eastern US. The long-term relationship between these two variables, as well as variability within each, provides a foundation for investigating the impact of changes in atmospheric moisture in climate model projections.

5.1. Recommendations for future work

This dissertation has identified several topics requiring further investigation, some of which have been presented in the preceding chapters. Overall, we find that this novel moisture transport approach has a wealth of possibilities for investigating relationships and changes in hydroclimatology. Here, we list six recommendations for future work investigating moisture transport associated with precipitation and other aspects of hydroclimatology.

1) This moisture transport approach in concert with classical weather typing or storm typing methodologies would likely produce new insights into the relationships between moisture supply, precipitation, and the mechanisms producing precipitation. We envision such a study investigating how moisture transport associated with various meteorological features, such as extratropical cyclones, frontal activity, or mesoscale convective systems, vary over time, and the effect of this variability on precipitation.
2) This dissertation borrows the integrated water vapor transport variable from the atmospheric rivers literature. While this variable neatly combines atmospheric moisture and horizontal velocity, this vertically integrated variable does not account for vertical placement of moisture within the atmospheric column. Future work might include water vapor content at multiple heights while establishing

patterns of moisture transport or analyze changes in the height of water vapor transport in each pattern over time.

3) While not considered in this dissertation, the phase of precipitation (and variability therein) associated with each moisture flux may greatly affect the impact of a precipitation event. We propose that future work consider the phase of precipitation associated with each moisture transport pattern, potentially in an investigation of winter rain/snow fractions in mid- to high-latitude regions.
4) This dissertation focuses entirely on water vapor transport and precipitation. However, water vapor transport is closely linked to other aspects of hydroclimatology. We suggest that future work investigate the relationship between water vapor transport and evapotranspiration, soil moisture, and sea surface temperatures. Any such study would couple well with this dissertation, as providing information on the sources of water vapor would close the moisture budgets between the atmosphere and land surface.
5) The moisture transport approach is useful in the eastern US because the region experiences precipitation from a wide variety of mechanisms and moisture fluxes. We recommend that similar studies be undertaken in other regions that are also influenced by complex precipitation climatologies to better understand the drivers of variability.
6) The information contributed by this dissertation creates a foundation for work examining the impact of water vapor transport in future climate projections. We look forward to research analyzing the future variability of water vapor transport

in the eastern US to assess if or how the long-term trends and relationships identified in this dissertation may carry forth in the future.

APPENDIX

Chapter 3: Supplemental Materials

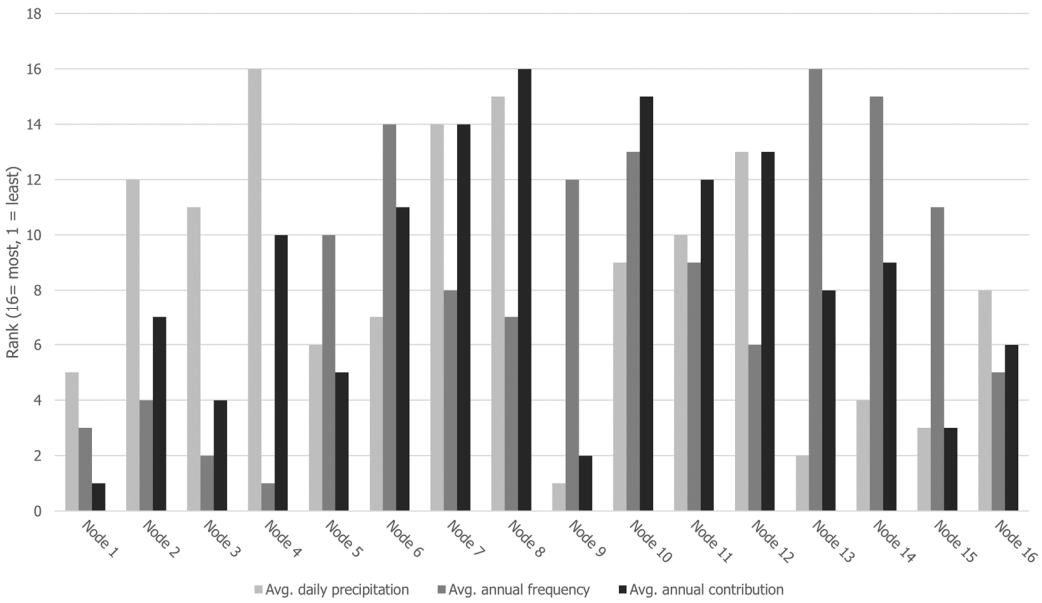

Supplemental Figure 3.1. Ranked average precipitation, average frequency, and average contribution to annual precipitation.

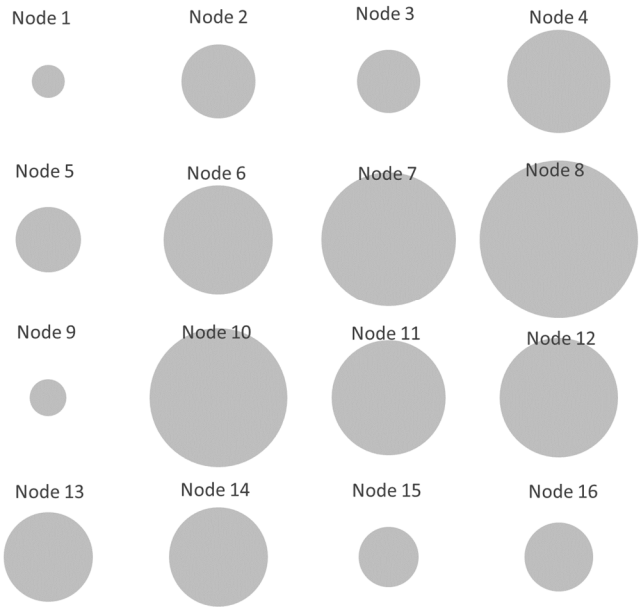

Supplemental Figure 3.2. Average annual contribution of each node; circle diameter represents contribution.

Chapter 4: Supplemental Materials

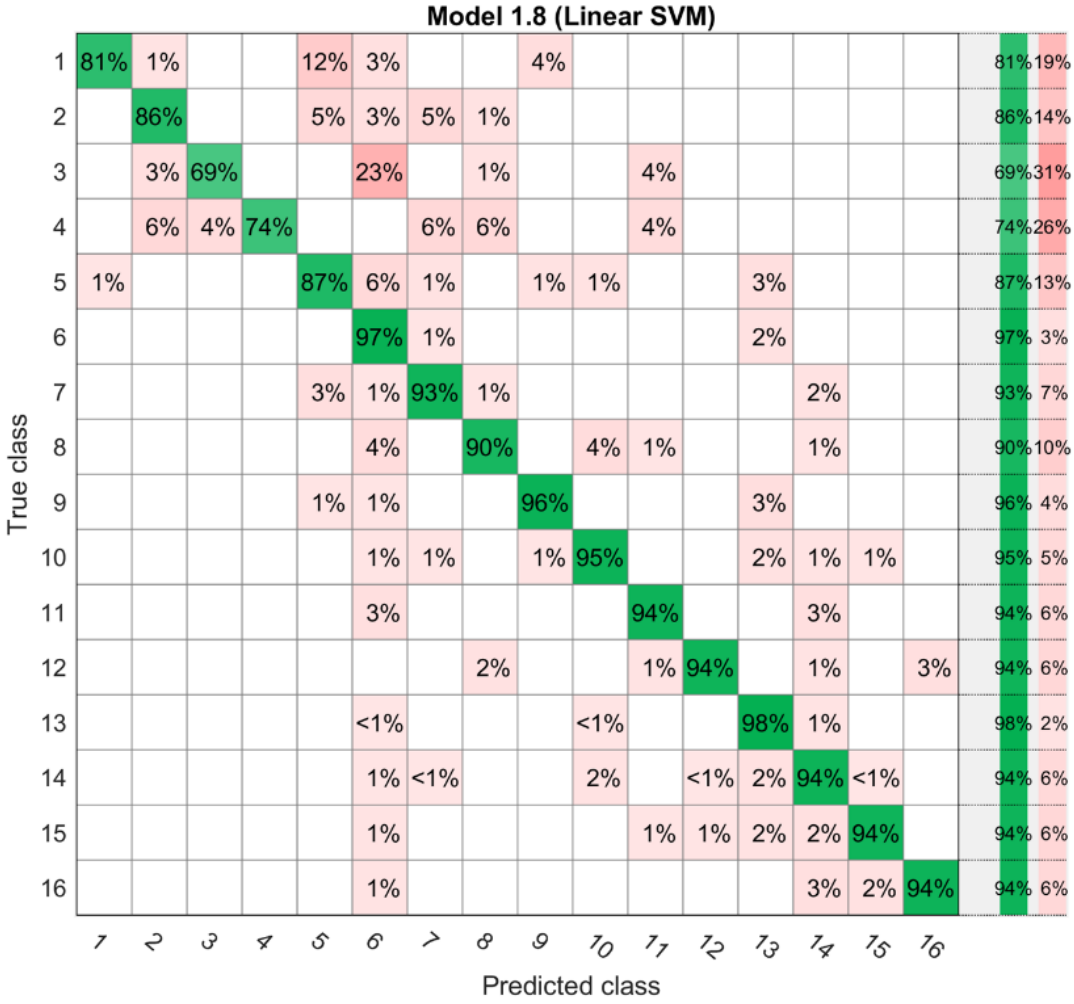

Supplemental Figure 4.1. Confusion matrix for linear SVM model with accuracy rate of 92.8%.

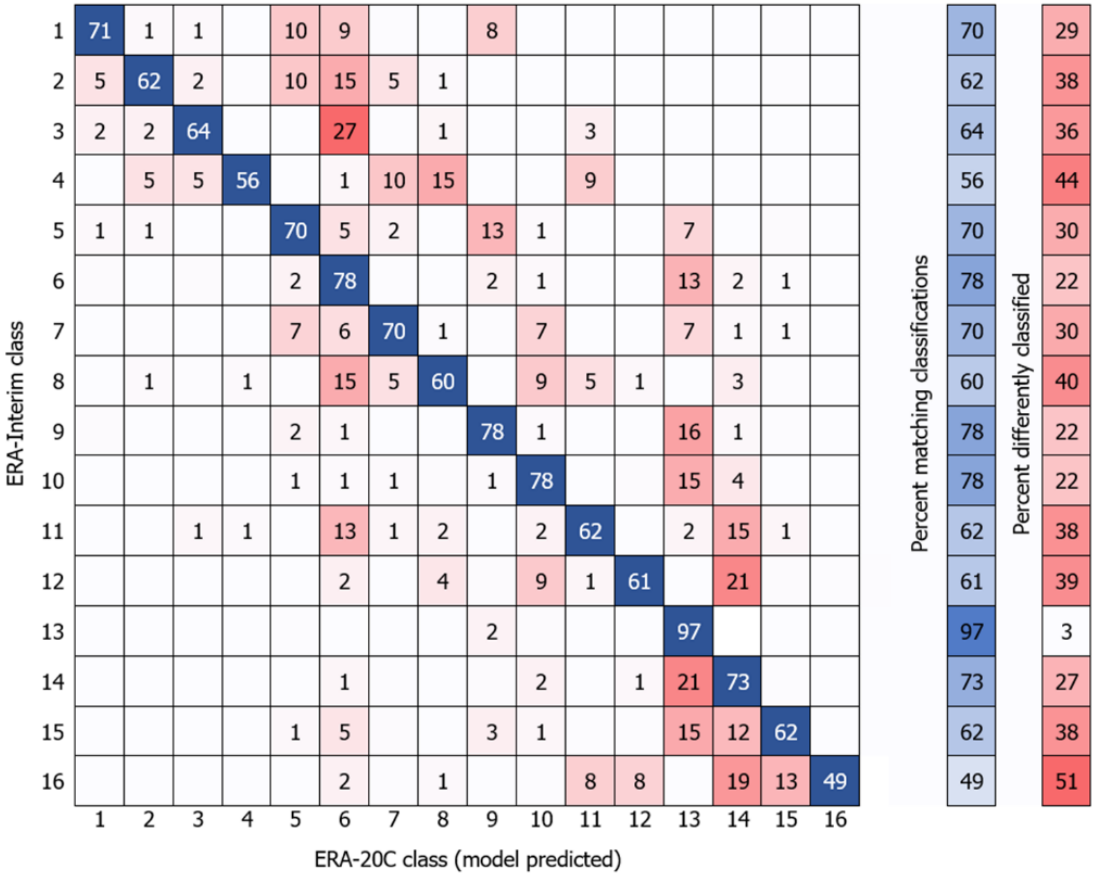

Supplemental Figure 4.2. Confusion matrix comparing percent of daily node assignments form ERA-Interim IVT (T&R) and from ERA-20C IVT for the overlap period of 1979-2010, with a matching node assignment rate of 73.7%.

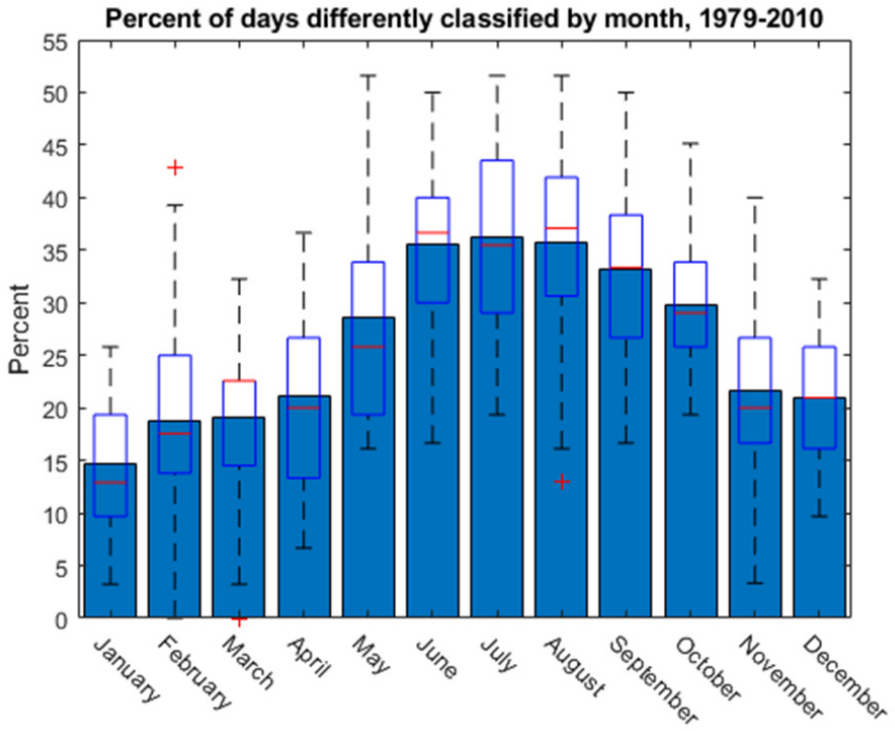

Supplemental Figure 4.3. Percent of days in each month that is classified differently between ERA-Interim daily IVT and ERA-20C IVT. Bars indicate overall percent of days differently classified. Boxplots display the annual variaion in percent of days differently classified.

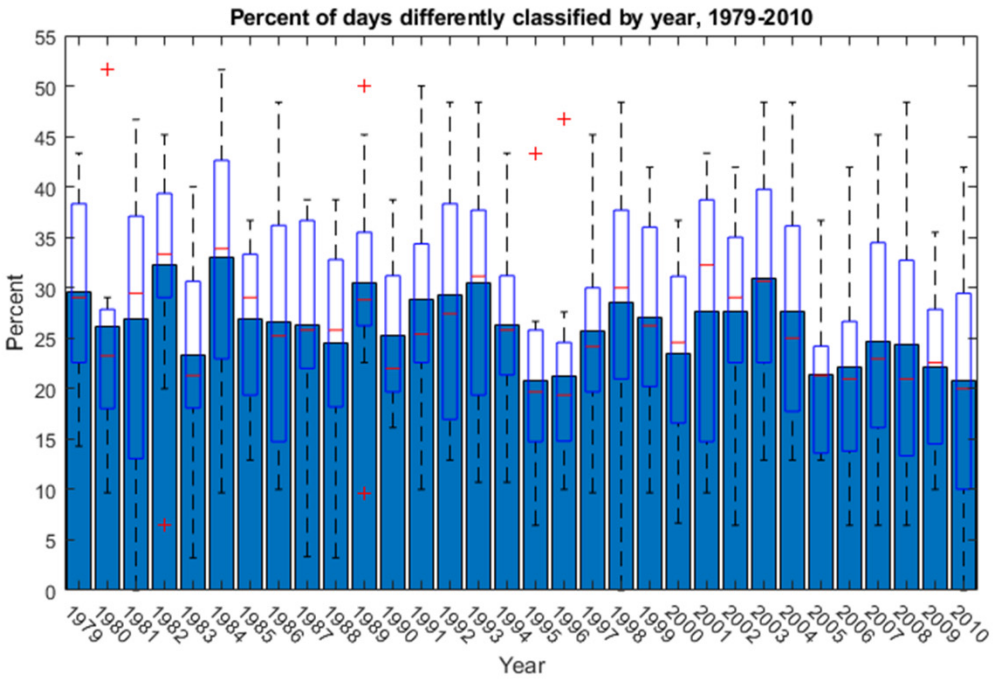

Supplemental Figure 4.4. Percent of days in each year that is classified differently between ERA-Interim and ERA-20C IVT. Bars indicate iverakk oercebt if days differently classified. Boxplots display monthly variations in percent of days differently classified for each year.

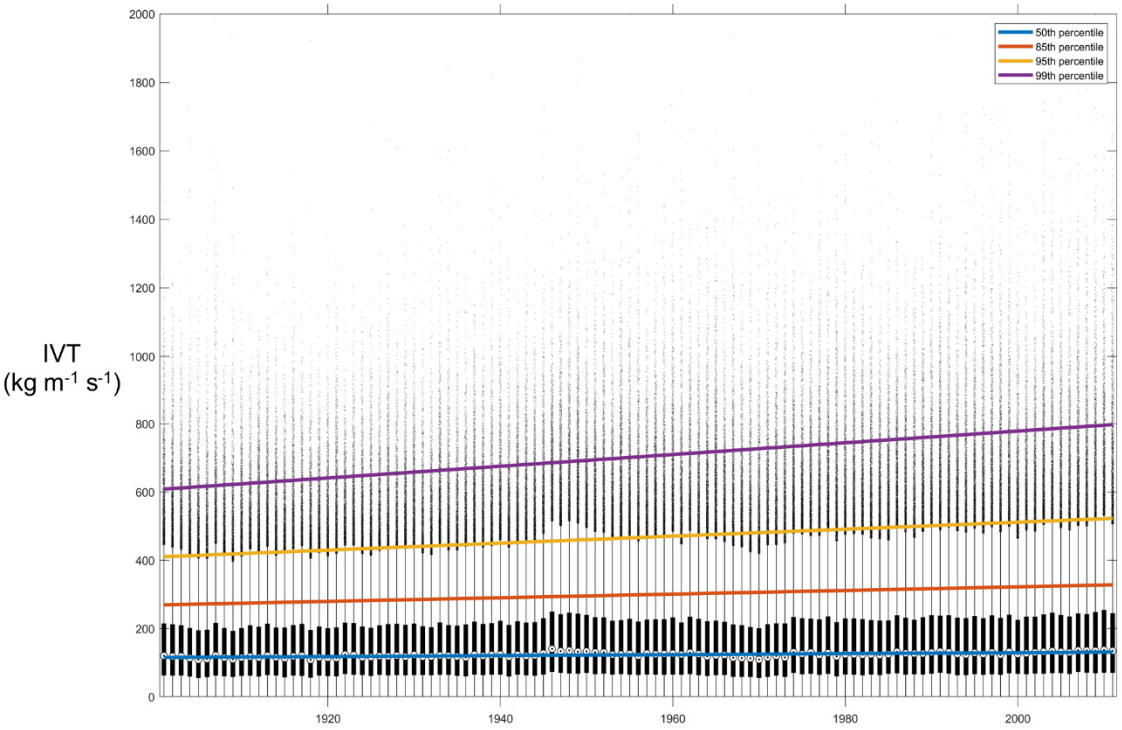

Supplemental Figure 4.5. The distribution of annual IVT. Boxplots show the 25th (bottom of the box), 50th (center circle), and 75th (top of box) percentiles of IVT. Trends in the 50th (blue), 85th (orange), 95th (yellow), and 99th (purple) percentiles of IVT are shown.

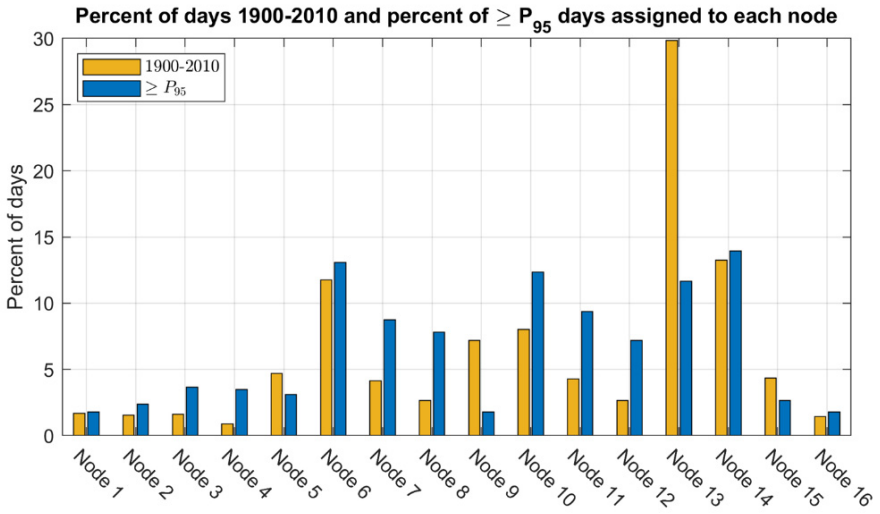

Supplemental Figure 4.6. Percent of days from 1900–2010 assigned to each node (yellow; left bar) with the percent of heavy precipitation days (≥P_{95} days) associated with each node (blue; right bar).

Supplemental Table 4.1. Significant increases in IVT (kg m^{-1} s^{-1}) per decade for each node at the 50th, 85, 95th, and 99th percentiles.

	P_{50}	P_{85}	P_{95}	P_{99}
Node 1	1.7	-	6.1	9.7
Node 2	-	-	6.8	12.9
Node 3	-	3.2	8.7	12.9
Node 4	2.7	4.5	9.1	14.2
Node 5	1.0	-	4.3	7.1
Node 6	-	1.6	4.5	8.2
Node 7	-	1.8	5.2	11.1
Node 8	-	3.0	6.5	9.2
Node 9	0.6	1.1	3.3	7.3
Node 10	0.5	-	3.5	8.8
Node 11	1.3	3.9	5.8	7.3
Node 12	-	3.1	7.4	12.2
Node 13	-	0.6	1.7	3.9
Node 14	-	1.2	2.9	4.7
Node 15	0.7	3.7	7.1	9.8
Node 16	2.2	3.9	5.7	9.4

ACKNOWLEDGEMENT OF PREVIOUS PUBLICATION

Chapter 2 of this dissertation is under review by the Journal of Hydrometeorology under the title “Patterns of Water Vapor Transport in the Eastern United States.” The majority of the writing in this paper is my own, with helpful advice from my advisor and coauthor as well as three anonymous reviewers.